

Bifluorescent analysis of α -synuclein aggregation *in vivo*

Kianna Mau

Thesis submitted to the University of Ottawa in partial fulfillment of the degree requirements for
Master of Science in Biochemistry with Specialization in Pathology and Experimental Medicine

Department of Biochemistry, Microbiology, and Immunology
Faculty of Medicine
University of Ottawa

© Kianna Mau, Ottawa, Canada, 2020

Abstract

Parkinson's disease is an incurable neurodegenerative disease characterized by motor deficits, owing to dopaminergic denervation in the nigrostriatal pathway. The abnormal formation of hallmark Lewy bodies underlies the disease process. The pre-synaptic protein alpha-synuclein (α -syn) has prion-like properties arising from its propensity to propagate, seed misfolding, and self-aggregate. Pathogenesis is postulated to arise in olfactory and enteric regions, exploiting connected neuronal pathways to ultimately propagate to the substantia nigra pars compacta. There is little known about the earliest stages of α -syn aggregation and its prion-like propagation mechanisms. Bimolecular fluorescence complementation of α -syn aggregates has allowed us to directly visualize aggregation in transgenic mice and mice transduced with an adeno-associated virus vector. Although our transgenic mice expressed BiSyn in a mosaic fashion that limited utility, we were successful in transducing neurons in the mouse striatum. This work has validated the AAV2/9-CMV-BiSyn approach as groundwork for future systematic studies.

Acknowledgements

I am incredibly grateful for my co-supervisors Drs. Doug Gray and John Woulfe, who supported and encouraged me throughout a challenging project. With great risk, they took me on as a graduate student, having no prior lab experience. Their knowledge and compassion were critical for my success. To Doug for always making himself available for my “quick” questions; for helping with my unique microscope issues; and for continuously empathizing when my health interfered with my studies. To John for helping me develop neuroanatomical awareness; for his histological guidance; and for sympathizing with the difficulties of such a perplexing project.

I would also like to thank Drs. Rashmi Kothary and Michael Schlossmacher, my thesis advisory committee members, for their knowledge, insight, and constructive criticism that helped me develop novel strategies throughout a puzzling project and thrive through, what seemed to be, continuous roadblocks.

Many thanks need to be given to Dr. Josée Coulombe, Senior Research Associate in the Gray/Woulfe lab, without whom I would have never achieved what I have in Science. She trained me in nearly all lab procedures and was patient with me from the start when I required instruction on the simplest of tasks. Because of Josée’s continuous support and assistance, and our ability to share ideas and fully understand each other’s blather, I have come so far and have learned an incredible amount. I am so thankful for the training and friendship gained while working with Josée as well as the other current and previous members of the Gray/Woulfe lab (especially Brennan, Sarah, Mei and Yvonne) and researchers at the Cancer Centre.

My success would not have been possible without the support of my family (Mom, Dad, Jerai and Jade) and Andrew in Kingston. They were all just a phone call away or a quick two-hour drive when I needed them.

Table of Contents

Abstract.....	ii
Acknowledgements	iii
Table of Contents.....	iv
List of abbreviations.....	vii
List of figures	x
List of tables	xi
1.0 Introduction.....	xii
1.1 Parkinson’s disease.....	xii
1.1.1 <i>Prevalence and risk factors</i>	xii
1.1.2 <i>Dopaminergic innervation and denervation</i>	xii
1.2 Pathological hallmarks and aetiologies.....	xvi
1.2.1 <i>Synucleins</i>	xvi
1.2.2 <i>Lewy pathology</i>	xvii
1.2.3 <i>SNCA mutations</i>	xviii
1.2.4 <i>Parkinson’s disease as a mitochondriopathy</i>	xix
1.2.5 <i>Environmental contributors</i>	xx
1.3 Prion diseases.....	xxii
1.3.1 <i>α-syn as a prion</i>	xxii
1.3.2 <i>Braak hypothesis</i>	xxiii
1.4 Enteric nervous system.....	xxvii
1.4.1 <i>Enteric implications in Parkinson’s disease</i>	xxix
1.4.2 <i>Evolution and function of the appendix</i>	xxxiii
1.4.3 <i>Immune contribution to Parkinson’s disease</i>	xxxiv
1.5 BiSyn.....	xxxvi
1.5.1 <i>Bimolecular fluorescence complementation</i>	xxxvii
1.5.2 <i>Tamoxifen-inducible Cre-lox system</i>	xl
1.6 Purpose.....	xli
2.0 Methods	xliv
2.1 Animal care.....	xliv
2.1.1 <i>Generation of BiSyn transgenic mouse lines</i>	xliv
2.1.2 <i>Genotyping</i>	xlvii
2.1.3 <i>Statistical analysis of litter sizes</i>	lii
2.2 Transgene expression experiment.....	lii
2.2.1 <i>Evaluation of BiSyn expression phenotype via histochemical technique</i>	lii
2.2.1.1 <i>Zygote and ovary extraction</i>	lv
2.2.1.2 <i>Embryo extraction</i>	lv
2.2.1.3 <i>Mouse embryonic fibroblast isolation</i>	lvi
2.2.1.4 <i>Brain and testis harvest for histochemical staining</i>	lvii
2.2.1.5 <i>Fixation and histochemical staining for β-gal</i>	lvii
2.2.1.6 <i>Tissue Freezing</i>	lvii

2.2.1.7 Microscopy.....	lviii
2.2.1.8 Statistical analysis of transgene expression at distinct developmental time points.....	lviii
2.2.2 <i>Assessing BiSyn expression in enteric neurons via immunofluorescence</i>	lviii
2.2.2.1 Tamoxifen-induced recombination in vivo.....	lviii
2.2.2.2 Whole mount gut sectioning.....	lix
2.2.3 <i>Evaluating restoration of transgene expression and functionality</i>	lix
2.2.3.1 DNA methyltransferase and histone deacetylase complex inhibitor treatments.....	lx
2.2.3.2 Inducible recombination in MEFs.....	lx
2.2.3.3 Rotenone-induced aggregation in MEFs.....	lxi
2.3 BiSyn transduction experiment.....	lxi
2.3.1 <i>rAAV preparation</i>	lxi
2.3.2 <i>rAAV injection</i>	lxi
2.3.3 <i>Tissue fixation</i>	lxii
2.3.4 <i>Tissue freezing</i>	lxii
2.3.5 <i>Immunofluorescence</i>	lxii
2.3.6 <i>Analysis</i>	lxv
3.0 Results.....	lxvi
3.1 Generation of BiSyn mouse lines.....	lxvi
3.1.1 <i>Comparative analysis of litters across the three BiSyn mouse lines</i>	lxvi
3.2 Expression in BiSyn/Cre transgenic mice.....	lxix
3.2.1 <i>Developing mice present with mosaic phenotype</i>	lxix
3.2.2 <i>Gametic variation in transgene expression</i>	lxxii
3.2.3 <i>Stochastic expression in regions critical to PD pathology</i>	lxxvii
3.2.4 <i>Expression is not restored in late passage MEFs</i>	lxxvii
3.2.5 <i>BiSyn system is functional in early passage MEFs and transfected cell lines</i>	lxxx
3.3 Delivery of BiSyn via AAV as an alternative model.....	lxxxii
3.3.1 <i>Pattern of striatal transduction with AAV2/9-CMV-BiSyn</i>	lxxxiv
3.3.2 <i>Viral propagation via CSF</i>	lxxxvii
3.3.3 <i>Viral propagation via structural connectivity</i>	xc
3.3.4 <i>Viral uptake into glial cells</i>	xc
4.0 Discussion.....	xcvi
4.1 BiSyn/Cre transgenic mouse model.....	xcvi
4.1.1 <i>Re-evaluating the ubiquitous transgenic model</i>	xcvi
4.1.2 <i>Tamoxifen-inducible recombination efficiency</i>	xcvii
4.1.3 <i>Zygotic genome activation</i>	xcvii
4.1.4 <i>Mosaicism attributed to position effects</i>	xcviii
4.2 AAV2/9-CMV-BiSyn model.....	ci
4.2.1 <i>Transduction specificity</i>	cii
4.2.2 <i>Expression patterns</i>	cii
4.2.3 <i>AAV propagation tendencies</i>	ciii
4.2.4 <i>Adult neurogenesis and Parkinson's disease</i>	civ
4.2.5 <i>Inflammation at the epicentre of PD pathogenesis</i>	cxi
4.2.6 <i>Future use of AAV2/9-CMV-BiSyn in the appendix</i>	cxiii
4.3 Conclusion.....	cxvi

References	cxviii
Contributions of Collaborators	cxxxiv
Appendices	cxxxv
Appendix A: Copyright permission for reproduction of Figure 1	cxxxv
Appendix B: Copyright permission for reproduction of Figure 2	cxxxvi
Appendix C: Copyright permission for reproduction of Figure 3	cxxxvii
Appendix D: Copyright permission for reproduction of Figure 4	cxxxviii
Appendix E: Copyright permission for reproduction of Figure 5	cxxxix
Appendix F: Copyright permission for reproduction of Figure 6	cxl
Appendix G: Copyright permission for reproduction of Figure 8	cxli
Appendix H: Copyright permission for reproduction of Figure 19	cxlii
Appendix I: Copyright permission for reproduction of Figure 20	cxliii
Appendix J: Copyright permission for reproduction of Figure 22	cxliv

List of abbreviations

α -syn	Alpha-synuclein
AAV	Adeno-associated virus
ATP	Adenosine triphosphate
β -gal	Beta-galactosidase
β -geo	Beta-galactosidase fused to neomycin
β -syn	Beta-synuclein
BDNF	Brain derived neurotrophic factor
BiFC	Bimolecular fluorescence complementation
BiSyn	Bimolecular fluorescence complementation of alpha-synuclein aggregates
CAG	Compound promoter with CMV enhancer and chicken β -actin promoter
cAMP	Cyclic adenosine monophosphate
CMV	Cytomegalovirus promoter
CNS	Central nervous system
CPu	Caudate-putamen (striatum)
Cre/ERT2	B6.Cg-Ndor1 ^{Tg(UBC-Cre/ERT2)1Ejb} mice
CSF	Cerebral spinal fluid
DA	Dopamine
DJ-1	Deglycase
DMEM	Dulbecco's modification of eagle's medium
DMSO	Dimethyl sulfoxide
DMV	Dorsal motor nucleus of the vagus nerve
DNMT	DNA methyltransferase
ENS	Enteric nervous system
FBS	Fetal bovine serum

γ-syn	Gamma-synuclein
GABA	Gamma-aminobutyric acid
GFP	Green fluorescent protein
GI	Gastrointestinal
GPI	Globus pallidus pars interna
G418	Geneticin selective antibiotic
HCG	Human chorionic gonadotropin
HDAC	Histone deacetylase complex
IF	Immunofluorescence
IRES	Internal ribosome entry site
LAG3	Lymphocyte-activation gene 3
LB	Lewy body
LC3	1A/1B-light chain 3
LRRK2	Leucine-rich repeat kinase 2
MEF	Mouse embryonic fibroblast
MPPP	1-methyl-4-phenyl-4-propionoxypiperidine
MPTP	1-methyl-4-phenyl-1,2,3,6-tetrahydropyridine
Neo	Neomycin
NSAID	Non-steroidal anti-inflammatory drug
OB	Olfactory bulb
OCT	Optimal cutting temperature embedding medium
Pac.4	Homozygosity for A30P and A53T mutant human <i>SNCA</i> transgenes
<i>PARK1</i>	<i>SNCA</i> gene mutations
<i>PARK4</i>	<i>SNCA</i> gene multiplications
PBS	Phosphate buffered saline pH 7.3
PD	Parkinson's disease

PEV	Position effect variegation
PFA	Paraformaldehyde
PINK1	PTEN-induced kinase 1
PMSG	Pregnant mare serum
PrP _c	Cellular prion protein
PrP _{Sc}	Infectious prion protein
rAAV	Recombinant adeno-associated virus
RMS	Rostral migratory stream
ROS	Reactive oxygen species
SAHA	Suberoylanilide hydroxamic acid
SNCA (mice)	Snca ^{Tg(Neo)} .Tg(SNCA) mice
SNpc	Substantia nigra pars compacta
SNr	Substantia nigra pars reticulata
SVZ	Subventricular zone
TH	Tyrosine hydroxylase
UCHL1	Ubiquitin carboxyterminal hydroxylase 1
VIP	Vasoactive intestinal peptide
vg	Viral genomes
X-gal	5-bromo-4-chloro-3-indolyl-beta-D-galactopyranoside
YFP	Yellow fluorescent protein
5-aza-dC	5-Aza-2'-deoxycytidine

List of figures

Figure 1: Nigrostriatal pathway in normal individuals and Parkinson's disease patients.

Figure 2: Simplification of vagal projections between the DMV and ENS.

Figure 3: Organization of the enteric nervous system.

Figure 4: Lewy pathology in myenteric neurons.

Figure 5: BiSyn strategy.

Figure 6: Tamoxifen-inducible activation of Cre recombinase.

Figure 7: Schematic diagram of BiSyn transgene elements.

Figure 8: Pedigree outlining the generation of the BiSyn/Cre/SNCA mouse line

Figure 9: Genotyping BiSyn mouse lines via terminal PCR.

Figure 10: Silencing in zygotic stages is alleviated in a stochastic fashion at the 8-cell stage.

Figure 11: Stochastic nature of β -gal expression in BiSyn/Cre littermates at gestation day e14.5.

Figure 12: BiSyn/Cre reproductive organs stained with X-gal yield mosaic phenotype in ovaries but not testes.

Figure 13: Stochastic mosaicism in PD-critical CNS regions from BiSyn/Cre mice.

Figure 14: Rotenone-treated MEFs display BiSyn fluorescence.

Figure 15: BiSyn expression and aggregation from rostral to caudal CPu regions.

Figure 16: BiSyn expression extends through the entirety of the neuron.

Figure 17: Viral transport occurs in antero- and retrograde directions.

Figure 18: AAV capsid uptake into glia that neighbour BiSyn-containing axon termini in the SNr.

Figure 19: Position effect variegation in the *Drosophila* eye.

Figure 20: Mechanism of rAAV transduction.

Figure 21: The rostral migratory stream.

Figure 22: LAG3 facilitates α -syn fibril transmission and toxicity.

List of tables

Table 1: Murine strain of origin for each transgenic derivative

Table 2: Primers used for genotyping transgenic mice via terminal PCR

Table 3: Antibodies used for immunofluorescence application

1.0 Introduction

1.1 Parkinson's disease

Parkinson's disease (PD) is an incurable neurodegenerative disease characterized by motor deficits. Dopaminergic atrophy in the substantia nigra pars compacta (SNpc) drives the disease-associated motor deficits, thereby limiting synaptic input to the caudate-putamen (CPU) and reducing signal output to the motor cortex.

1.1.1 Prevalence and risk factors

Primarily affecting the elderly population, PD prevalence is on the rise. From 2005 to 2030, there has been a predicted prevalence increase of nearly two-fold^{1,2}, with the number of PD-diagnosed Canadians expected to be greater than 163,000 persons³. The risk of PD development is greater in elderly individuals, males, Caucasians, and people who experience chronic stress; PD incidence is not constrained to particular geographical locations^{2,4–10}. Females and cigarette smokers tend to have reduced PD risk due to the neuroprotective benefits of estrogen^{10–15} and specifically of nicotine on the dopamine system^{2,8,16,17}.

1.1.2 Dopaminergic innervation and denervation

Dopamine (DA) is a catecholamine transmitter molecule derived from dietary amino acids. There are four central nervous system (CNS) pathways where DA plays a crucial role: mesolimbic, mesocortical, tuberoinfundibular, and nigrostriatal. The nigrostriatal pathway is paramount to the coordination of voluntary motor activity and its degeneration results in Parkinsonism.

The SNpc is the major site of dopaminergic atrophy in PD. DA neurons residing in the SNpc project axons through the medial forebrain bundle, located in the lateral hypothalamus,

and onto γ -aminobutyric acid (GABA) neurons in the CPu¹⁸. These regions are topographically connected such that the caudolateral SN has efferents extending into the caudal CPu, while the rostromedial CPu receives afferents from the rostromedial SN¹⁸.

Striatal GABAergic neurons host two types of transmembrane G-protein coupled receptors that bind dopamine: D1 and D2 receptors. While D1 receptors are located exclusively on post-synaptic neurons, D2 receptors have a presynaptic localization. Their actions are also opposing; D1 receptor activation positively regulates cyclic adenosine monophosphate (cAMP) levels while stimulation of D2 receptors inhibits intracellular cAMP accumulation [reviewed in ¹⁹]. Activation of DA receptors in the CPu modulates globus pallidus pars interna (GPi) activity. D1 receptor binding facilitates the direct pathway while binding of D2 receptors activates the indirect pathway. The two pathways generate a net reduction in inhibitory output from the GPi, permitting excitatory thalamic output to the motor cortex (Figure 1) [reviewed in ²⁰].

Nigral dopaminergic neurons have a susceptibility to degeneration that other DA neurons do not possess^{21,22}. Seemingly a faulty system in the concept of PD, the oxidative degradation of cytosolic DA and its metabolites produce reactive oxygen species (ROS) and impair mitochondrial respiration^{23–26}. DA neurons in the SN have a lower capacity for sequestering DA into vesicles leading to an accumulation of cytosolic DA and thus an increase in ROS; this deficit is more pronounced in males^{9,27}. While excess cytosolic DA triggers oxidative stress, leading to cytotoxicity and activation of apoptotic signalling cascades, low DA levels can create a lapse in neuronal signalling. If these low levels are chronically maintained, signalling efficacy is reduced and neuronal atrophy occurs [reviewed in ²⁷]. In Parkinsonism, not only is there accumulated cytosolic DA but moreover, synaptic DA release is reduced due to the degradation of nigral neurons. In combination, the natural antioxidant glutathione has reduced levels in the SN of PD patients and there exists a corresponding deficiency in glutathione reductase activity^{26,28–30}. These nigral deficits collectively alter the firing pattern of GABA neurons in the GPi^{31,32}, which disturbs succeeding thalamo-cortical communication²⁰.

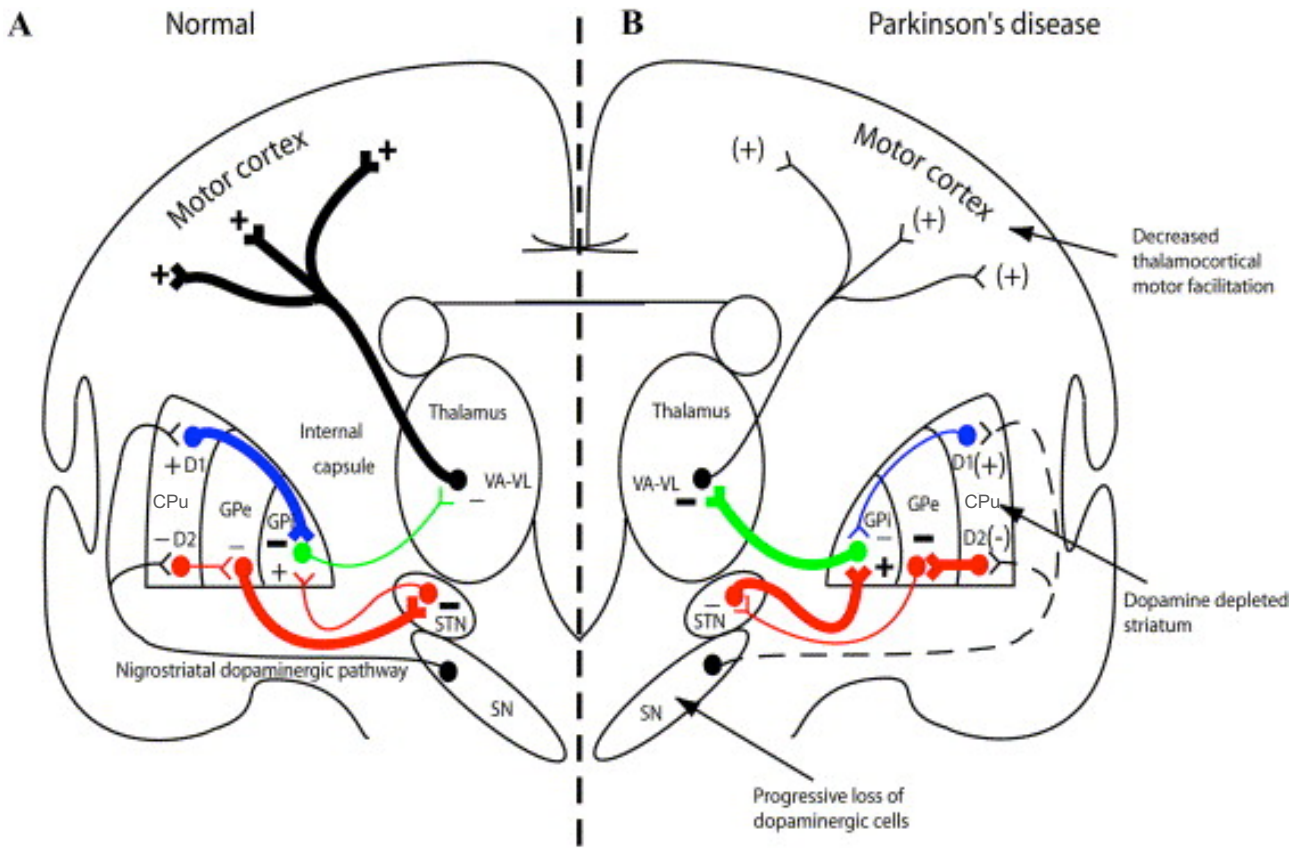


Figure 1: Nigrostriatal pathway in normal individuals and Parkinson's disease patients.

(A) In a healthy brain, DAergic neurons in the SNpc release DA at synapses in the CPU. The DA D1 and D2 receptors function distinctly from one another such that the direct and indirect pathways that ultimately project to the globus pallius pars interna (GPi) cause a net reduction in inhibitory output from the GPi. This facilitates activation in the motor cortex from increased thalamic output.

(B) In PD, loss of DAergic neurons in the SNpc reduces DA release in the CPU, thereby leading to elevated GPi activation, driving an increased inhibitory output in the thalamus. Heightened thalamic inhibition decreases output in the motor cortex, which causes the motor deficits observed in PD.

Adapted from ³³. Permission to reproduce found in Appendix A.

1.2 Pathological hallmarks and aetiologies

Alpha-synuclein (α -syn) is the primary component of Lewy bodies (LBs), the pathological hallmark of Parkinson's disease. Notorious for misfolding and self-aggregating, α -syn loses its functional capacity and renders neurons susceptible to degeneration. Several genetic causes of PD have been identified, some of which involve α -syn mutations. The majority of PD cases, however, arise sporadically, underlining the importance of environmental factors.

1.2.1 Synucleins

The synucleins are a family of proteins termed by Maroteaux and colleagues at Stanford University in 1988 for their localization in the presynaptic nerve terminal and along the nuclear membrane³⁴. Their nuclear localization, however, was later shown to be the result of antibody cross-reactivity³⁵. There are three synuclein isoforms: alpha, beta, and gamma (α -syn, β -syn and γ -syn, respectively). The synucleins adopt an amphipathic α -helical motif upon interaction, which facilitates binding to lipid vesicles and membranes^{36,37}.

α -syn is a critical protein in PD pathogenesis. It has a 140 amino acid sequence encoded by the *SNCA* gene located on chromosome 4q21^{38,39}. It was originally purified from amyloid plaques in human Alzheimer's disease brains, and was accordingly known as the precursor to the non-amyloid β component⁴⁰. α -syn is involved in synaptic vesicle transport and docking at the plasma membrane by working closely with cysteine-string protein- α to chaperone the folded state of the SNARE protein synaptobrevin-2⁴¹⁻⁴⁴. It also has an important role in recycling DA at the synaptic cleft by regulating dopamine transporter activity, which pumps DA back into the cytosol^{45,46}. The proper function of α -syn therefore modulates the synaptic release and reuptake of DA in the CPU. α -syn also binds vesicular monoamine transporter-2, elucidating its role in sequestering cytosolic DA into vesicles⁴⁷. Moreover, α -syn has been shown to reduce

activity of tyrosine hydroxylase (TH), the rate limiting enzyme in DA synthesis, thereby offering a regulatory mechanism in DA biosynthesis^{48–50}.

β -syn is a 134 amino acid protein encoded by the *SNCB* gene located on chromosome 5q35^{38,39}. It was originally deemed the bovine phosphoneuroprotein-14-kDa^{51,52}, which was later recognized to be the equivalent of β -syn in humans³⁸. α - and β -syn have similar molecular weights and show 61% sequence resemblance; they are both localized to presynaptic nerve terminals³⁹. Despite their similarities, only α -syn is found in LBs⁵³. In fact, β -syn actually prevents the fibrillation of α -syn⁵⁴.

Although the γ isoform is the original synuclein that was isolated from the electric ray (genus *Torpedo*) at Stanford in 1988^{34,37} and again in the rat dorsal-root ganglion in 1995^{37,55}, it was actually identified much later and separately from the other two. γ -syn is a 127 amino acid protein encoded by the *SNCG* gene. In the late 1990's this synuclein isoform was well known for its role as the human breast cancer-specific gene, wherein overexpression was correlated with breast cancer malignancy⁵⁶. In 1998, Clayton and George aligned several cDNA sequences, demonstrating that the breast cancer-specific gene and *SNCG* are homologous, both encoding the protein that was thereafter called γ -syn³⁷.

1.2.2 Lewy pathology

α -syn was first linked to PD in 1997 when a familial autosomal dominant point mutation was detected in four distinct Italian and Greek kindreds with PD⁵⁷. The point mutation at site 209 in the *SNCA* gene leads to a subsequent A53T mutant α -syn protein, which has a truncated α -helix and extended β -sheet, facilitating the protein's self-aggregation propensity⁵⁷ (discussed further in section 1.3.1). In 1998, a German group identified a distinct point mutation in the *SNCA* gene with a resultant A30P mutant α -syn protein, which also yields a PD phenotype⁵⁸.

These genetic discoveries prompted others to assess the role of α -syn in Parkinsonism. Soon after, insoluble α -syn was found to be the primary component of LBs^{53,59}. First identified in 1912 by Friedrich Lewy, LBs were described as proteinaceous spherical cytoplasmic inclusions within the dorsal motor nucleus of the vagus nerve (DMV), among other nuclei, in post-mortem PD brains⁶⁰. Gonzalo Rodriguez Lafora confirmed Lewy's findings in his 1913 publication, calling such inclusions *cuerpos intracelulares de Lewy*⁶¹. Konstantin Trétiakoff uncovered analogous inclusions in the SNpc and similarly designated them LBs in his 1919 doctoral thesis⁶².

More than α -syn alone resides in these tangles of proteinaceous particles. In fact, it was ubiquitin that was first identified as a LB component in 1988⁶³. While ubiquitin localizes to the periphery⁶³, α -syn comprises the core. When considering the importance of ubiquitin in the adenosine triphosphate (ATP) dependent proteolytic pathway, the aggregated α -syn likely becomes ubiquitinated to flag it as a target for protein degradation. Other proteins can exist in LBs (e.g., microtubule-associated proteins), however, only α -syn and ubiquitin are consistent components⁶³.

Misfolding of α -syn is fundamental in PD pathogenesis. Proteins have the tendency to transition from a high-energy unfolded state to a minimal energy native state⁶⁴. While misfolded proteins have a higher energy state than natively folded proteins, they maintain the tendency to develop a minimized energy state. Curiously, in the case of the high-energy partially folded α -syn protein, the minimal energy state is in the form of amyloid fibrils⁶⁵. Seemingly, fibrillation acts as a protective mechanism.

1.2.3 SNCA mutations

Mutations to the *SNCA* gene are collectively referred to as *PARK1* mutations, while multiplications of the whole gene are deemed *PARK4* mutations. *SNCA* triplication has an

autosomal dominant inheritance pattern and yields a pathological phenotype that differs from classic Parkinson's disease^{66,67}. This variation causes doubling of wildtype α -syn expression⁶⁶, which yields an early-onset, rapid-progressive form of PD with signs of dementia and autonomic dysfunction⁶⁷. *SNCA* duplication also leads to a PD phenotype, however this form has a wide variation in progression rate and age of onset⁶⁸; signs of dementia are uncommon and presentation of autonomic dysfunction is mild in the presence of *SNCA* duplication⁶⁸⁻⁷⁰.

1.2.4 Parkinson's disease as a mitochondriopathy

Although important for synaptic function and despite the association between misfolded α -syn and neuronal atrophy, α -syn itself is not essential for organism survival. *Snca* null mice are not only viable, but also have a similar lifespan to wildtype mice⁷¹. They do however have over a 20% reduction in total cardiolipin mass compared to wildtypes⁷². Cardiolipin is a mitochondrial-specific phospholipid. In response to mitochondrial damage, cardiolipin is translocated from the inner to the outer mitochondrial membrane where it binds 1A/1B-light chain 3 (LC3) to induce mitophagy. α -syn is actually a regulator of LC3-induced mitophagy by competing for the same binding site on cardiolipin⁷³.

When α -syn binds membranes, it forms an amphipathic α -helix, which impedes fibril formation⁷⁴. Therefore, when lipid levels are high, α -syn has an extensive α -helical conformation and fibrillation does not occur⁷⁴. When lipid levels are low however, α -syn remains in its partially folded intermediate conformation, which has a higher propensity to self-dimerize, thereby accelerating insoluble fibril formation⁷⁴⁻⁷⁸. Self-dimerization occurs in an antiparallel fashion such that the N-terminal domain of one α -syn monomer aggregates with the C-terminal domain of another^{75,76}. This offset ratio of lipid to protein occurs when high levels of α -syn exist within vesicles. Resultant fibrillation can disrupt the vesicular membrane and cause leakage of

aggregated α -syn, which can seed the formation of further aggregates (see section 1.3.1 for further details)⁷⁴.

Cardiolipin plays a key role in mitigating synucleinopathy. From the outer mitochondrial membrane, cardiolipin binds monomeric α -syn, pulls it out of pathogenic fibrils, and promotes its refolding⁷³. However, mutated α -syn has a lower affinity for the cardiolipin binding site and is less capable of refolding, thereby reducing its capacity for managing LC3-induced mitophagy⁷³.

Despite its central role in the disease process, α -syn is not the only player in PD. The most common genetic form of early-onset PD stems from autosomal recessive *Parkin* mutations⁷⁹. This is a slow-progressing form of the disease, clinically similar to idiopathic PD⁷⁹. *Parkin*, *PTEN-induced kinase 1 (PINK1)*, and *deglycase (DJ-1)* gene mutations confer mitochondrial dysregulation⁸⁰. For example, while monomeric DJ-1 drives mitophagy in the presence of oxidative stress, thereby helping cells maintain mitochondrial homeostasis, mutant DJ-1 is unable to homodimerize in a stable environment^{81,82}. This autosomal recessive mutation therefore leads to a cascade of mitophagy and fosters subsequent neuronal atrophy⁸².

1.2.5 Environmental contributors

Given that familial cases encompass only 10-20% of all diseased individuals⁸³, environmental contributors are paramount to the disease process. Relevant in recent years, exposure to pesticides has increased the incidence of sporadic PD cases. In 1998, a rural agricultural region in France applied insecticides to crops via air-assisted spraying. This application method releases excess toxins into the surrounding environment, including water supplies, and therefore utilizes greater volumes in the application process due to environmental leaching. Despite occupying only 1% of total agricultural area in France, this region consumed 21% of the country's insecticides. Inhabitants had a 20% higher PD prevalence than any other French region⁸. Similarly, a study from 1987 revealed that the "Garden of Quebec" (i.e., a rural

region with the largest amount of agricultural production in the province) had the highest PD prevalence compared to any other rural region in Quebec. In 1982, this region consumed 59% of the provincial total for organophosphates and carbamates⁸⁴. Research focussed on pesticides has demonstrated their potential to trigger PD pathology. Due to the increase in scientific data, some of these pesticides have been banned from commercial use (e.g., the carbamate insecticide rotenone was banned in 2016) and are currently used in laboratory settings to expand the field's understanding of PD.

The aforementioned insecticide rotenone is a mitochondrial complex I inhibitor. Intranigral rotenone injection in rodents leads to accumulation of ROS and reduced ATP synthesis, which encourage accumulation of intracellular α -syn, promote its misfolding, and prevent its degradation^{75,76,85}. When rotenone is administered peripherally in rodents, which more closely resembles authentic human exposure, not only does it lead to uniform nigrostriatal lesions but it renders enteric neurons susceptible to neurodegeneration, leading to increased gastrointestinal (GI) transit time and weight loss, both of which are early non-motor features of Parkinson's disease^{86,87}.

Further support for environmental origins of PD dates back to 1982 when an illicit synthetic heroin caused an outbreak of PD cases in California. In attempt to produce the meperidine analog 1-methyl-4-phenyl-4-propionoxypiperidine (MPPP), the toxic 1-methyl-4-phenyl-1,2,3,6-tetrahydropyridine (MPTP) was a resultant by-product found in the injected substance of 7 case reports. MPTP selectively kills SNpc dopaminergic neurons, causing chronic deficiencies in striatal DA, thereby leading to Parkinsonism^{88,89}. Videos of 5 original Californian cases were recently reviewed with reference to current knowledge of PD. Notably, akinesia was a prominent motor feature in all cases. While some of these patients presented with a tremor-dominant subtype known to be a milder, slower progressing form of PD, the others showed signs of the more severe form featuring bradykinesia, akinesia, and muscular rigidity⁹⁰.

An intriguing novel hypothesis of aberrant α -syn from dietary sources was described by Killinger and Labrie in 2017⁹¹. Since all α -syn from dietary meat (e.g., cow, chicken, pig) contains the A53T variant⁹², they suggest that α -syn from vertebrate food products can seed α -syn aggregation⁹¹. This proposed exogenous source of α -syn seeding relies on the prion-like properties of α -syn and a GI breaching mechanism.

1.3 Prion diseases

Accurate prion composition was first hypothesized by Stanley Prusiner in 1982, proposing that prions are infectious proteinaceous particles lacking nucleic acid⁹³. Post-translational modifications to the innate cellular prion protein (PrP_c) modify its conformation from a highly α -helical structure to a favourable β -sheet conformer, which facilitates infectious activity^{94,95}. These infectious prion proteins (PrP_{Sc}), first identified in the prion disease scrapie, are capable of converting innate PrP_c into infectious PrP_{Sc}, which have the propensity to self-oligomerize⁹⁶. PrP_{Sc} transmission leads to fatal diseases including scrapie, kuru, and Creutzfeldt-Jakob disease. Thirty years after the publication of his initial prion hypothesis, Prusiner extrapolated the role of prions to neurodegenerative diseases with insight into both the sporadic and inherited transformations^{83,97}.

1.3.1 α -syn as a prion

Similar to the conversion of PrP_c to PrP_{Sc}, misfolded α -syn acquires an extended β -sheet portion and reduced α -helical structure, facilitating its self-aggregation tendency⁵⁷. This conformational change predisposes the prion-like properties of α -syn in the sense that misfolded α -syn is capable of propagating from cell-to-cell and acts as a template for promoting misfolding and aggregation. In accordance, synthetic and preformed α -syn fibril injections into rodent CPU induce LB inclusion formation and subsequent degeneration in both the CPU and SNpc,

amounting to motor deficits^{98,99}. Further, A53T and A30P α -syn mutants have an increased capacity to self-dimerize compared to wildtype α -syn. The altered protein conformations accelerate a β -sheet conformational shift, thus promoting oligomer and aggregate formation⁷⁸. Similar to prion disease, PD can be inherited in 10-20% of cases or can arise sporadically⁸³.

1.3.2 Braak hypothesis

In 2003, Heiko Braak and colleagues developed a staging hypothesis for idiopathic Parkinson's disease based on Lewy pathology in brains at autopsy¹⁰⁰. The group appreciated the presence of the GI and olfactory symptomology and pathology throughout the disease process, especially in the prodromal and preclinical phases¹⁰¹. They recognized that the first regions in the CNS to show α -syn inclusions are the DMV, olfactory bulb, and anterior olfactory nucleus^{100,102}. These regions are connected to the enteric nervous system (ENS) and nasal cavity, and are therefore at the forefront of environmental exposures, laying ground for the group's "dual-hit hypothesis"^{103,104}. Their claim that little inter-individual variation in their suggested caudorostral pathological spread, their postulated anterograde propagation through olfactory regions, and the hypothesized staging based largely on Lewy pathology rather than neurodegeneration are heavily criticized in the literature [for example ¹⁰⁵⁻¹⁰⁷, reviewed in ^{108,109}]. The group has recently addressed the latter caveat, highlighting the apparent neuroprotective role of LBs and the regional vulnerabilities that may attribute to their presence¹¹⁰. Detailed review of this hypothesis is currently beyond the scope of this project; nonetheless the proposed process merits explanation.

An unknown neurotropic pathogen, likely a virus, was suggested to possess prion-like properties, enabling it to propagate from neuron to neuron^{102,103}. It is suggested that pathogens enter the nasal cavity, some being swallowed with nasal secretions in saliva^{103,104}. Despite a lack in evidence for this proposition, the intestinal epithelium is disrupted in biopsies from

Parkinson's patients. Occludin, a tight junction protein, is significantly downregulated in the colon¹¹¹. There is also an association between gut inflammation and PD, similar to that observed in irritable bowel disease, which parallels enteric glial dysregulation¹¹². Further, chronic stress, a PD risk factor, exacerbates intestinal permeability to neurotoxins by reducing the presence of tight junction proteins⁸⁷. If pathogens are able to penetrate the single layer of epithelial cells that line the GI tract, they could surely enter unmyelinated axons from the submucosal plexus that reside just microns from the lumen¹⁰⁴. While axonal and transneuronal transport are important means of intra- and interneuronal communication upon which neurons depend for survival, infectious diseases are postulated to also manipulate these routes to spread their pathogenicity¹¹³. By this framework, pathogens would be able to travel from the ENS to CNS. Each neuron along this route would therefore acquire the neurotropic agent and pass it onto the next neuron in its connective pathway, seemingly using the vagus nerve as a propagation highway (Figure 2). Supporting the role of the vagus nerve in PD pathogenesis, two large cohort studies, one using data from nationwide Danish registers and the other Swedish, demonstrated that full truncal vagotomy is associated with reduced PD risk^{114,115}. As mentioned previously, misfolded α -syn has prion-like qualities, which could very well make the misfolded protein itself the propagating agent described by Braak and colleagues. This hypothesis relies on retrograde propagation of α -syn aggregates through the ENS, resulting in a domino effect in connective structures, first receiving α -syn pathology followed by subsequent atrophy¹⁰².

Interestingly, Francisco Pan-Montojo and colleagues have produced a model that almost perfectly replicates the proposed Braak hypothesis^{116,117}. By chronically administering rotenone via oral gavage, they were able to track the spread of α -syn aggregates through the ENS, vagus nerve, and CNS in mice. Despite a lack of rotenone and thus mitochondrial complex I inhibition either systemically or in the CNS, both inflammation and α -syn phosphorylation were observed in enteric and DMV neurons after 1.5 months of treatment¹¹⁶. α -syn aggregate propagation

central nervous system

enteric nervous system

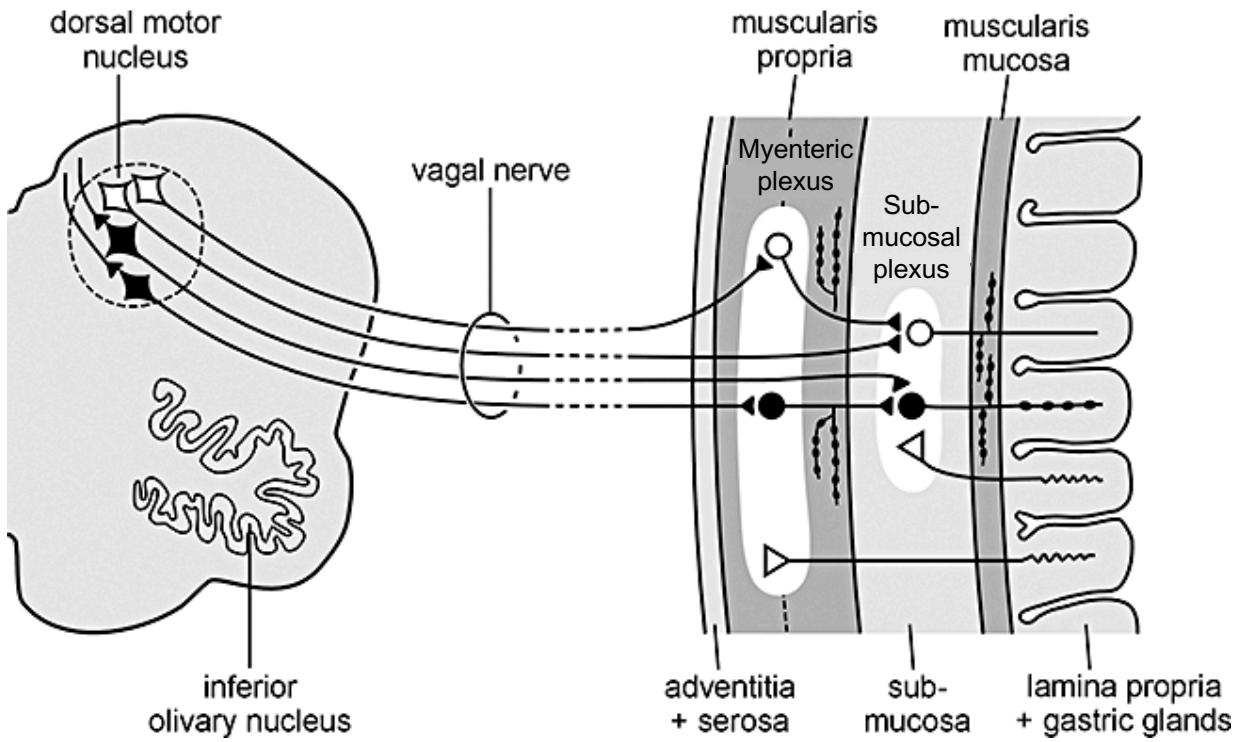


Figure 2: Simplification of vagal projections between the DMV and ENS.

A hypothesized neurotropic pathogen enters the submucosal plexus at VIPergic axon termini (black circular cell somas) after crossing the epithelial lining of the mucosa. Manipulating retrograde axonal and transneuronal transport mechanisms, the pathogen would be able to reach the preganglionic cholinergic neurons (black diamond cell somas) in the DMV.

Adapted from ¹⁰³. Permission to reproduce found in Appendix C.

occurred only in connected neuronal pathways and the spread was time-dependent¹¹⁶. After 3 months of treatment, mice showed significant motor impairments corresponding to SNpc dopaminergic degeneration¹¹⁶. In a subsequent study, they performed partial or truncal vagotomy in mice prior to rotenone treatments¹¹⁷. While partial vagotomy slowed the propagation of α -syn aggregates to the DMV, it did not preclude SNpc degeneration altogether¹¹⁷. However, truncal vagotomy was capable of preventing nigral degeneration in the ipsilateral hemisphere, again confirming the importance of the vagus nerve for aggregate propagation¹¹⁷. Moreover, the group demonstrated that α -syn is released from enteric neurons and absorbed by presynaptic fibers of sympathetic neurons¹¹⁷. From there, protein inclusions are transported in a retrograde fashion to the soma where they accumulate¹¹⁷.

1.4 Enteric nervous system

The ENS is the largest of three divisions of the autonomic nervous system¹¹⁸. Over 200 million enteric neurons are intrinsically arranged into thousands of compact ganglia that frame the ENS¹¹⁹. Enteric ganglia are arranged into reflex circuits, which, dating back to 1899, were shown to foster peristalsis independently of the CNS^{120,121}. These enteric ganglia provide full enteric control over fluid flux through the mucosa, muscle activity and regional blood flow [reviewed in ^{119,122}].

The vagus nerve originates in the DMV and embodies substantial arborization through the upper GI tract and digestive organs, extending 40,000 to 50,000 axons^{122,123}. Despite most vagal axons sharing synapses with enteric ganglia, very few enteric neurons actually respond to vagal stimulation, emphasizing the substantial independence of the ENS^{122,124,125}.

Arranged into several neuronal plexuses, the ENS innervates the many layers of muscle fibers and connective tissues comprising the GI tract. The two major distinctions include the myenteric and submucosal plexuses (Figure 3), which form a communication network¹²⁶.

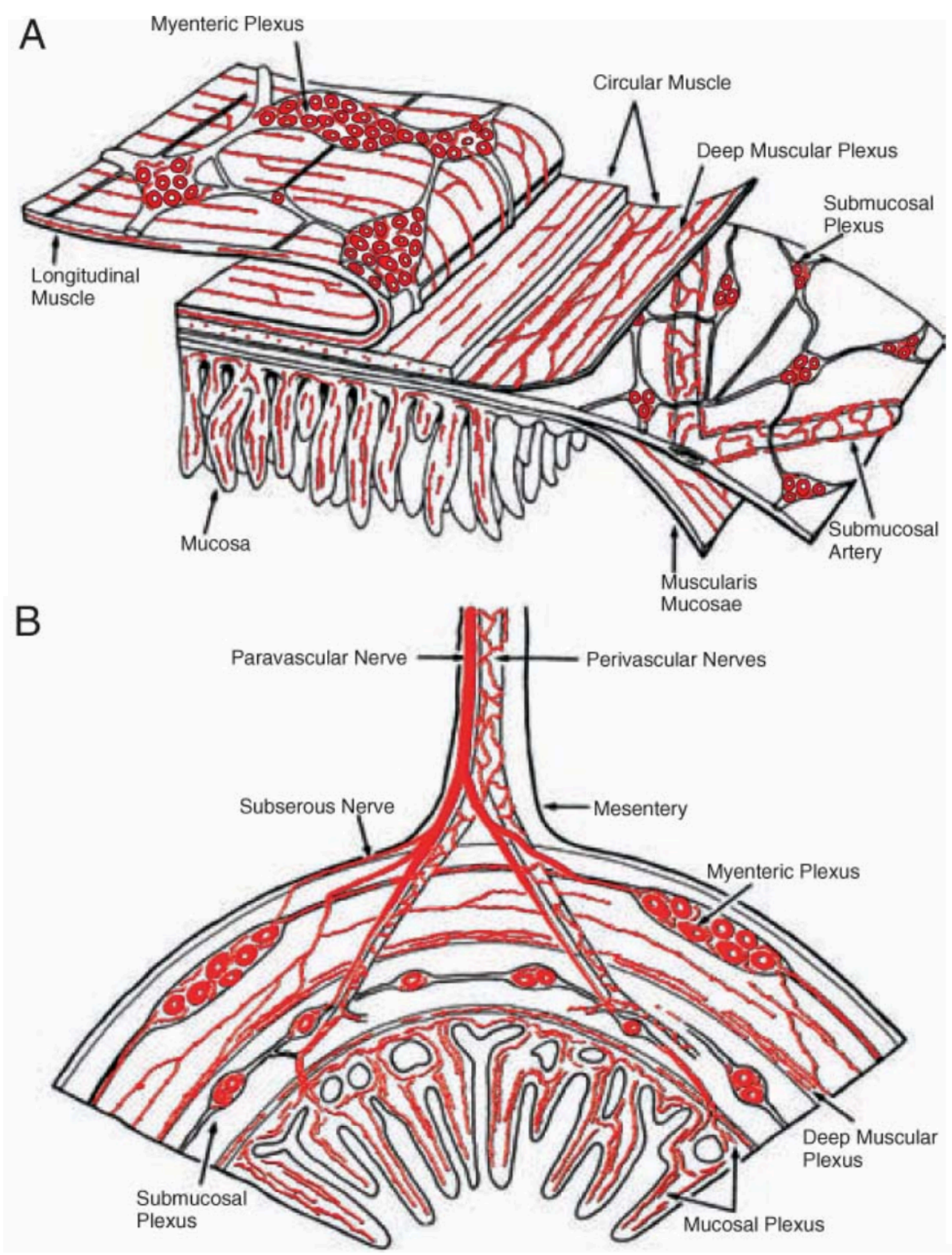


Figure 3: Organization of the enteric nervous system.

(A) Wholemout depiction highlights the layering of distinct muscle fibers and connective tissue with intricate design incorporating enteric plexuses into each distinct layer between the innermost luminal surface and the outermost mesentery.

(B) Transverse view shows the ganglia in the major submucosal and myenteric plexuses. The submucosal plexus, located in the submucosa, lies in close proximity to the luminal space and some of its axons can extend within microns. Submucosal neurons communicate extensively with the myenteric plexus, which lies between the circular and longitudinal muscle layers of the muscularis. The enteric neuronal plexuses are depicted in red.

From ¹¹⁹. Permission to reproduce found in Appendix D.

1.4.1 Enteric implications in Parkinson's disease

Despite CNS disturbance being the driver of classic PD motor deficits, emerging evidence suggests that the origin of the disease process lies outside the CNS itself. An abundance of non-motor symptomology is associated with PD, many of which involve the GI tract. Constipation is the most common autonomic feature with at least a 2-fold higher incidence in PD patients than controls¹²⁷. In fact, the Honolulu-Asia Aging Study, a longitudinal study including over 8000 individuals, showed that there is a significant negative correlation between PD incidence and number of bowel movements per day¹²⁸. Studies have shown that constipation can arise more than 20 years prior to development of typical motor features, with the shortest estimated precedence being 6 years^{127,129–131}.

Not only are GI symptoms evident, but GI pathology has also been correlated with the observed deficits. Nearly half of submucosal neurons secrete vasoactive intestinal peptide (VIP)¹³². VIP is a secretomotor neurotransmitter that stimulates smooth muscle relaxation via secretion of cAMP and chloride ions in mucosal enterocytes^{133,134}. Heightened VIP concentrations are therefore associated with diarrhea¹³⁴. The contrary is observed in PD patients and this finding is associated with VIP neuronal susceptibility to LB accumulations (Figure 4A-C), which lead to motor neuron disinhibition in GI distal smooth muscles^{101,135,136}. Pathology thereby impairs smooth muscle reflex relaxation and brands constipation a prominent feature in PD patients.

In 1995, Singaram and colleagues collected colon samples from 11 advanced PD patients and 22 control subjects who underwent colonoscopy for other reasons. 9 of the 11 PD patients showed a significant loss of DA neurons in the myenteric plexus compared to the control subjects¹³⁷. A separate study confirmed the presence of Lewy pathology in myenteric DA neurons (Figure 4D)¹³⁶. Substantial enteric dopaminergic atrophy has also been demonstrated in an MPTP model, however these mice displayed colonic hypermotility¹³⁸. In fact, DA has been

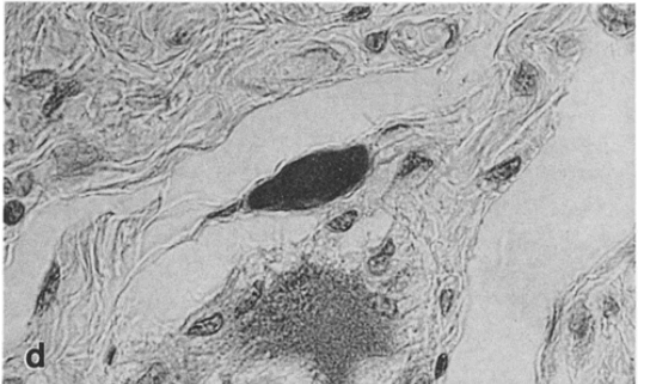
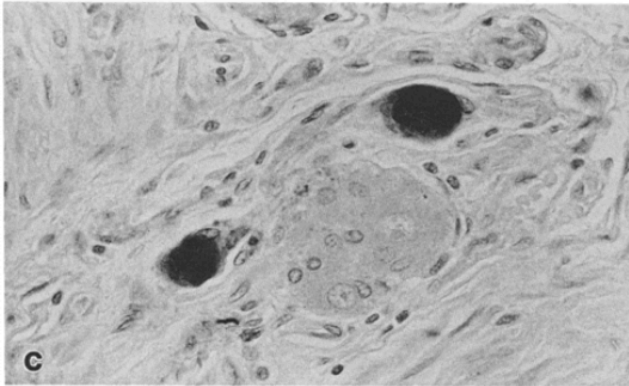
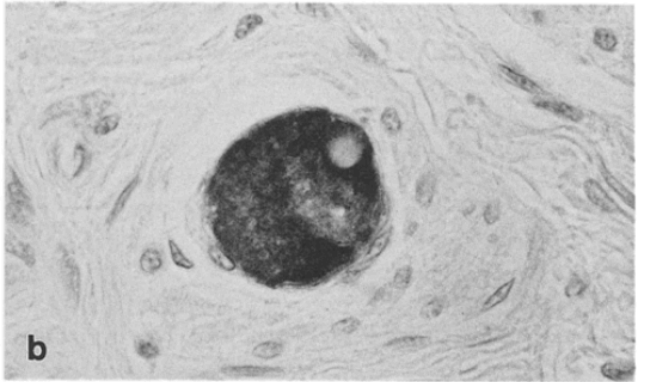
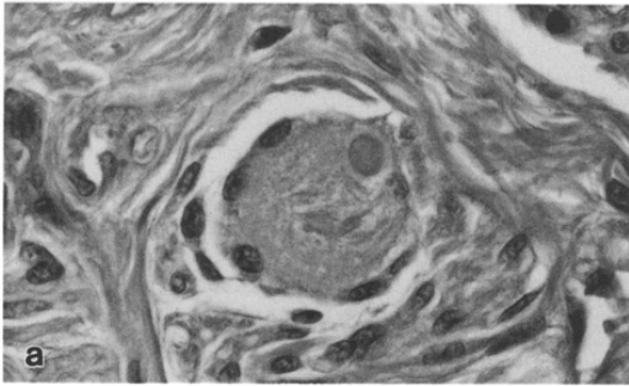


Figure 4: Lewy pathology in myenteric neurons.

(a) Pronounced LB in the cytoplasm of a myenteric neuron in the esophagus of a PD patient. Section is stained with hematoxylin and eosin.

(b-c) LBs in VIP-immunoreactive somas in sections adjacent to that in (a).

(d) LB in a TH-immunoreactive myenteric neuron in the esophagus of a PD patient.

From ¹³⁶. Permission to reproduce found in Appendix F.

shown to inhibit gastric motility, and this altered behavioural response is dependent on DA binding at presynaptic D2 receptors on cholinergic neurons in the myenteric plexus¹³⁹. Together these data create uncertainty surrounding the clinical relevance of enteric DA neuronal pathology and subsequent degeneration, especially with constipation being such a prominent feature in PD patients.

1.4.2 Evolution and function of the appendix

Charles Darwin hypothesized that the evolution of the hominoid appendix was stimulated by the mammalian shift from a leaf-based to fruit-based diet, which corresponded to a reduction in caecum size. This reduction is partly related to the amount of plant matter that a species consumes, with obligate herbivores having the largest caeca due to its critical function in breaking down cellulose by secreting the enzyme cellulase^{140,141}. Rather than diet alone however, it is now evident that multiple environmental factors have led to the convergent evolution of the appendix in a number of species¹⁴².

For centuries, scientists have postulated the appendix to be a vestigial organ. It has even been argued to be an exaptive structure with poor design. This assertion is largely supported by the rare occurrence of ulcerative colitis in patients who had undergone appendectomy previous¹⁴³. Further supporting the structure's poor design is the common condition appendicitis, which involves the occlusion of the appendiceal lumen often as the result of lymphoid hyperplasia in response to bacterial or viral insult¹⁴⁴. In 2007, six percent of industrialized nation residents experienced inflammation of the appendix¹⁴⁵. The presence of GI diseases highlight the tendency of the appendiceal lymphatic tissue to acquire chronic pathological inflammation¹⁴⁰.

Prior to civilization, the vermiform appendix likely had an evolutionary advantage. There remain regions of the world where amenities like clean drinking water and access to cooked food are not readily available, and consequently diarrheal illness is common¹⁴⁶. An endogenous

recovery mechanism following diarrheal illness would therefore be advantageous¹⁴⁶. In fact, the appendix is highly associated with lymphatic tissue and houses bountiful beneficial bacteria. After diarrheal insult, the gut is in a state of dysbiosis, and the colonic microbiome can be replenished with the bacteria stored in the vermiform appendix^{142,145}. Perhaps unsurprisingly then, appendectomy is a risk factor for GI disorders like irritable bowel syndrome^{147,148}.

Further, appendicitis is rare in developing nations. While this may, in part, be contributed to dietary distinctions like reduced fiber intake in industrialized countries^{149,150}, epidemiological data instead suggests that excessive hygienic practices are the culprit of appendectomy¹⁵¹. The industrialized lifestyle lacks immune stimulation, rendering it hyperactive, and causing a wide range of immune-related diseases (e.g., asthma, allergies, etc.)¹⁴⁵. Laboratory rabbits are the only animal, aside from humans, that live in an excessively hygienic environment and possess an appendix¹⁴⁶. It is likely that from studying these animals, we decided the appendix to have little functional importance for so many years. However, rabbits appendectomized at birth show reduced lymphatic development at two months of age and have reduced titers of circulating lymphocytes, highlighting the functional importance of the appendix in antibody production¹⁵².

1.4.3 Immune contribution to Parkinson's disease

Due to its association with the inflammatory disorders leprosy¹⁵³ and Crohn's disease^{153,154} and its enhanced expression in immune cells including macrophages¹⁵⁵, *leucine-rich repeat kinase 2 (LRRK2)* mutations may indicate immunological malfunction in PD. The LRRK2 G2019S mutation is the most common cause of genetic PD, and may account for as high as 40% of cases in certain populations¹⁵⁶. It has an autosomal dominant inheritance pattern, and can arise sporadically in 2% of cases, with a pleomorphic phenotype^{157–159}. Michael Schlossmacher's research group at the University of Ottawa has recently demonstrated that LRRK2 modulates inflammation following pathogenic insult. Although mice lack an appendix and the mouse cecum was not assessed, immune cells infiltrated the spleen (i.e., another

lymphatic organ) more robustly in LRRK2 G2019S mutant mice challenged with bacterial infection compared to wildtypes¹⁶⁰. This benefit was mediated by an augmented relationship between LRRK2 and the actin-regulatory network in myeloid cells, thereby enhancing their chemotactic response, which was also recognized in a previous study^{160,161}. Despite this apparent gain-of-function effect in response to bacterial insult, the mutant mice generated more ROS than wildtypes in both the periphery and CNS and showed higher concentrations of α -syn when challenged with a virus¹⁶⁰. This finding provides further evidence for the potential of a viral neurotropic pathogen having the capacity to initiate PD development and indicates an immunological contribution.

Since LRRK2 has an elevated concentration in macrophages, enteric-immune interactions are additionally supported in PD. Muscularis macrophages are strategically located within myenteric ganglia and are found adjacent to enteric neuronal fibers in the muscularis externa^{162–164}, where they maintain enteric homeostasis by harmonizing neuronal apoptosis and neurogenesis¹⁶⁵. The remarkable ability of the ENS to regenerate likely provides protection from environmental insult. However, the interaction between muscularis macrophages and the ENS is hypothesized to foster pathogenesis in various diseases, supported by enteric functional alterations in response to macrophage-mediated inflammation of the mucosa [reviewed in ¹⁶⁶].

Further, the vagus nerve densely innervates the mammalian caecum^{125,167,168}, making the appendiceal ENS an intriguing site for PD pathogenesis. Our lab has previously shown that the vermiform appendiceal mucosa in patients without underlying synucleinopathy contains an abundance of α -syn inclusions within nerve bundles¹⁶⁹. Since the number of α -syn inclusions is far greater in the appendiceal mucosa than other regions of the GI tract, we postulate that blood-borne pathogens have potential to trigger initial α -syn oligomerization due to the lack of barrier between the blood and ENS. In addition, the regional blood supply is both easily accessible and controlled by neurons residing in the appendiceal mucosa, making it an attractive location for pathogenesis^{119,122,169}.

A recent study based on nationwide Swedish register data suggests that appendectomy can reduce PD risk by nearly 20%, furthering support for an appendiceal role in PD pathogenesis¹⁷⁰. Appendectomy at least 20 years prior to PD diagnosis prolonged the age at diagnosis by 1.6 years¹⁷⁰. Moreover, rural inhabitants had over 25% reduced PD risk after appendectomy, while urban residents did not show any benefit¹⁷⁰. This not only highlights the appendix as a critical structure in PD development, but also points to an interaction between the appendix and environmental factors, in particular pesticides, which have far greater exposure in rural regions.

Interestingly, gut dysbiosis is a prominent feature in PD patients^{171–173}. These microbiota irregularities modify short chain fatty acid concentrations, which may, in part, underlie some of the autonomic symptoms experienced in Parkinsonism¹⁷³. In 2016, Sampson and colleagues demonstrated that human PD-derived gut bacterial implantation in mice fostered subsequent motor impairment, which was not observed in that from healthy human controls¹⁷⁴. In fact, a case study from 2011 revealed that faecal transplant in a PD patient reduced impairments associated with PD symptomology¹⁷⁵. Researchers have since shown the impressive relationship not only between the brain and gut, but also the microbiome. Since the appendix is thought to play an important role in maintaining flora homeostasis, gut dysbiosis broadens the potential for pathogenesis in the appendix.

1.5 BiSyn

Given that the self-dimerization of α -syn is important for the α -helix to β -sheet conformational shift and acceleration of neurotoxic aggregate formation⁷⁸, we have developed a novel system that enables visualization of dimerized α -syn for the purpose of assessing the earliest initiation and propagation mechanisms in the PD process. Our system utilizes bimolecular fluorescence complementation to enable visual identification of α -syn dimers,

henceforth called the *BiSyn* system. *BiSyn* appreciates the antiparallel nature of α -syn aggregation.

Our system was designed to address major gaps in the literature regarding the most premature steps of α -syn aggregation and propagation. While many groups have set out to track the pattern of aggregate spread and molecular mechanisms of disease in the SNpc itself, the innovative technology to enable visualization of the first aggregates and the ability to observe how they spread was not previously available.

1.5.1 Bimolecular fluorescence complementation

Our *BiSyn* strategy depends on bimolecular fluorescence complementation (BiFC) to enable visualization of α -syn dimers (Figure 5). The concept of BiFC was first described in 2000 when Ghosh and colleagues at Yale University demonstrated that green fluorescent protein (GFP) can be split into non-fluorescent fragments with the capacity to reconstitute into the native conformation via antiparallel leucine zippers¹⁷⁶. Two years later, Hu and colleagues named the strategy after using the same leucine zipper technique to reconstitute non-fluorescent yellow fluorescent protein (YFP) fragments that were fused to cellular proteins, permitting for the first time direct visualization of protein interactions¹⁷⁷.

Researchers have been using fluorescent proteins to visualize α -syn for nearly two decades in attempt to illuminate the events that precede aggregation. McLean and colleagues fused α -syn to GFP in 2001, demonstrating that the protein's subcellular distribution and aggregation pattern changes with respect to different α -syn mutations¹⁷⁸. These researchers appreciated the lack of direct methodology for visualizing α -syn and pursued approaches to fill this gap. In 2006, the group used fluorescence lifetime imaging to directly demonstrate the antiparallel oligomerization of intracellular α -syn for the first time⁷⁵. It was in 2008 when the group first adopted the BiFC approach to study the interaction between α -syn and the molecular

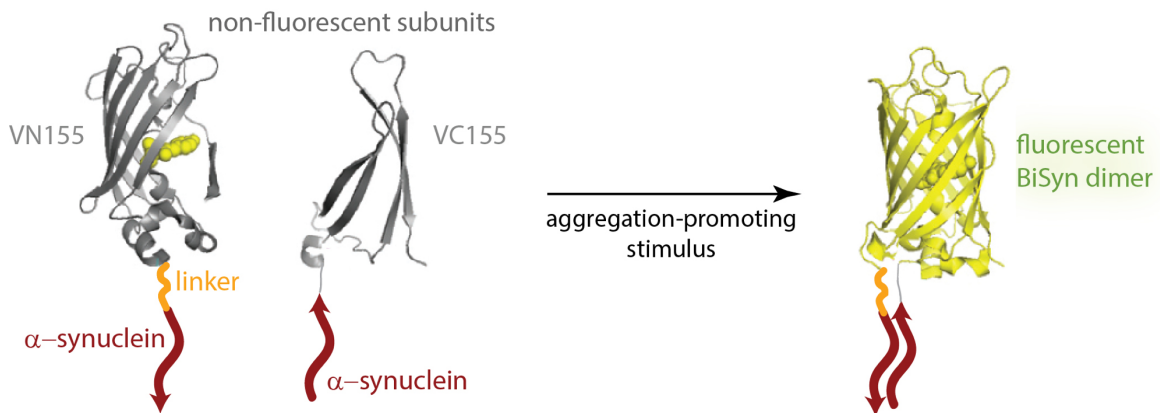


Figure 5: BiSyn strategy.

Non-fluorescent Venus-YFP fragments are fused to α -syn monomers, such that their antiparallel aggregation brings the Venus-YFP fragments within sufficient proximity that they can reconstitute into their native 3-dimensional configuration, thus placing an endogenous fluorescent probe on α -syn dimers.

chaperone protein Hsp70⁷⁶. In 2013, the group used this novel tool in rats, demonstrating its ability to enable direct visual identification of α -syn oligomers¹⁷⁹. Two years ago, McLean and her former MassGeneral Institute colleagues demonstrated for the first time the pathology and behavioural characteristics associated with BiFC of α -syn in mice⁷⁷. Herein, mice were injected intranigrally with the two distinct fragments of Venus-YFP- α -syn genetic sequences (i.e., one with α -syn fused to Venus-YFP at the C-terminus, and the other at the N-terminus) engineered into an adeno-associated virus. After 4 weeks, fluorescence associated with α -syn aggregation was observed in cell bodies and projections in the SN as well as fibers in the CPu, providing further evidence for the anterograde spread of α -syn oligomers through the nigrostriatal pathway⁷⁷. Our group adopted a similar BiFC strategy in 2014, using a single genetic sequence in conditional transgenic mice.

1.5.2 Tamoxifen-inducible Cre-lox system

Cre-lox recombination is a powerful tool in the realm of mouse genetics. It allows researchers to control the timing and site-specific location of gene activation or suppression. In our case, the Cre-lox system is used to induce ubiquitous BiSyn expression. This recombination mechanism was initially used in 1987 when Brian Sauer demonstrated binding of Cre recombinase to loxP sites with subsequent excision and ligation, first in yeast *Saccharomyces cerevisiae* and thereafter in a mammalian kidney cell line^{180,181}. Five years later, Picard and colleagues recognized the role of the hormone-binding domain on steroid receptors as genetic regulatory switches and theorized the manipulation of such a system to induce genetic alterations¹⁸². Metzger and Chambon later combined the two techniques to design a conditional recombination complex by fusing Cre recombinase to a mutant binding domain on the human estrogen receptor, enabling tamoxifen-inducible recombination¹⁸³. Under normal physiological conditions, the ligand Hsp90 sequesters the estrogen receptor in the cytoplasm, which thereby

prevents Cre-mediated recombination¹⁸². However, the synthetic compound tamoxifen generates the active metabolites 4-OH-tamoxifen and endoxifen, which have high affinities for the active site on the estrogen receptor, interfering with Hsp90 interaction and thus allowing Cre to enter the nucleus where it can recombine the DNA (Figure 6)^{184,185}. This was taken one step further by Hayashi and colleagues at Harvard University, who enabled ubiquitous expression of this inducible recombination complex¹⁸⁵. Since α -syn expression does not initiate until 11 weeks gestation in humans and gestation day 9.5 in mice^{186,187}, we designed the BiSyn system to be tamoxifen-inducible via the Cre-lox system. In accordance, we can activate BiSyn in adulthood, preventing any potential interference during mouse development.

1.6 Purpose

The initial mechanisms that underlie α -syn aggregation are not well understood and the method in which the toxic species are able to spread from cell-to-cell is unknown. We designed the BiSyn model to elucidate these principles. Herein I describe the validation of our novel system and provide *in vitro* and *in vivo* data to support its proper functioning. We intend to use BiSyn in future endeavours to assess the appendiceal origin in Parkinson's disease.

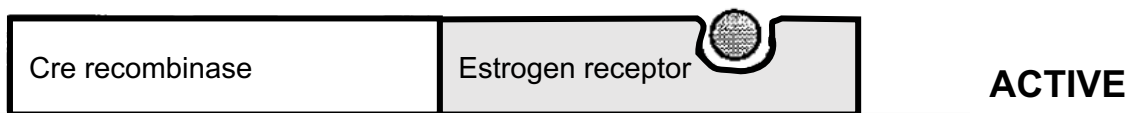
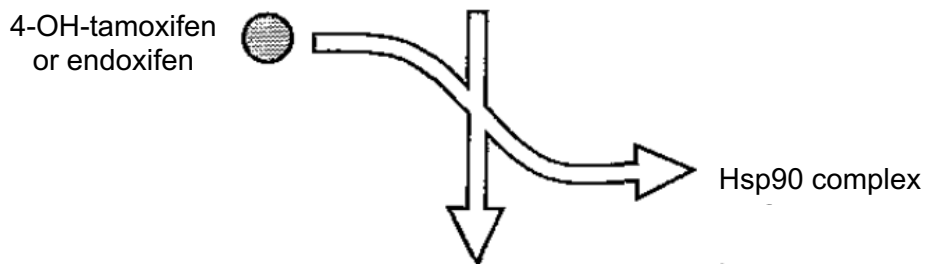
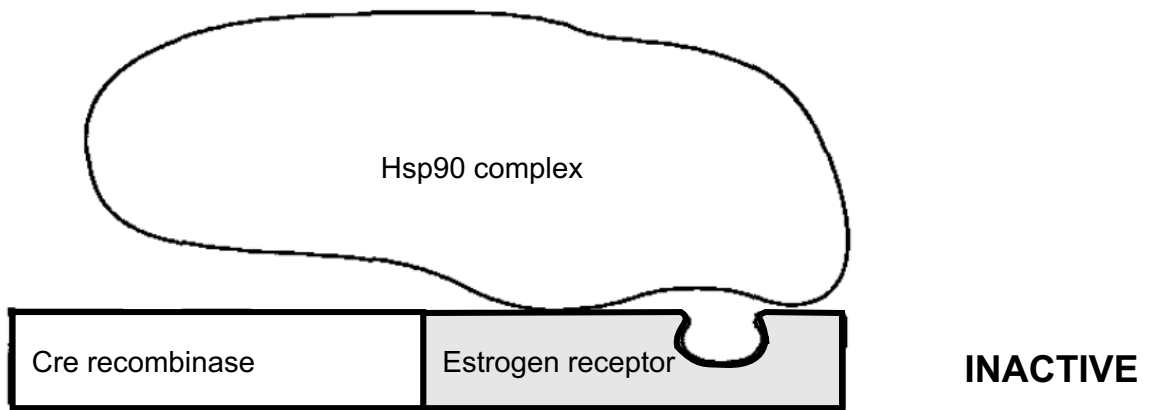


Figure 6: Tamoxifen-inducible activation of Cre recombinase.

Hsp90 interacts with the estrogen receptor and sequesters it in the cytoplasm. Since Cre recombinase is fused to the estrogen receptor via a mutant gene, it is unable to enter the nucleus. When tamoxifen is introduced, its metabolites bind the active site on the estrogen receptor which interrupts its interaction with Hsp90 and enables nuclear translocation. Once in the nucleus, Cre is able to recombine genetic sequences.

Adapted from ¹⁸². Permission to reproduce found in Appendix G.

2.0 Methods

2.1 Animal care

All mice in this study were bred and housed in the University of Ottawa Animal Care and Veterinary Services and were given a standard chow diet and water *ad libitum*. All mouse protocols (breeding #OHRI-2150; experimental #OHRI-1957) were approved by the University of Ottawa Animal Care Committee. Mating plug checks were performed by University of Ottawa Animal Care and Veterinary Services.

2.1.1 Generation of *BiSyn* transgenic mouse lines

R1 embryonic stem cells from the Nagi laboratory (in a 129Sv background with agouti coat colour) were transfected with plasmid pDG473, which encodes our *BiSyn* reporter whose expression is driven by cytomegalovirus (CMV) enhancer and chicken β -actin promoter (henceforth, CAG promoter) and dependent on Cre-mediated excision of a floxed beta-galactosidase (β -gal) fused to neomycin (β -geo) and three downstream polyadenylation signals (Figure 7)¹⁸⁸. These cells underwent selection using 200 μ g/mL Geneticin Selective Antibiotic (G418; ThermoFisher Scientific, #11811031) for 7-10 days and individual colonies were isolated, expanded and tested for expression of β -gal. *BiSyn* chimeras were then generated by aggregating selected clones of embryonic stem cells with morulas from CD-1 mice (white coat). The chimeras with a significant amount of 129Sv contribution (assessed by coat colour) were crossed with CD-1 wildtype mice. Offspring showing a complete agouti colour were indicative of originating from our embryonic stem cells and were genotyped to confirm the presence of the transgene (see section 2.1.2 for genotyping details and Table 1 for primer information). Chimeras that produced transgenic offspring were used as founders for the *BiSyn* mouse line

Figure 7: Schematic diagram of BiSyn transgene elements.

The CAG promoter (white) drives transgene expression. Following is a floxed β -geo cassette (purple). The β -gal-neomycin fusion (β -geo) enables selection for transgenic cells in culture with G418, while the β -gal acts as a reporter sequence, easily identifiable via histochemical staining with X-gal. In the presence of tamoxifen, Cre recombinase binds LoxP sites (blue) to excise the floxed β -geo cassette, facilitating transgene recombination. Upon recombination, the two Venus- α -syn sequences (VN155-linker- α -syn and VC155- α -syn; yellow and red) are transcribed into a single mRNA strand. The internal ribosome entry site (IRES) sequence (grey) allows both Venus- α -syn sequences to be transcribed from the single strand of mRNA; the first initiates at the normal 5' cap, while the second initiates at the IRES and is translated in a cap-independent manner.

Created in SnapGene by Madison T. Gray.

and were bred to 129Sv wildtype mice to maintain the same background. BiSyn mice were then intercrossed to eventually achieve a homozygous genotype.

B6.Cg-Ndor1^{Tg(UBC-Cre/ERT2)^{1Ejb}} mice (hereafter, Cre/ERT2) were acquired from Jackson Laboratories^{189,190}. BiSyn mice were crossed with Cre/ERT2 mice to generate BiSyn/Cre F1 mice. These BiSyn/Cre mice were intercrossed to achieve a homozygous genotype for the BiSyn transgene with a heterozygous Cre/ERT2 genotype. Jackson Laboratories noted that attempts to achieve homozygosity for the Cre/ERT2 genotype was unattainable, likely indicating embryonic lethality due to targeted knockout of *Ndor1*. All offspring were genotyped to assess their transgene composition (see section 2.1.2 for genotyping details and Table 2 for primer information).

To generate the BiSyn/Cre/SNCA mouse line, multiple crosses were performed. Firstly, heterozygous BiSyn mice were crossed with *Snca*^{Tg(Neo).Tg(SNCA)} mice (hereafter SNCA)¹⁹¹. These SNCA mice have a knockout of endogenous *Snca* with insertion of neomycin (Neo) in its place. They are also homozygous for the A30P and A53T mutant human *SNCA* transgenes (*Pac.4*; see section 1.2.2 for details regarding these mutations). The resultant BiSyn/SNCA F1 mice were backcrossed to the SNCA line to enrich the the SNCA transgenes for two generations. Secondly, a BiSyn/Cre F1 mouse was crossed with an SNCA mouse to introduce the Cre/ERT2 genotype. The resultant BiSyn/Cre/SNCA F1 mouse was crossed with a BiSyn/SNCA N2 mouse to generate what is now known as the BiSyn/Cre/SNCA mouse line (Figure 8). Details regarding mouse background strains are listed in Table 1.

2.1.2 Genotyping

3 to 4-week-old transgenic weanlings were tagged and an ear clipping was taken for genotyping. For all experiments, upon euthanization of adult mice, tail clippings were used to confirm the genotype. Other specimens were acquired for genotyping as indicated. Terminal PCR was performed on DNA extracted from ear, tail, or alternative specimens using

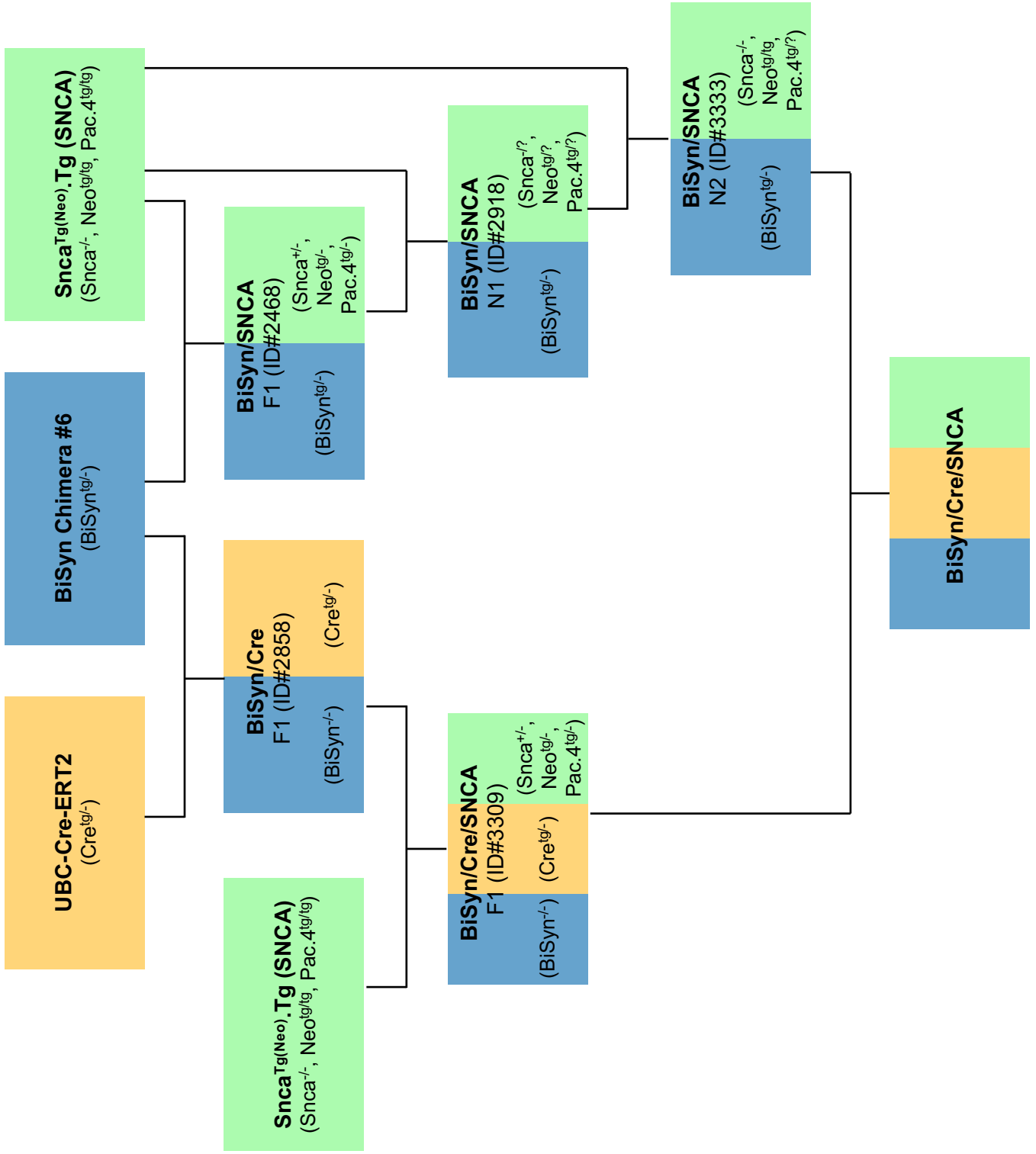


Figure 8: Pedigree outlining the generation of the BiSyn/Cre/SNCA mouse line

Table 1: Murine strain of origin for each transgenic derivative

Transgene/Knockout	Strain of origin	Mouse lines
BiSyn	129svJ	BiSyn
		BiSyn/Cre
		BiSyn/Cre/SNCA
Cre/ERT2	C57BL/6	BiSyn/Cre
		BiSyn/Cre/SNCA
Snca^{Tg(Neo)}	129svJ	BiSyn/Cre/SNCA
	C57BL/6	
Pac.4	FVB/N	BiSyn/Cre/SNCA
	129S6//SvEvTac	

*Note: The Snca knockout and Pac.4 transgenic were compounded into one mouse line, which we received from the Schlossmacher lab at the University of Ottawa. See ¹⁹¹ for details.

REDEExtract-N-Amp Tissue PCR Kit (Sigma, #SLCD1176). 10 μ L sample preparation was performed using REDEExtract-N-Amp ReadyMix (Sigma, #SLCC7047). BiSyn, Pac.4, SNCA, Neo and UCHL1 (ubiquitin carboxyterminal hydrolase 1) analyses were performed using a gel of 1% agarose in tris-acetate and EDTA buffer. Cre/ERT2 analyses were performed using a gel of 1.2% agarose in sodium borate buffer. Both gels were made with RedSafe Nucleic Acid Staining Solution (iNtRON, #21141). Primers used are listed in Table 2.

2.1.3 Statistical analysis of litter sizes

All relevant mating data was exported from SoftMouse (i.e., mouse colony management system: Softmouse.net) to Microsoft Excel for each of the three BiSyn mouse lines. There was a total of 146 BiSyn litters, 165 BiSyn/Cre litters, and 143 BiSyn/Cre/SNCA litters used for comparative analysis of litter sizes. Averages and standard deviations of litter sizes were computed for each mouse line. I performed a one-way analysis of variance (ANOVA) to assess whether there was a significant difference between litter sizes for the three mouse lines. Tukey-Kramer post-hoc test was performed to identify which litter sizes were different from each other.

2.2 Transgene expression experiment

Thorough expression analysis was performed in BiSyn/Cre mice to ensure ubiquitous expression of our novel transgene. BiSyn and BiSyn/Cre/SNCA lines were used as supplementary where indicated.

2.2.1 Evaluation of BiSyn expression phenotype via histochemical technique

To evaluate transgene expression throughout development, as well as in sex organs and brain regions critical to Parkinson's disease, histochemical staining for β -gal was used. This method allows us to assess raw BiSyn expression prior to recombination.

Table 2: Primers used for genotyping transgenic mice via terminal PCR

Transgene/ Knockout	Primers	Sequence 5' to 3'
BiSyn	BiSyn-5-Forward BiSyn-5-Reverse	TGTGGCAGAAGCAGCAGG CCATGCCGAGAGTGATCC
	YFP-Forward YFP-Reverse	AAGCTGACCCTGAAGCTGATCTGC CTTGTAGTTGCCGTCGTCCTTGAA
	β -gal-Forward β -gal-Reverse	TACGATGCGCCCATCTACAC TACCCGTAGGTAGTCACGCA
Cre/ERT2	Cre200-Forward Cre200-Reverse	ATTGCTGTCACTTGGTCGTCCC GGAAAATGCTTCTGTCCGTTTGC
Snc^{aTg(Neo)}	Sncadel-Forward Sncadel-Reverse	TCACCTCAATGCAAACCAA CAGCTCCCTCCACTGTCTTC
	Neo-Forward Neo-Reverse	CATACGCTTGATCCGCGTAC AATATCACGGGTAGCCAACG
Pac.4	Pac.4-Forward Pac.4-Reverse	CCTCCTGTAGCTGGGCTTT ACCACTCCCTCCTTGGTTTT
UHL1	Up-Forward Up-Reverse Pgk-Reverse	CAGCTTGTCTTGGTTGTTGG CTGGACCACCATCTGCTTAC AAGCGAAGGAGCAAAGCTGC

2.2.1.1 Zygote and ovary extraction

BiSyn^{tg/tg}/Cre^{tg/-} females underwent superovulation using 5 units gonadotropin from pregnant mare serum (PMSG; Sigma, #G4877) followed by 5 units human chorionic gonadotropin (HCG; Sigma, #CG5-1vI) 46 hours later. Females were mated with BiSyn^{tg/tg}/Cre^{tg/-} males at the time of HCG intraperitoneal injection. Gestation ages of e0.5, e1.5, and e2.5 were used for zygote harvest following positive copulation plug.

Females were euthanized via CO₂ inhalation followed by cervical dislocation. The ovaries and uterus were immediately excised together. Fat was trimmed and ovaries were removed to access the infundibulum. The ovaries were kept in ice cold phosphate buffer (pH 7.4) until fixation.

The uterine horns were then separated, and the zygotes were flushed from the infundibulum. If they required further growth, they were placed in warm M16 medium with sodium bicarbonate and lactic acid, without penicillin and streptomycin (Sigma, #SLBV7181) in an incubator at 37°C until appropriate growth was achieved. We found it optimal to use a 96-well tissue culture plate to proceed with staining. The various solutions could be changed using a 200µL long plastic pipette tip used to load protein gels.

2.2.1.2 Embryo extraction

Gestation ages of e12.5, e14.5, and e16.5 were used for embryo harvest following positive copulation plugs. Females were euthanized via CO₂ inhalation followed by cervical dislocation. Embryos were immediately dissected from the uterine lining and their respective amniotic sacs. They were placed in ice cold phosphate buffer (pH 7.4) until fixation.

2.2.1.3 Mouse embryonic fibroblast isolation

BiSyn/Cre embryos were extracted as described in section 2.2.1.2 under sterile conditions. Separate scissors and forceps were used for each layer to prevent contamination of interior tissue with external material. After dam euthanization the uterine horns were immediately removed without allowing them to come in contact with the dam's exterior. They were placed in 1X phosphate buffered saline pH 7.3 (PBS). In a laminar flow hood, each embryo was removed from the uterus and amniotic sac separately and instruments were sterilized between individuals. Embryos were rinsed in PBS. Heads and internal red organs were discarded. One limb from each embryo was collected for genotyping. Carcasses were transferred to individual plates containing sterile 1X 0.25% trypsin in HBSS solution (Corning, Mediatech Inc., #25-050-CI) and were minced into fine pieces. They were then incubated for 10 minutes at 37°C. Tissue was homogenized by vigorously pipetting up and down 20-30 times. 1X Dulbecco's modification of eagle's medium with 4.5g/L glucose, L-glutamine and sodium pyruvate (DMEM; Corning Mediatech Inc., #10-013-CV) with 10% fetal bovine serum (FBS) was added. Cells were centrifuged at 230g for 5 minutes at room temperature to pellet. Supernatant was aspirated and cells were resuspended in DMEM+10%FBS and plated in 3 X 10cm plates per carcass. When full confluency was achieved (~48 hours), cultures were treated with 1X 0.05% trypsin, 0.53mM EDTA solution (Corning Mediatech Inc., #25-052-CI) and pelleted. For storage, cells from one 10cm dish were resuspended in 1mL of FBS+10% dimethyl sulfoxide (DMSO) and placed in a cryovial at -80°C. For growth to immortalization, mouse embryonic fibroblasts (MEFs) were resuspended in DMEM+10%FBS. If cultures required gene selection, they were continuously cultured in 400ug/mL G418, which was added at each cell passage.

2.2.1.4 Brain and testis harvest for histochemical staining

Adult BiSyn^{+/+}/Cre^{-/-} mice (n=10) were euthanized via asphyxiation in a CO₂ chamber followed by cervical dislocation as a secondary measure. Brains were harvested and cut into 6 pieces coronally using a razor blade. Testes were also excised from the males (n=5). Brain sections and testes were placed in ice cold phosphate buffer (pH 7.4) until fixation.

2.2.1.5 Fixation and histochemical staining for β -gal

Tissues (ovaries, testes, embryos and brains) were fixed in 0.8% glutaraldehyde-containing fixative solution for 20 minutes. Zygotes and MEFs were fixed in 4% paraformaldehyde for 20 minutes. Following respective fixation, tissues, zygotes and MEFs were stained for β -gal positivity to assess transgene expression. Specimens were washed in PBS for 3 X 10 minutes then incubated in 0.04% X-gal (5-bromo-4-chloro-3-indolyl-beta-D-galactopyranoside; ThermoFisher Scientific, #R0404) histochemical stain overnight at 37°C. Sections were placed in PBS and moved to 4°C overnight to enhance pigmentation.

2.2.1.6 Tissue Freezing

X-gal stained tissue was placed in 15mm X 15mm X 5mm cryomold intermediate disposable vinyl specimen molds (Tissue-Tek, #4566), embedded in Tissue Plus O.C.T. Compound (OCT; Fisher HealthCare, #4585), and frozen in cold isopentane. The University of Ottawa Department of Pathology processed the stained brain sections. Ovaries were cut at 10 μ m thickness using a Leica CM1850 cryostat (Leica Biosystems, USA). -15 to -16°C was optimal for cutting ovaries, and it was critical that excess fat was removed prior to freezing to maintain the integrity of the tissue while cutting. Frozen testes became desquamate and could not be cut without severe tainting at any temperature tested between -15 to -25°C.

2.2.1.7 Microscopy

Brain and ovary sections were analyzed under Olympus BX50F microscope (Olympus Optical Co. Ltd., Japan) and images were captured using attached PixeLINK camera (Ottawa, Ontario, Canada) and processed using PixeLINK μ Scope Professional (version 21.1x64).

Whole testis and embryos were imaged using Leica MZFL111 (Leica Microscopy Systems Ltd., Switzerland) and images were captured using attached PixeLINK camera (Ottawa, Ontario, Canada) and processed using PixeLINK μ Scope Professional (version 21.1x64). MEFs were imaged using an EVOS microscope with built-in camera (Advanced Microscopy Group, USA).

2.2.1.8 Statistical analysis of transgene expression at distinct developmental time points

Zygotes at the 2-cell, 4-cell, 8-cell, morula, and blastocyst stages were categorized by expression phenotype as homogenous +, homogenous -, or mosaic. A χ^2 test for independence was performed to assess whether developmental stage and expression phenotype were related. Statistical analyses were conducted using Microsoft Excel.

2.2.2 Assessing *BiSyn* expression in enteric neurons via immunofluorescence

To evaluate transgene expression in key enteric neuronal plexuses without commensal β -gal interference, tamoxifen-induced recombination was conducted, and immunofluorescence (IF) staining was used.

2.2.2.1 Tamoxifen-induced recombination in vivo

20mg/mL tamoxifen (Sigma, #T5648) was dissolved in a 98% corn oil, 2% ethanol solution. 9 to 11-week old *BiSyn/Cre* mice were transferred to disposable cages. They were

treated once daily for five days with 180mg/kg tamoxifen¹⁸⁹ via oral gavage using disposable feeding tubes (Harvard Instruments, #72-4448) to stimulate recombination.

2.2.2.2 Whole mount gut sectioning

Mice were euthanized via asphyxiation in a CO₂ chamber followed by cervical dislocation as a secondary measure. I adopted the method used by Schock and colleagues for whole mount intestine sectioning¹⁹² to assess transgene expression in the myenteric and submucosal plexuses in duodenum and jejunum regions. I made minor alterations to the whole mount protocol to optimize the methodology in my lab setting. Rather than using silicone for flat fixing intestinal tissue, I made a 3% agarose gel in sodium borate buffer. While the original method provides instruction for constructing boxes to encase the OCT, I filled 20mm X 25mm X 5mm cryomold intermediate disposable vinyl specimen molds (Tissue-Tek, #4557) with OCT. When flat freezing the tissue, I used a metal tool sharpener to dull the edges of the double-edged razor blades for safer handling. After heat-transferring the tissue onto the OCT block and covering it with a layer of OCT, I used a single-edged razor blade to reinforce the pentagonal shape of the OCT box where the additional OCT layer was added. This allowed for smoother cutting on the cryostat.

Sections containing myenteric and submucosal plexuses were stained via IF with anti-alpha-synuclein [MJFR1] antibody (see section 2.3.5 for staining details and Table 3 for antibody information).

2.2.3 *Evaluating restoration of transgene expression and functionality*

The possibility of restoring BiSyn expression and the assessment of transgene functionality were explored in MEFs isolated from our BiSyn mouse lines.

2.2.3.1 DNA methyltransferase and histone deacetylase complex inhibitor treatments

Immortalized BiSyn/Cre and BiSyn/Cre/SNCA MEFs were counted using a Vi-CELL XR Cell Viability Analyzer (Beckman Coulter, USA, #478389). A density of 5.0×10^5 cells/well in a 12-well plate was used. 24 hours after plating, MEFs were treated with 0.25, 0.5, 1.0, and 2.0 μ M suberoylanilide hydroxamic acid (SAHA) for 24 hours; 0.25, 0.5, and 1.0 μ M 5-Aza-2'-deoxycytidine (5-aza-dC) for 48 hours; the combined treatment of 0.5 μ M SAHA (24 hours)+ 0.25 μ M 5-aza-dC (48 hours); or PBS as a control for 48 hours. These concentrations were added to 1.5 mL DMEM+10%FBS.

Following treatments, MEFs were rinsed in phosphate buffer (pH 7.4) and stained with X-gal to assess whether expression was restored (see section 2.2.1.5 for X-gal staining details).

2.2.3.2 Inducible recombination in MEFs

NIH3T3 MEFs transfected with BiSyn plasmid pDG473 were counted using a Vi-CELL XR Cell Viability Analyzer (Beckman Coulter, USA, #478389). The required number of cells (5.0×10^6 cells/well in a 6-well plate X number of wells required as per experiment) was transferred to an Ependorf tube then placed in a centrifuge at 230g for 4 minutes to pellet. The supernatant was aspirated. To promote transgene recombination, NIH3T3/DG473 MEFs were treated with 10 viral genomes (vg)/cell adenovirus Cre in 100 μ L DMEM+10%FBS. Cells were gently vortexed then placed in an incubator at 37°C for 1 hour. Alternatively, BiSyn/Cre/SNCA MEFs (passage 3) were treated with 100nM tamoxifen (Sigma, #T5648) in a 6-well plate with 2.0 mL DMEM+10%FBS for 48 hours. Following treatment, they were counted in the same manner, pelleted and supernatant aspirated.

2.2.3.3 Rotenone-induced aggregation in MEFs

Recombined NIH3T3/DG473 or BiSyn/Cre/SNCA MEFs were plated on uncoated sterilized coverslips with 4.25×10^6 cells/well in a 6-well plate. Cells were treated with rotenone (Sigma, #R8875) dissolved in DMSO at concentrations of 1, 10, and 100nM. 72 hours post-treatment, coverslips were washed in PBS then fixed in 4% paraformaldehyde (PFA) for 15 minutes. BiSyn/Cre/SNCA MEFs were then stained via IF with anti-alpha-synuclein [MJFR1] antibody (see section 2.3.5 for staining details and Table 3 for antibody information).

2.3 BiSyn transduction experiment

Adeno-associated virus (AAV) containing our constitutive BiSyn cassette flanked by inverted terminal repeats was used to transduce mouse CPu. I performed a thorough analysis for transduced brains to determine the efficiency and spread of transduction.

2.3.1 rAAV preparation

Vector Biolabs re-engineered the constitutive CMV-BiSyn cassette into a hybrid AAV2/9. Virions were purified using CsCl. The final stock titer was 4.9×10^{13} vg/mL. The recombinant AAV (rAAV) was stored at -80°C in a 5% glycerol PBS storage solution.

2.3.2 rAAV injection

Three 11-week old wildtype male littermates were used to test rAAV transduction in the CPu. Mice were injected with buprenorphine HCl (0.1mg/kg) from McGill University Comparative Medicine Animal Resource Center subcutaneously at induction. They were anesthetized with isoflurane inhalation. Stereotaxic surgery was performed as described previously¹⁹³, but with injection into the CPu (ML 2mm, AP 0.5mm, DV -4mm). 2 mice were injected with 2µL rAAV

($\sim 9.8 \times 10^{10}$ vg) and 1 mouse was injected with 2 μ L of PBS at a rate of 1 μ L over 10 minutes. The needle was held in place for 5 minutes before removal to avoid viral efflux during retraction.

The same injections were later performed in 8-week-old UCHL1-KO mice. Wildtype control *UCHL1*^{+/+} (n=4), heterozygous *UCHL1*^{+/-} (n=4) and knockout *UCHL1*^{-/-} (n=2) mice were generated by intercrossing *UCHL1*^{+/-} mice.

2.3.3 Tissue fixation

An anesthetic cocktail was prepared containing 50mg/mL ketamine and 20mg/mL xylazine from McGill University. Mice were injected with 0.1mL/10g body weight anesthetic (100mg/kg ketamine and 16mg/kg xylazine) at 28 days post-infection (dpi). Perfusion was performed using PBS followed by 4% PFA. Brains were removed and placed in 10% buffered formalin phosphate (Fisher Scientific, #192274) overnight, then sunk in 20% sucrose (Sigma, #SULE133-18) in PBS to limit freezing artefact.

2.3.4 Tissue freezing

Fixed brains were cut in half coronally using a razor blade. They were frozen in isopentane. Frozen brain halves were embedded in OCT in a 15mm X 15mm X 5mm cryomold intermediate disposable vinyl specimen mold (Tissue-Tek, #4566), which was then frozen in isopentane. It was more optimal, however, to embed brains in OCT prior to freezing, then freeze the brain in the OCT box as this modified method reduced freezing artefact. Brains were cut at 10 μ m thickness using a Leica CM1850 cryostat. -17 to -18°C was optimal for cutting frozen brain tissue.

2.3.5 Immunofluorescence

Fixed and frozen sections were washed in PBS and blocked in 5% normal goat serum for 30 minutes, then incubated in the indicated primary antibody (Table 3) overnight at 4°C in a

Table 3: Antibodies used for immunofluorescence application

Antibody	Source	Catalog Number	Dilution
Rabbit recombinant anti-α-synuclein [MJFR1]	Abcam	Ab138501	1:300
Rabbit anti-tyrosine hydroxylase [EP1533Y]	Abcam	Ab75875	1:100
Rabbit anti-GFP chip-grade	Abcam	Ab290	1:500
Rabbit anti-AAV capsid protein VP1	Bioss Antibodies	Bs-10180R	1:100
Goat ant-rabbit IgG Alexa Fluor 594	LifeTech	A32740	1:500

humidity box. Sections were washed in PBS then incubated in a red fluorescent secondary antibody (Table 3) for 40 minutes in the dark. They were rinsed in PBS. Coverslips were applied onto a slide using VectaShield Antifade Mounting Medium with DAPI (Vector Laboratories, H-1200).

2.3.6 Analysis

Brains were analyzed and imaged using ZEISS AxioScan.Z1 fluorescent slide scanner (Carl Zeiss Canada Ltd., Serial No. 4631001022) with ZEISS ZEN imaging software at 20X magnification. Images were processed using ZEN 2 blue edition software. High magnification images were taken on a Zeiss Airyscan confocal microscopy in the imaging core facility of Faculty of Medicine, University of Ottawa. High magnification z-stack images were composed on Axioskop II fluorescence microscope with Zeiss AxioCam attachment (Carl Zeiss Canada Ltd., Toronto, Ontario) and processed using Zeiss Axiovision software.

3.0 Results

3.1 Generation of BiSyn mouse lines

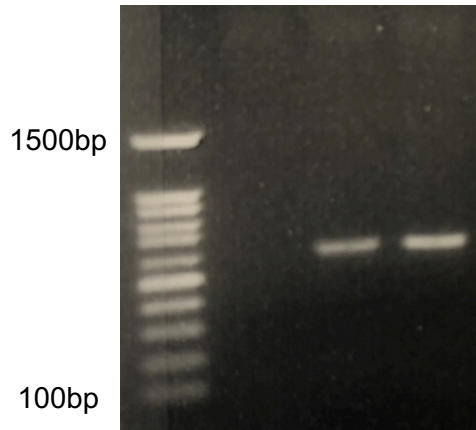
The first BiSyn mouse was created by injecting transfected embryonic stem cells into a blastocyst, producing a BiSyn chimera. Of the 12 BiSyn chimeras generated, one chimeric male produced transgenic offspring, which was confirmed via terminal PCR (Figure 9A). This male (BiSyn Chimera #6) is the sole founder of the BiSyn mouse line.

BiSyn mice were crossed with UBC-Cre-ERT2 transgenic mice to produce the BiSyn/Cre mouse line, or they were crossed with SNCA mice to produce an intermediate BiSyn/SNCA mouse line. Endogenous SNCA knockout and presence of Cre and Pac.4 transgenes were confirmed via terminal PCR (Figure 9B-D). BiSyn/Cre mice were crossed with SNCA mice to produce the BiSyn/Cre/SNCA F1 generation. The BiSyn/SNCA mice were backcrossed with SNCA mice twice before crossing with the BiSyn/Cre/SNCA F1 mice to produce the BiSyn/Cre/SNCA mouse line.

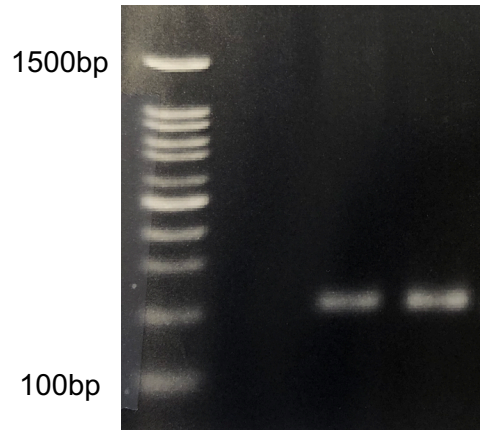
3.1.1 Comparative analysis of litters across the three BiSyn mouse lines

A one-way ANOVA was conducted to compare the effect of background strain on litter size in BiSyn, BiSyn/Cre, and BiSyn/Cre/SNCA mouse lines, showing a statistically significant result [$F(2,451)=9.02$, $p<0.001$]. Post-hoc comparisons using the Tukey-Kramer test indicated that the mean litter size for the BiSyn/Cre/SNCA mouse line ($M=6.90$, $SD=2.52$) was significantly larger than both the BiSyn ($M=5.72$, $SD=2.41$) and BiSyn/Cre ($M=5.82$, $SD=2.91$) mouse lines. However, there was no statistically significant difference between the litter sizes for the BiSyn and BiSyn/Cre mouse lines. Taken together, these results suggest that as the background strains were more highly intercrossed, the hybrid mice had increased vigour, which is evident in the larger litter sizes.

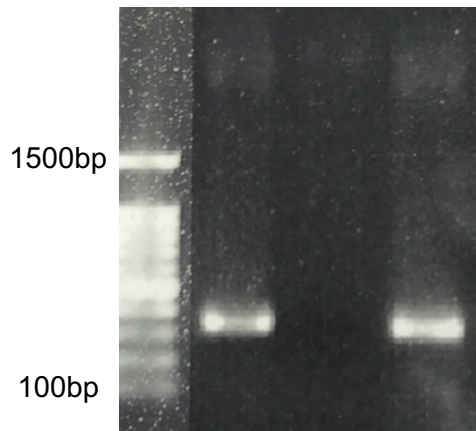
A



B



C



D

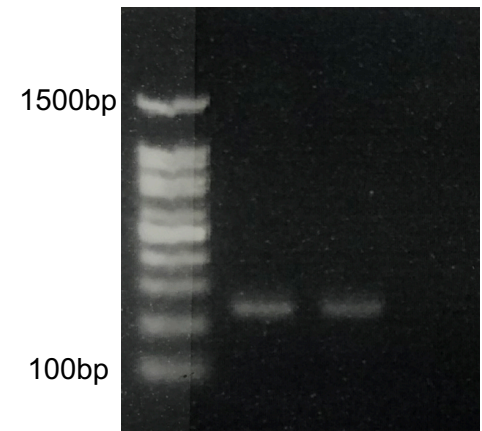


Figure 9: Genotyping BiSyn mouse lines via terminal PCR.

(A) The BiSyn-5 primers generate a 583-base pair (bp) product, confirming the presence of the BiSyn transgene in lanes 2 and 3, but not in lane 1.

(B) Genotyping for Cre recombinase using the Cre200 primers generates a 200bp product (lanes 2 and 3), or no band in the absence of Cre (lane 1).

(C) Endogenous Snca knockout is assessed using Sncadel primers, which generate a 354bp when Snca is present (lanes 1 and 3), or no band in null samples (lane 2).

(D) Pac.4 primers generate an ~250bp product, confirming transgene presence (lanes 1 and 2). No band indicates that the transgene is not present (lane 3).

3.2 Expression in BiSyn/Cre transgenic mice

In order to utilize a transgenic mouse model effectively, careful characterization should be conducted prior to experimentation. Although our BiSyn transgenic mice were designed to yield ubiquitous transgene expression, I have demonstrated that expression is highly stochastic across individuals, tissues, and the lifespan.

3.2.1 Developing mice present with mosaic phenotype

Our BiSyn/Cre transgenic mice provided the opportunity to isolate unique cell lines for the purpose of *in vitro* studies. In particular, we were interested in utilizing MEFs and primary SN neurons to assess the validity and mechanisms behind exosome-mediated α -syn aggregate propagation. Therefore, it was critical that we ensured ubiquitous transgene expression at various developmental time points. To evaluate transgene expression through development, we used X-gal histochemical staining. This method enables assessment of β -gal positivity, which, in the case of the BiSyn transgene construct, is not dependent on the efficiency of tamoxifen-induced recombination, making this a better estimate for raw expression compared to an approach that would assess expression of our Venus- α -syn fragments post-recombination.

There was no β -gal positivity at the 2-cell stage (Figure 10A; n=6). One 4-cell zygote displayed mosaic expression, while all others were negative for β -gal expression (Figure 10B; n=13). The 8-cell stage displayed all possible expression phenotypes (Figure 10C – E; n=33), with the majority favouring mosaicism (Figure 10G). Despite all BiSyn/Cre mice being homozygous for the BiSyn transgene, ubiquitous expression was never achieved beyond the 8-cell stage. In fact, the 8-cell stage is the only time point when homogeneity of expression was present (Figure 10E). The 8-cell stage marks a shift in transgene expression such that 90% of morulae (n=10) and 100% of blastocysts (Figure 10F; n=8) display β -gal positivity in a stochastic fashion. A χ^2 test for independence was performed ($\chi^2=36.993$), yielding a statistically

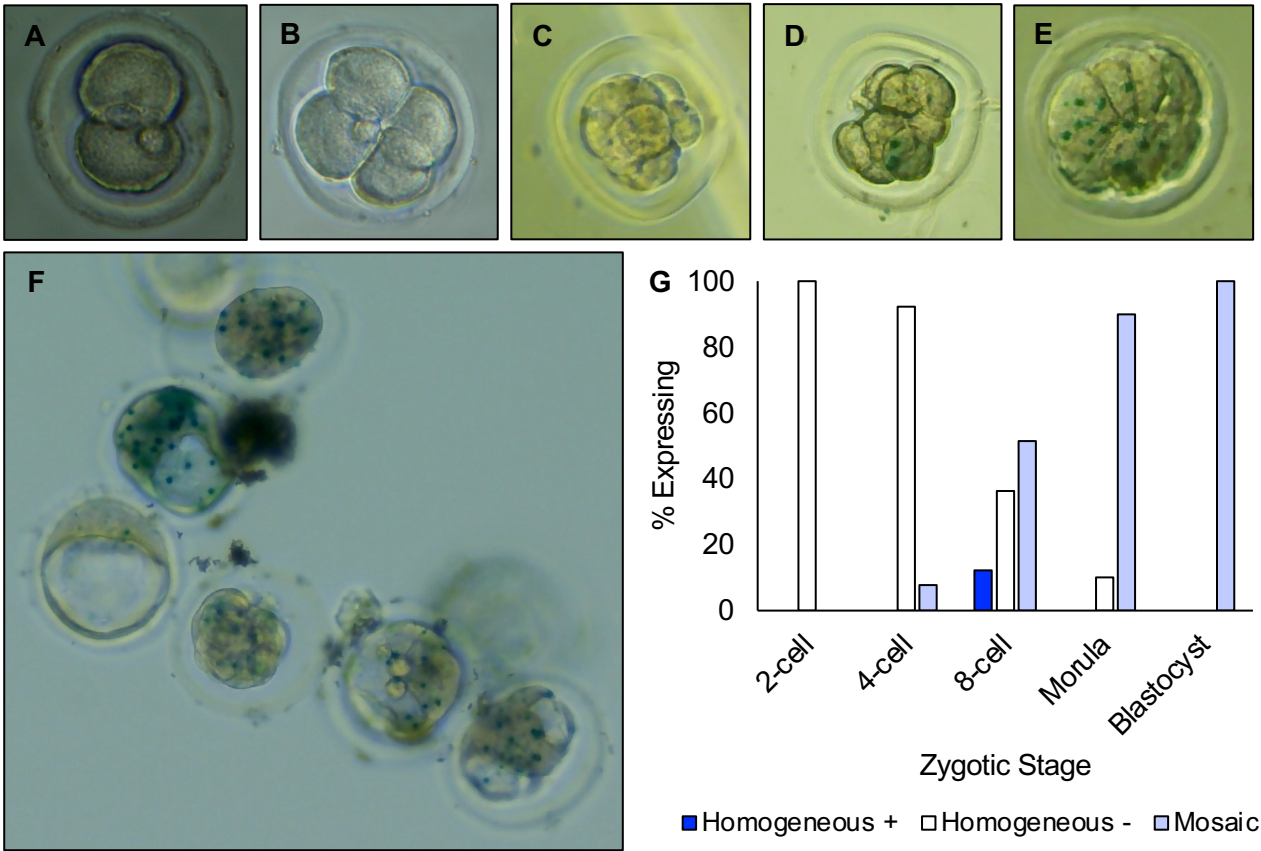


Figure 10: Silencing in zygotic stages is alleviated in a stochastic fashion at the 8-cell stage.

(A) 2-cell zygotes lack β -gal positivity.

(B) Similarly, nearly all 4-cell zygotes are negative for transgene expression.

(C-E) There are 3 expression phenotypes at 8-cell stage, at which time zygotes display (C) homogeneity of negative staining, (D) mosaic expression, or (E) homogeneity of β -gal positivity.

(F) As cells multiply further and form into blastocysts, all individuals display β -gal positivity, however stochasticity of expression phenotype is evident at this stage.

(G) There is a clearly defined shift at the 8-cell stage when individuals begin expressing the BiSyn transgene. Beyond the 8-cell stage, however, homogeneous β -gal positivity is not observed, and all individuals display a mosaic expression phenotype.

significant result ($p=0.000012$). These data indicate that developmental stage has an effect on expression phenotype.

Since MEFs and primary SN neurons are isolated at gestation day e14.5, I assessed whole embryo expression at this time point along with MEFs isolated from our transgenic mice. Of the 16 distinct MEF cultures isolated from BiSyn/Cre mice, none of them displayed β -gal positivity. Whole embryos showed a wide variation in mosaic phenotype (Figure 11A-C).

3.2.2 Gametic variation in transgene expression

Since the zygotic expression data were surprisingly stochastic, I was interested in assessing whether gamete expression is the potential cause of expression variability. In pursuit of answering this question, I stained whole testes and ovaries with X-gal, then used cryo-techniques and microscopy to further evaluate expression in oocytes.

The testis expresses over 77% of all protein coding genes, far more than any other tissue type¹⁹⁴. X-gal stained testes demonstrate thorough β -gal positivity throughout (Figure 12A and B). These results are consistent with X-gal stained testes from three years previous when the BiSyn/Cre mouse line was generated (Figure 12B), indicating that our transgene has remained intact over time. Silencing is thus not the result of mutation or deletion of the transgene.

Beginning as early as the oocyte, β -gal expression is stochastic. Ovarian cross-section demonstrates mosaic expression throughout the medulla with reduced β -gal positivity in the cortex (Figure 12D). While β -gal positivity is completely absent in some follicles (Figure 12E), other follicles maintain expression in granulosa cells throughout the epithelium (Figure 12F). Some follicles, however, preserve β -gal expression within oocytes (Figure 12G). There is ~3-fold more oocytes that do not exhibit expression compared to those that show β -gal positivity.

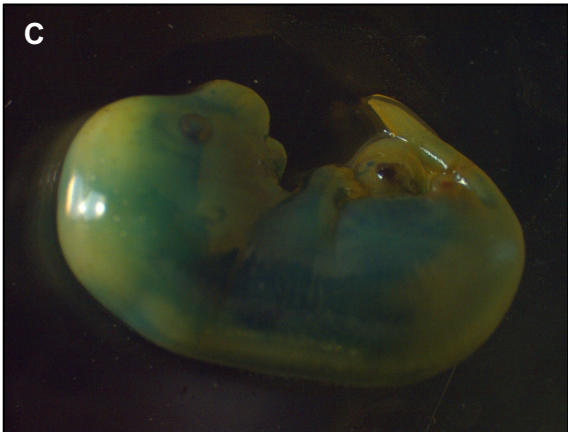
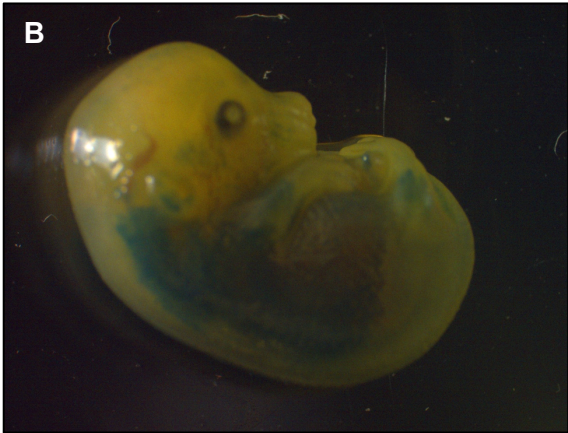
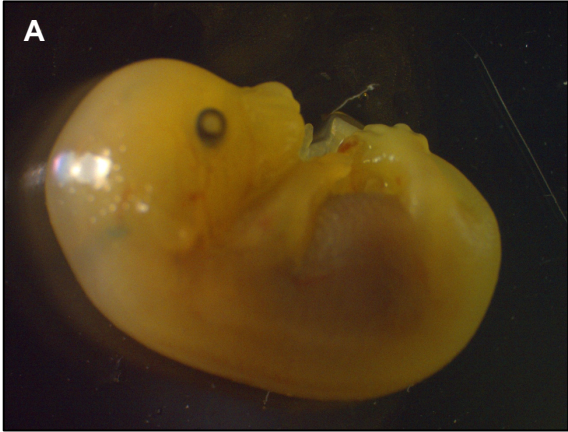


Figure 11: Stochastic nature of β -gal expression in BiSyn/Cre littermates at gestation day e14.5.

Histochemical coloration X-gal staining reveals (A) minimal, (B) moderate, or (C) high levels of β -gal positivity in littermates at gestation day e14.5.

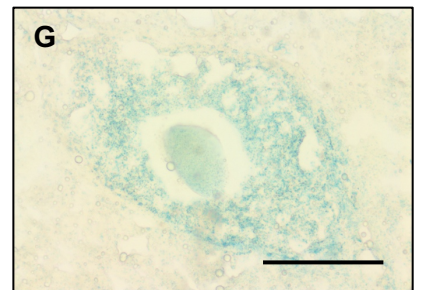
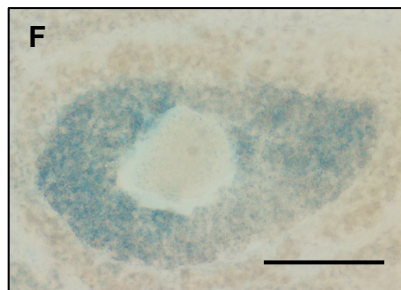
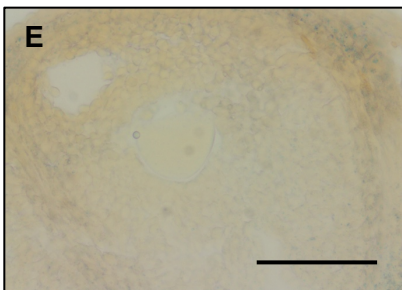
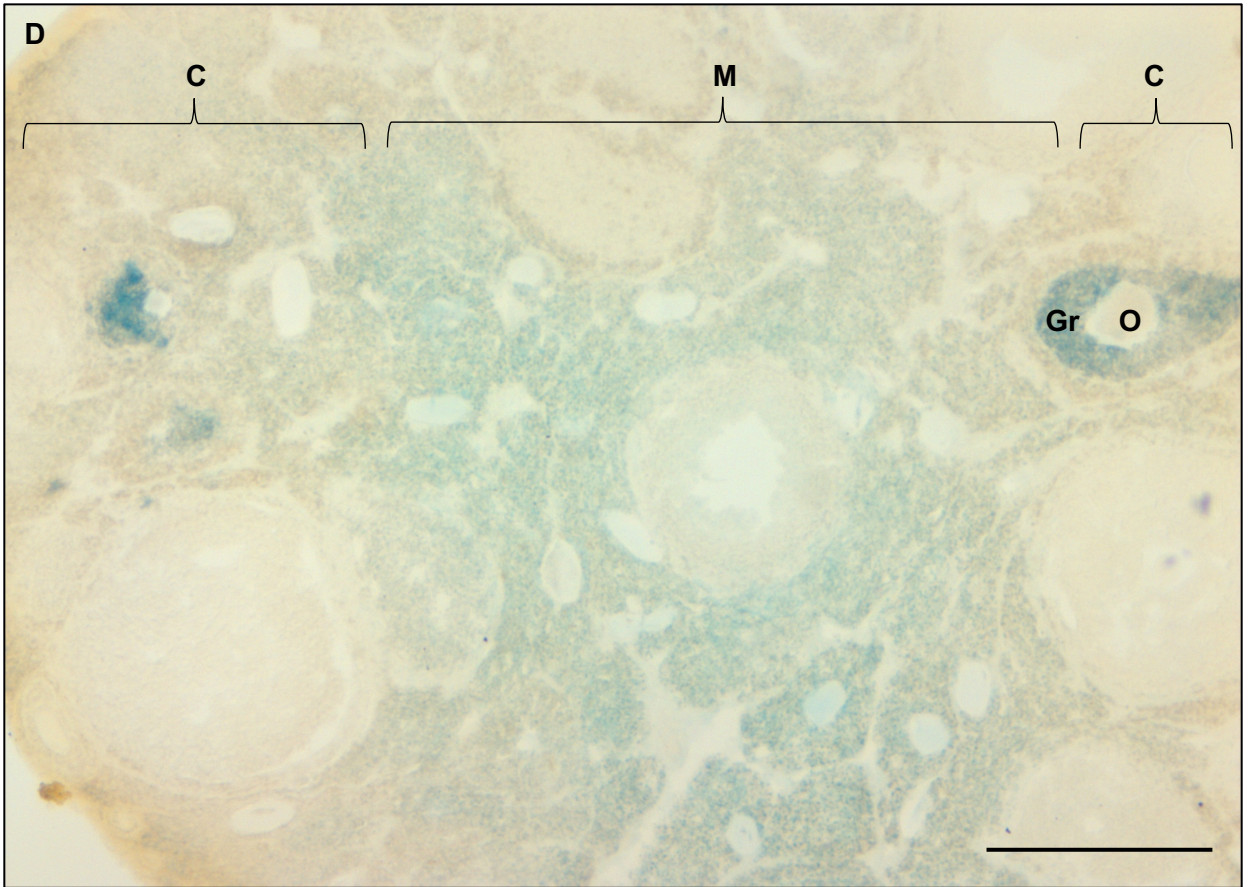
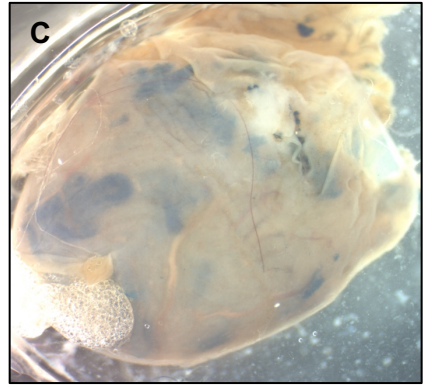
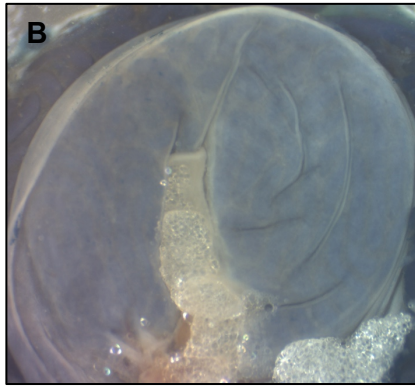
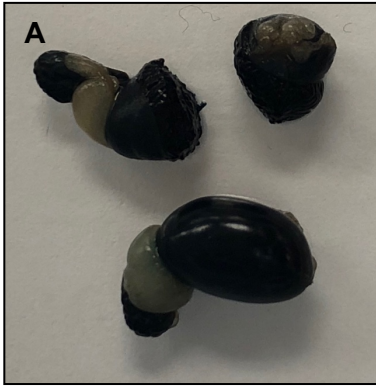


Figure 12: BiSyn/Cre reproductive organs stained with X-gal yield mosaic phenotype in ovaries but not testes.

(A) Testes show thorough penetration of β -gal positivity through the entire breadth of the testis. Expression appears ubiquitous.

(B) Testis stained three years prior yields a similar ubiquitous expression phenotype.

(C) On the contrary, a testis that was harvested from a tamoxifen-treated, Cre hemizygous mouse shows a mosaic expression phenotype as a result of inefficient recombination.

(D) Cross-section of X-gal stained ovaries reveals mosaic transgene expression throughout.

(E) Increased magnification of X-gal stained ovaries reveals the presence of some follicles lacking B-gal expression entirely.

(F) The majority of follicles display mosaic β -gal positivity in granulosa cells within the follicular epithelium.

(G) A small portion of follicles yield some degree of maintained β -gal positivity.

G = granulosa cells; O = oocyte; C = cortex; M = medulla.

Scale bars = (D) 300 μ m; (E-G) 100 μ m.

3.2.3 Stochastic expression in regions critical to PD pathology

Despite the observed mosaicism throughout development, we wanted to address whether PD-critical regions (i.e., SN and CPu in the brain, and neuronal plexuses in the GI tract) preserved sufficient expression to use these transgenic mice for *in vivo* studies. Using the same X-gal staining and cryo-techniques, I have confirmed that the stochastic nature of expression observed throughout development and in ovaries persists into the adult brain. β -gal positivity was observed in the CPu and hippocampus, but not SN, of ~50-60% of mice; however, the number of expressing cells in these two regions was minimal (Figure 13A–F, I). Both within a single brain and between brains of littermates, expression stochasticity is evident (Figure 13G–I). High levels of expression were not observed in any of the PD critical brain regions (Figure 13I).

The myenteric plexus of the GI tract was also considered in expression analyses. Since β -gal is an enzyme involved in lactose fermentation, X-gal staining can label both our transgene and endogenous species that typically exist in enterocytes¹⁹⁵. I therefore treated mice with tamoxifen and used an IF technique with human α -syn antibody. Unfortunately, there was no antibody specificity observed, likely indicating insufficient expression in our sample specimens.

3.2.4 Expression is not restored in late passage MEFs

Before pursuing alternative approaches, I wanted to first identify whether transgene expression could be restored, which would therein preclude the need to develop a novel system. Although the CAG promoter is widely used and evidence supports its ability to drive ubiquitous expression¹⁹⁶ with high efficiency¹⁹⁷, two distinct research groups have shown that it can become hypermethylated, thereby causing unstable transgene expression^{198,199}. These separate studies have identified distinct DNA methyltransferases (DNMTs) that regulate this hypermethylation tendency; while DNMT3b was the culprit in one report¹⁹⁸, DNMT1 was the

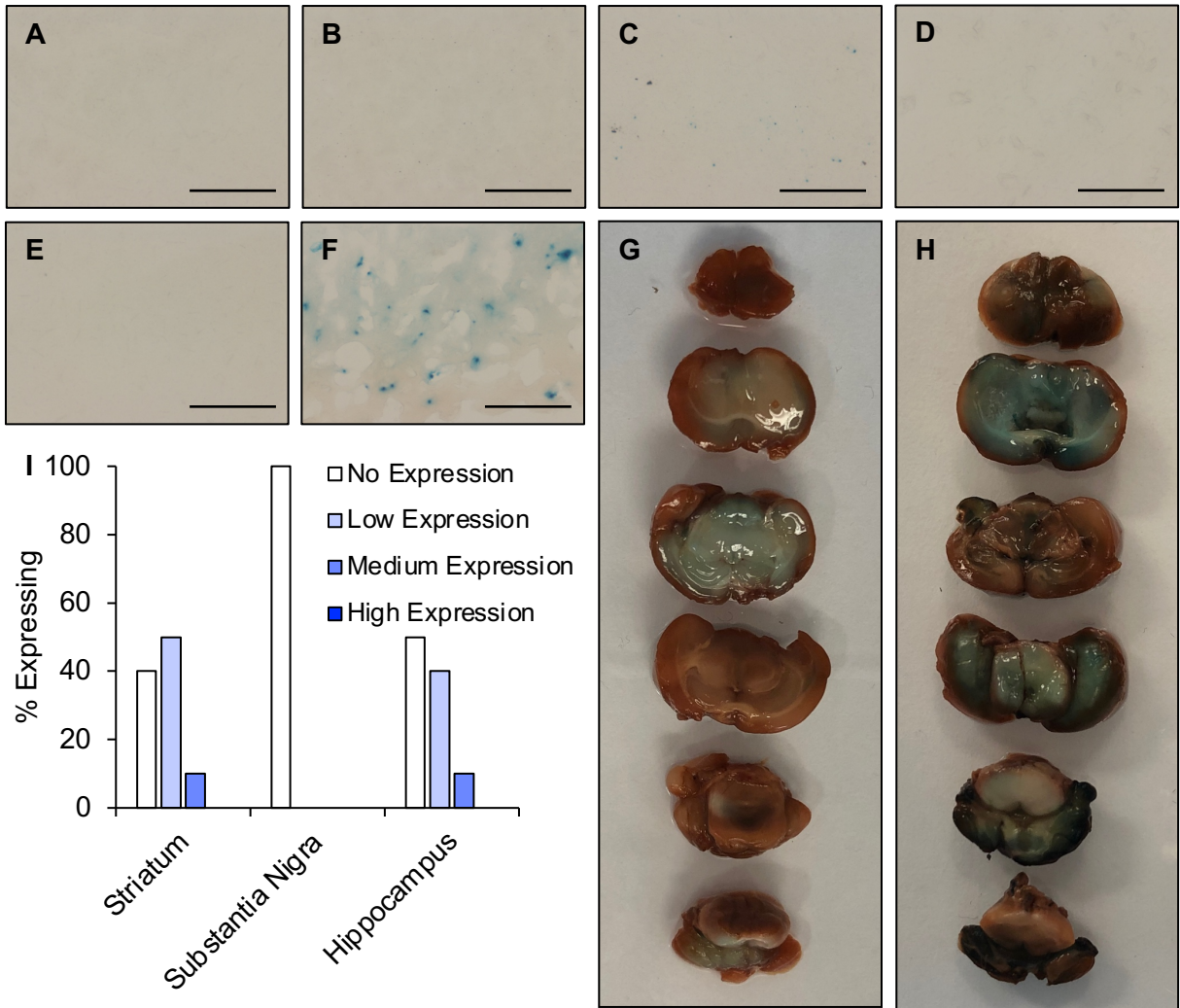


Figure 13: Stochastic mosaicism in PD-critical CNS regions from BiSyn/Cre mice.

(A, B) SN sections showed no transgene expression.

(C) Some mice preserved low to medium levels of stochastic expression in the striatum.

(D) However, slightly fewer individuals did not display any striatal β -gal positivity.

(E, F) Similarly, in the hippocampus some mice displayed low to medium levels of mosaic expression (E), while an equal number of individuals did not have any β -gal positivity (F).

(G, H) Macroscopic view of sectioned brains following X-gal staining reveals the stochasticity of expression with varied levels in different regions of the same brain and between two brains from individuals of the same BiSyn homozygous litter.

(I) High levels of expression were never achieved in the brain regions critical for PD and DLB pathologies. The mice that displayed β -gal positivity in the CPu were not consistently the same individuals with hippocampal positivity, further confirming the stochasticity of expression.

Scale bars = (A-F) 100 μ m.

driver of silencing in another¹⁹⁹. 5-aza-dC has been shown to reverse DNA hypermethylation caused by DNMT1 and 3b²⁰⁰. If our transgene was similarly becoming hypermethylated, 5-aza-dC should be able to restore expression. We also considered deacetylation as our mechanism of silencing. Although this has not previously been shown to affect the CAG promoter to our knowledge, silencing of the CMV promoter, which is a component of the more complex CAG promoter, has been associated with deacetylation. Some researchers have reversed CMV promoter silencing²⁰¹ or have enhanced transgene expression driven by the CMV promoter²⁰² via histone deacetylase complex (HDAC) inhibitors that selectively inhibit class I and II HDACs. If our CAG promoter was similarly undergoing deacetylation, then treatment with SAHA (i.e., an inhibitor of class I and II HDACs [reviewed in ²⁰³]) should restore expression.

To address whether transgene expression can be restored via 5-aza-dC or SAHA exposure, I treated BiSyn/Cre MEFs with these inhibitors. At low concentrations, these treatments did not restore expression. At high concentrations, treatments restored expression in only a few cells, and these concentrations were cytotoxic, leading to cell death. The combined treatment was also insufficient. Together, these data indicate that transgene expression cannot be restored by 5-aza-dC and SAHA treatments. This suggests that neither hypermethylation nor deacetylation of the BiSyn transgene are the likely drivers of stochastic silencing.

Considering incomplete recombination (Figure 12C) in conjunction with lack of expression homogeneity, our transgenic mice were deemed unfit for *in vivo* experimentation. It was therefore pertinent that we consider alternative approaches to answer questions regarding the initiation and propagation mechanisms of α -syn aggregates.

3.2.5 BiSyn system is functional in early passage MEFs and transfected cell lines

Despite lack of expression, I wanted to ensure that our transgene was functional before using it in a novel system. In theory, α -syn aggregation promotes the assembly of Venus-YFP reporter protein fragments into their 3-dimensional conformation, which is fluorescent. To test

the functionality of our system, I exposed transfected NIH3T3 MEFs and BiSyn/Cre/SNCA (see section 2.2 and Table 2 for details regarding this mouse line) MEFs to rotenone, a mitochondrial complex I inhibitor. Of the MEF cultures isolated from BiSyn/Cre/SNCA embryos (n=10), 40% displayed stochastic expression, however this expression diminished once MEFs reached immortalization. Possibly, the FVB background enriched an expression phenotype, whereas expression in the parent BiSyn/Cre mice was diluted in their rich C57BL/6 lineage. Nonetheless, stochastic mosaicism is prominent regardless of the background.

A specific BiSyn/Cre/SNCA MEF culture that displayed relatively high levels of β -gal positivity in early passages was used to test the functionality of our BiSyn system alongside NIH3T3 MEFs transfected with the conditional BiSyn construct. Recombination was stimulated using either 4-OH-tamoxifen for systems that contained endogenous Cre or adenovirus Cre for those that did not. The recombined samples were then treated with a range of rotenone concentrations to stimulate aggregation. 100nM rotenone was sufficient to induce Venus-YFP fragment reconstitution, for both MEF cultures (Figure 14D, H). However, the pattern of fluorescence is remarkably distinct for each cell type. NIH3T3 MEFs exhibited disperse, whole-cell fluorescence. Intriguingly, the BiSyn/Cre/SNCA MEFs displayed punctate signal, which is typically observed in PD patients and models. These data indicate that the aggregation-promoting stimulus rotenone is able to stimulate Venus-YFP fragment reconstitution and thus emit fluorescence, confirming BiSyn functionality.

3.3 Delivery of BiSyn via AAV as an alternative model

Vector Biolabs re-engineered our BiSyn expression cassette into a hybrid AAV vector and generated a stock of virions. The resultant AAV2/9-CMV-BiSyn uses the replication genes from AAV2 in combination with the capsid genes from AAV9. AAV9 capsid presentation has been shown to effectively transduce almost entirely into neurons in the ENS₂₀₄. To validate the novel AAV2/9-CMV-BiSyn approach, two wildtype mice were injected stereotactically with our

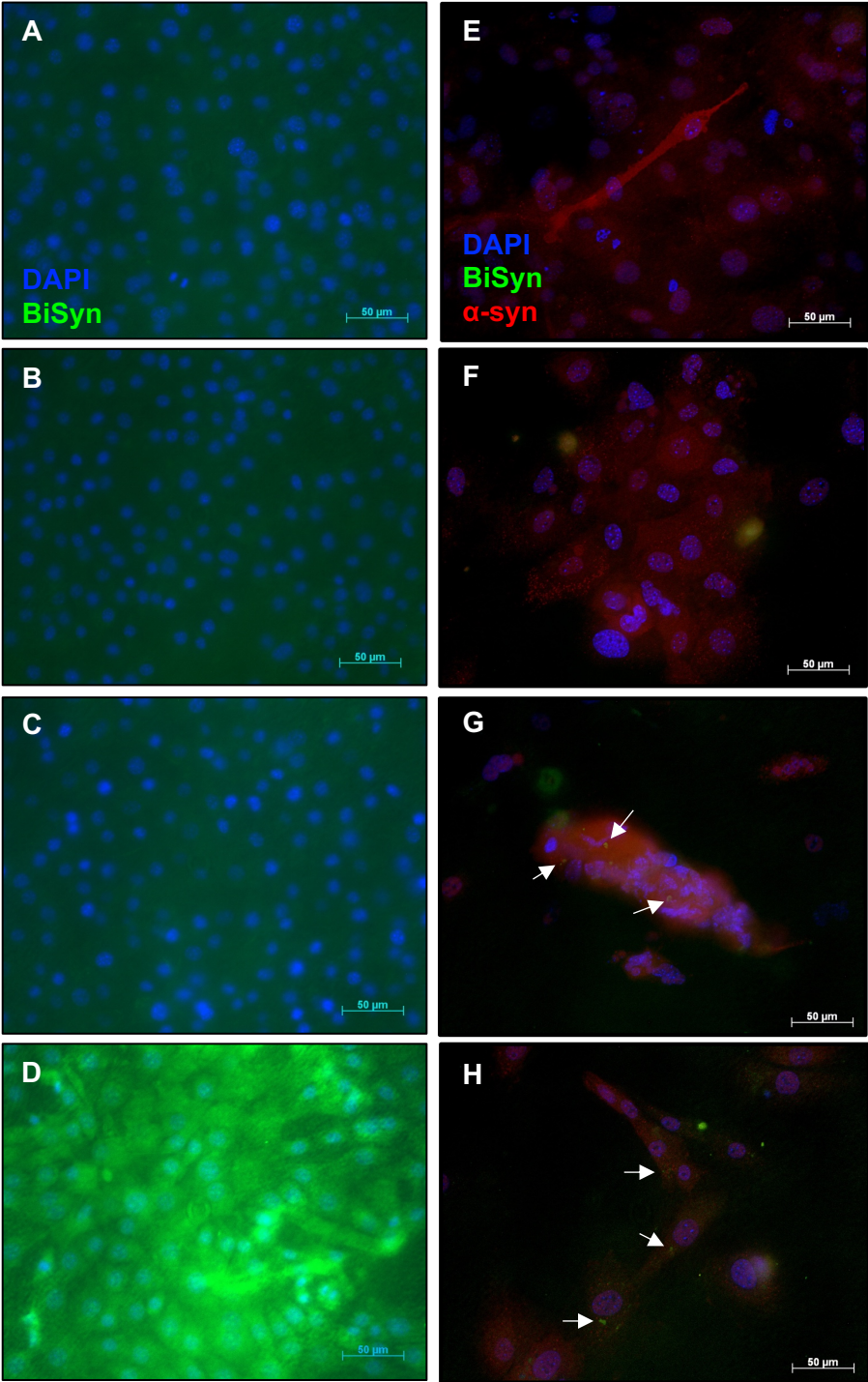


Figure 14: Rotenone-treated MEFs display BiSyn fluorescence.

(A-D) NIH3T3 MEFs (n=4) treated with (A) 0.1% DMSO control, (B) 1nM rotenone, (C) 10nM rotenone, and (D) 100nM rotenone show BiSyn signal (green) only at the highest concentration of the toxin.

(E-H) Immunofluorescence staining with anti- α -synuclein [MJFR1] antibody on BiSyn/Cre/SNCA MEFs (n=1) treated with (E) 0.1% DMSO and (F) 1nM rotenone display α -syn positivity (red) without evidence of Venus-YFP reconstitution. Treating these cells with higher concentrations of (G) 10nM and (H) 100nM rotenone present with a punctate pattern of BiSyn signal (white arrows).

Scale bars = 50 μ m.

virus and one with PBS as a control in the CPu. I performed a thorough analysis of these wildtype brains, outlined below. Subsequently, we moved toward a UCHL1 knockout mouse line²⁰⁵, performing the same injection in wildtype (n=2), hemizygous (n=4), and null (n=2) mice as a pilot investigation for the effect of glutathione deficiency on BiSyn aggregation. Unfortunately, the virus had been thawed too many times leading up to the injections and transduction did not occur in these brains. We have taken this into consideration for future experiments and have recently injected two additional wildtype mice with a fresh aliquot of our virus for future investigation. Herein, I present the data from the initial two wildtype mice. I recognize the limitation in such a small sample size, but further experiments were precluded by the suspension of laboratory work necessitated by the COVID-19 pandemic. Rather than making sophisticated claims from these data, I present them as evidence for validating the AAV2/9-CMV-BiSyn approach as preliminary to future systematic studies.

3.3.1 Pattern of striatal transduction with AAV2/9-CMV-BiSyn

A thorough analysis of the CPu was performed using IF staining with an antibody against human α -syn, showing that AAV2/9-CMV-BiSyn transduced cells throughout the ipsilateral CPu, but not the contralateral (Figure 15A, D, G, J, M). Although a previous graduate student, Madison Gray, assessed the specificity of the MJFR1 antibody for α -syn²⁰⁶, I used an anti-GFP antibody to ensure its specificity for our BiSyn fragments. The two methods presented a similar expression pattern (data not shown). BiSyn was present in rostrosuperior regions of the CPu (Figure 15B), extending into laterosuperior CPu regions residing next to the cortex and the anterior horn of the lateral ventricle at the level of the injection site (Figure 15E), and through to caudosuperior regions (Figure 15K, N). Fewer cells displayed Venus-YFP reconstitution in CPu regions furthest from the injection site compared with the vast number of cells emitting BiSyn signal surrounding the injection site. An extended region of α -syn positivity was present around the needle tract, giving evidence for transduction in the medial CPu (Figure 15F, H, L).

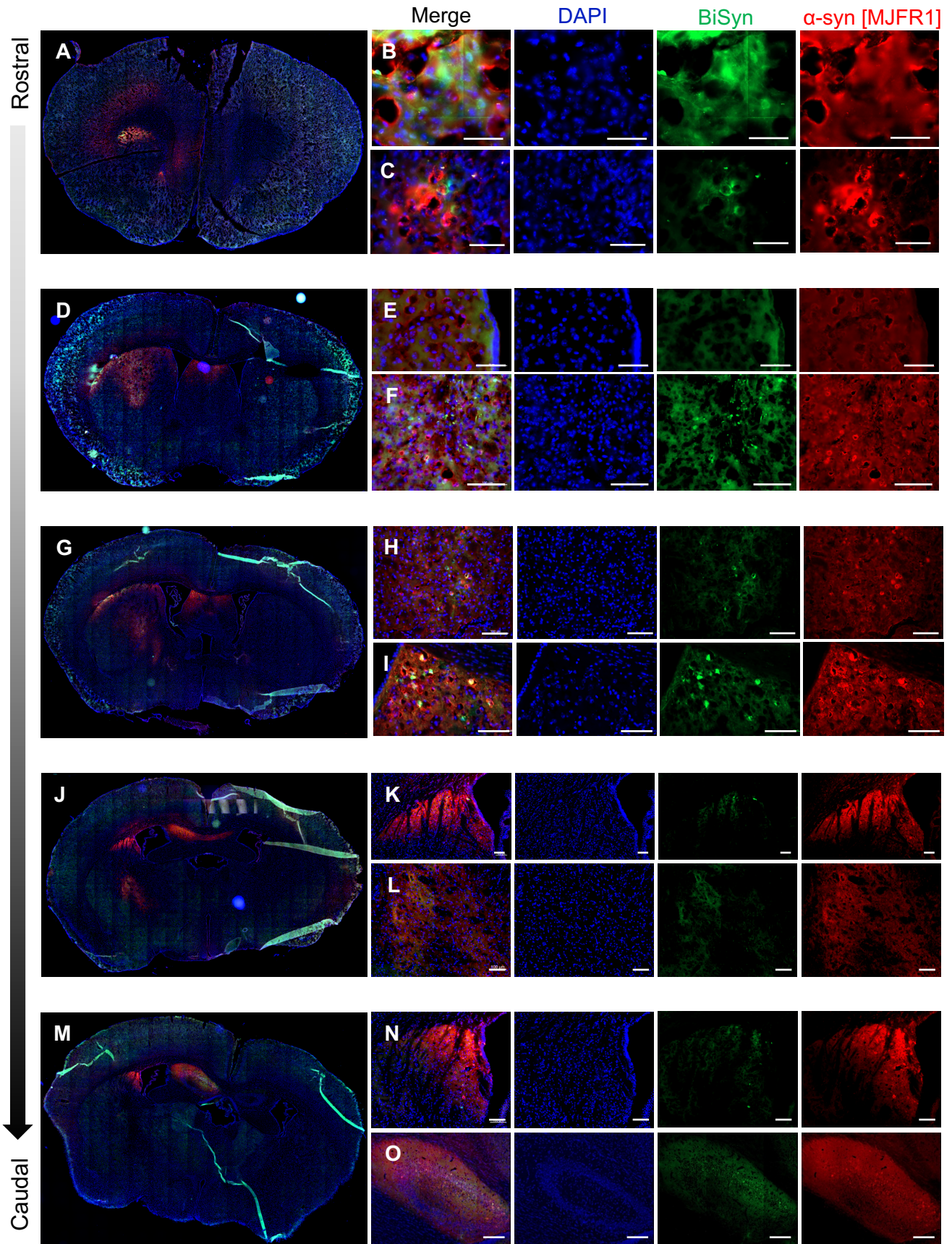


Figure 15: BiSyn expression and aggregation from rostral to caudal CPu regions.

(A-O) Immunofluorescence staining with anti- α -synuclein [MJFR1] antibody was performed on 10 μ m thick brain sections.

(A-C) α -syn positivity co-localizing with some BiSyn signal is present in the ipsilateral (B) rostral CPu and (C) the medial nucleus accumbens.

(D-F) At the level of the injection site, high levels of α -syn positivity and BiSyn signal are present in the (E) subventricular zone and (F) medial CPu.

(G-I) Caudal to the injection site, maintained expression and BiSyn signal are present in laterosuperior and (H) medial CPu areas as well as (I) both hemispheres of the lateral septal nucleus, dorsal fornix, and septofimbrial nucleus.

(J-L) Further in the caudal direction, BiSyn signal is present at lower levels in the (K) superior and (L) medial CPu.

(M-O) In the most caudal CPu region examined, (N) α -syn positivity and low levels of BiSyn puncta are present in the superior CPu adjacent to the lateral ventricle. (O) The superior CA3 hippocampal layer also exhibits α -syn positivity and Venus-YFP reconstitution.

Scale bars = (B, C, E) 50 μ m; (F, H, I, K, L, N) 100 μ m; (O) 200 μ m.

Transduced cells appear to be neuronal. High magnification imaging reveals BiSyn signal throughout the soma, extending into dendrites and dendritic spines, as well as axons and terminal buttons (Figure 16A, B). Since SNpc dopaminergic neurons degenerate in Parkinson's brains, which in turn leads to striatal dopaminergic denervation, I wanted to identify whether transduction occurred in dopaminergic axon terminals at the CPu injection site. Herein, CPu sections were stained with an anti-TH antibody (i.e., marker of catecholaminergic neurons), demonstrating that BiSyn is, in fact, present in TH+ axon terminals in the CPu (Figure 16B). This indicates that our hybrid AAV is able to transduce in both cell bodies and axon terminals at the CPu injection site.

3.3.2 *Viral propagation via CSF*

α -syn positivity and Venus-YFP reconstitution was not confined to the CPu. There is evidence that the virus was transported through cerebral spinal fluid (CSF). α -syn positivity was present in the lateral septal nucleus, dorsal fornix, and septofimbrial nucleus; structures which lie between the anterior horns of the lateral ventricle (Figure 15I). The right anterior horn neighbours the ipsilateral laterosuperior CPu, which displayed rostrocaudal BiSyn expression. These structures showed greater expression on the ipsilateral side to the injection site, however expression was also present at slightly lower levels on the contralateral side.

In the hippocampal region caudal to the septum, there was transduction of cells throughout the superior part of the CA3 layer (Figure 15O). Venus-YFP reconstitution, was present throughout these regions, though puncta were not observed.

α -syn positivity and BiSyn signal were present in a confined region of the dopamine-rich nucleus accumbens in both the mice analyzed. More specifically, these transduced cell bodies appear to be located within the ipsilateral rostral migratory stream (RMS; Figure 15C).

The CPu does not have direct connections with these structures, which suggests that the virus was transported through CSF. Despite these regions showing high levels of

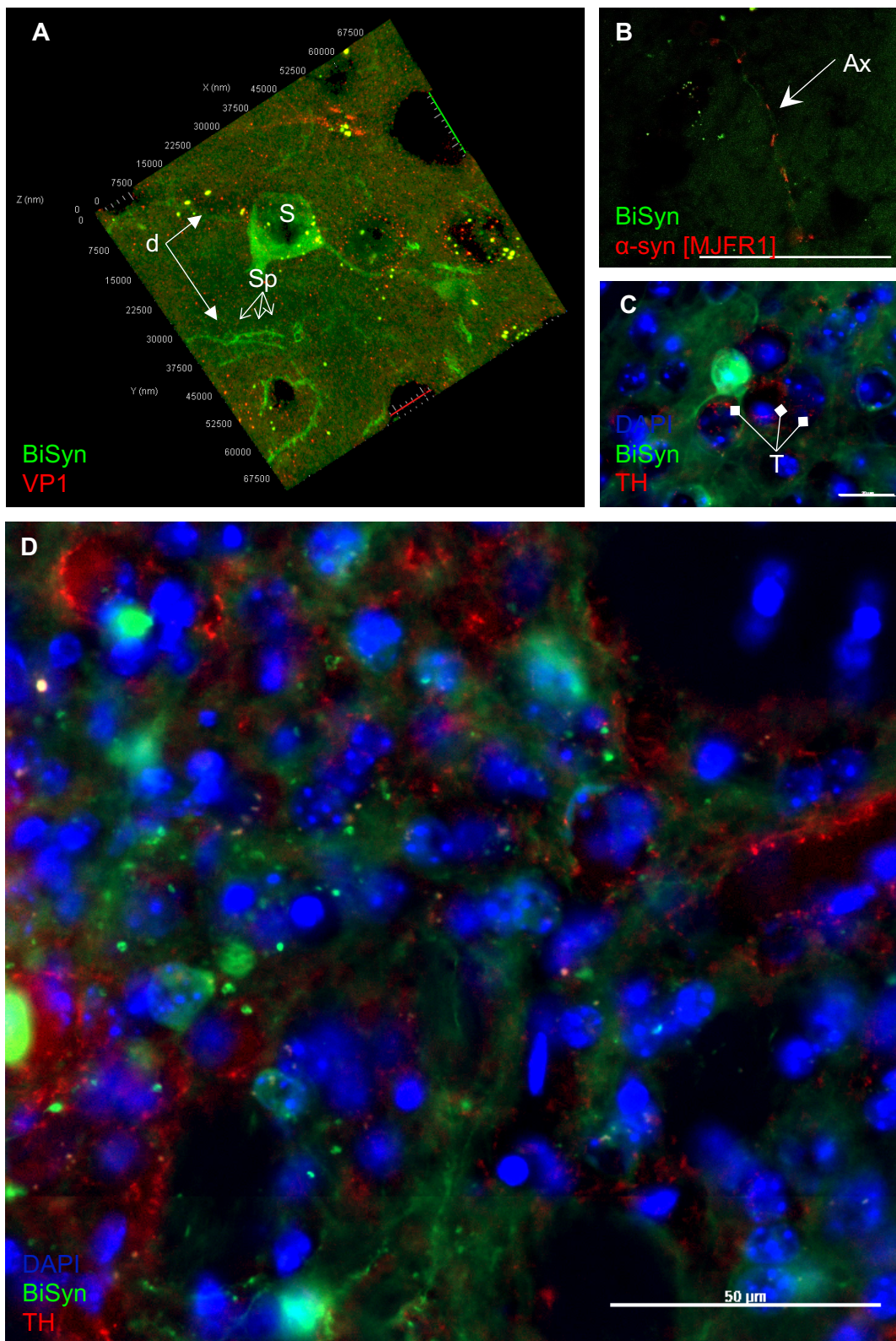


Figure 16: BiSyn expression extends through the entirety of the neuron.

(A, B) Venus-YFP fluorescence (green) is observed in the soma, the dendritic processes and dendritic spines (A) as well as axons co-labelling with anti- α -synuclein [MJFR1] antibody (B).

(C) IF staining with anti-TH antibody showing a neuron containing BiSyn signal surrounded by TH+ axon terminals in the CPu.

(D) From the same section as that in (C), several TH+ axon terminals containing BiSyn signal (co-labelling appears orange) are observed.

Ax = axon; d = dendrite; S = soma; Sp = dendritic spine; T = axon terminal.

Scale bars = (B, D) 50 μ m; (C) 20 μ m.

expression, viral spread via CSF did not result whole-brain transduction. Regions that have direct neuronal connections with the CPu displayed significantly greater expression levels than any other brain region, with the exception of these named regions that all reside adjacent to the anterior horns of the lateral ventricle.

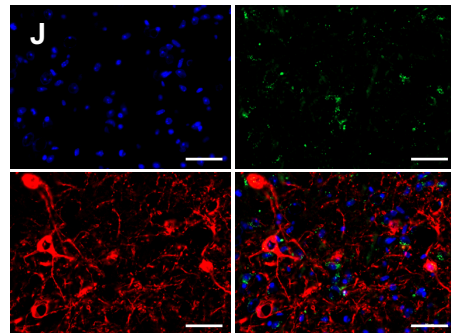
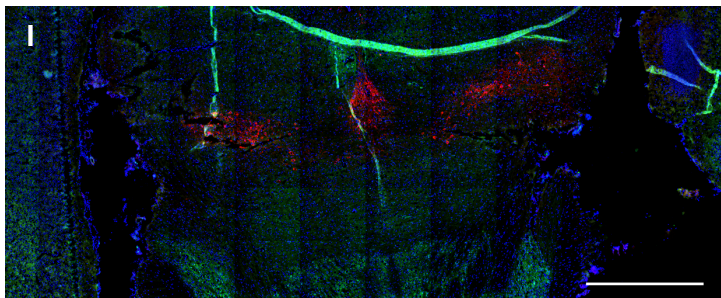
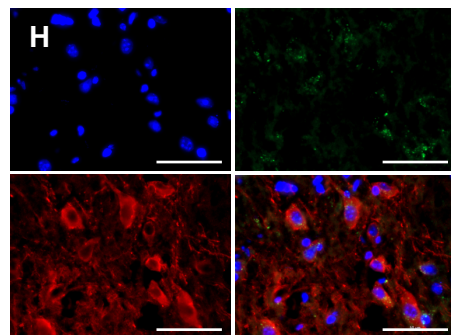
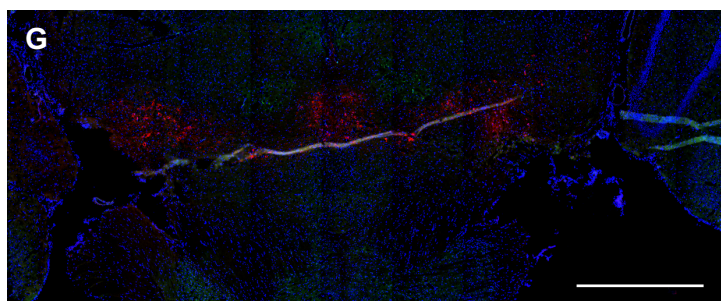
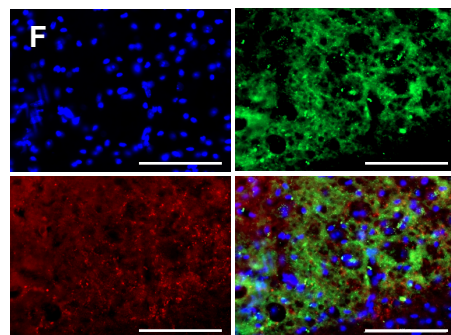
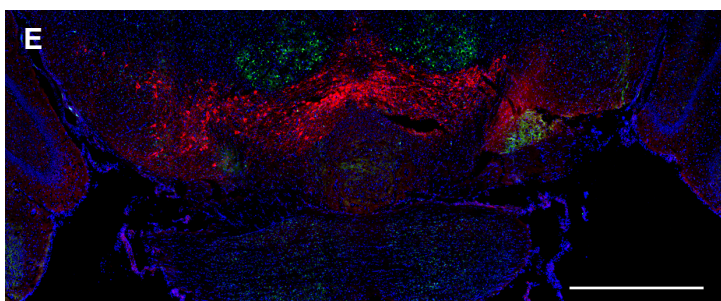
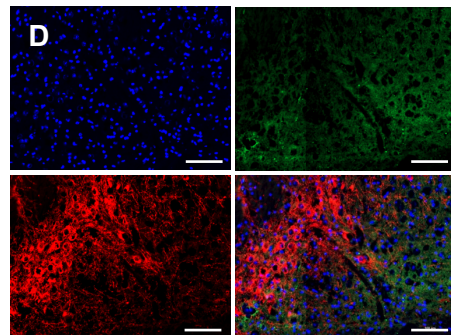
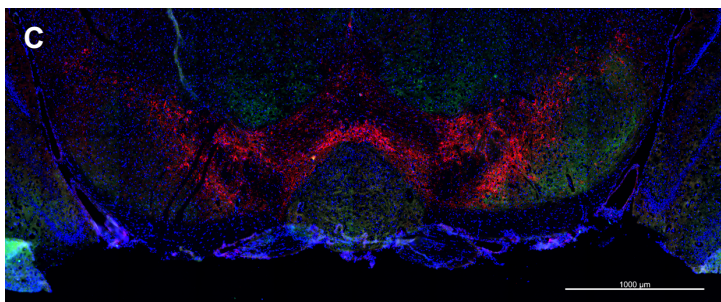
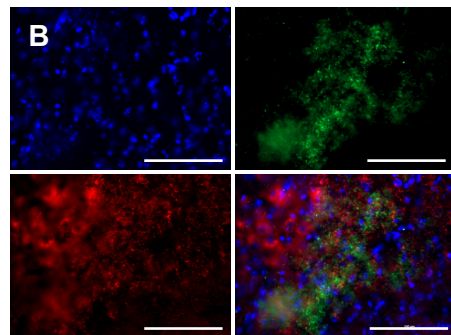
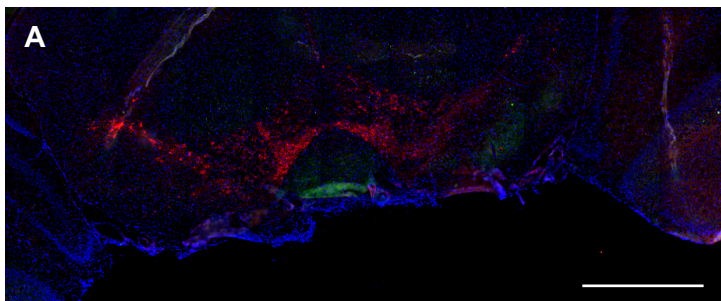
3.3.3 Viral propagation via structural connectivity

Due to the immense interconnectivity between the CPu and SN, and the importance of this nigrostriatal circuitry in PD, I investigated viral transport between these regions. Similar to the CPu, I performed a thorough analysis throughout the SN. Immunostaining with anti-TH antibody revealed the presence of BiSyn signal throughout the SN, however at lower levels in the most rostral and caudal regions (Figure 17A, C, E, G, I). BiSyn signal was observed in TH+ SNpc neuronal somas, with some occurrence of puncta (Figure 17D, H, J). There was also BiSyn signal in the substantia nigra pars reticulata (SNr); despite lack of evidence for Venus-YFP reconstitution in SNr cell bodies, there was an abundance of TH+ axon terminals containing BiSyn fluorescence (Figure 17B, D, F). This limited data confirms that AAV9 capsid presentation enables transport in both anterograde and retrograde directions, which was demonstrated in a previous study²⁰⁷. Interestingly, the furthest caudal SN level shows BiSyn puncta in both TH+ and non-dopaminergic somas (Figure 17J), which may provide evidence for the cell-to-cell propagation of BiSyn since only the TH+ axons project to the CPu.

3.3.4 Viral uptake into glial cells

Initially, we intended to use the anti-viral capsid protein VP1 antibody as our primary marker of viral propagation throughout the brain. Despite the abundance of BiSyn expression at 28dpi, we did not observe any VP1+ neurons. Instead, positive staining was located within glia (Figure 18). These VP1+ glia appeared to be microglial. This pattern of staining was observed in

Rostral



Caudal

Figure 17: Viral transport occurs in antero- and retrograde directions.

(A, C, E, G, I) Immunofluorescence staining with anti-TH antibody (red) throughout the SN shows some colocalization with Venus-YFP reconstitution (green).

(B) At the rostral SN level, BiSyn signal is present in axons.

(D) The interface of TH+ cell bodies in the SNpc and TH+ axon terminals in the SNr with BiSyn co-localization in both.

(F) There is an abundance BiSyn signal in TH+ axon terminals in the SNr.

(H) TH+ SNpc cell bodies contain BiSyn puncta.

(J) Although very little BiSyn signal remains in caudal SN regions, both TH+ and TH- cell bodies show punctate BiSyn inclusion bodies, which may indicate cell-to-cell propagation of aggregates.

Scale bars = (A, C, E, G, I) 1000 μ m; (B, D, F) 100 μ m; (H, J) 50 μ m.

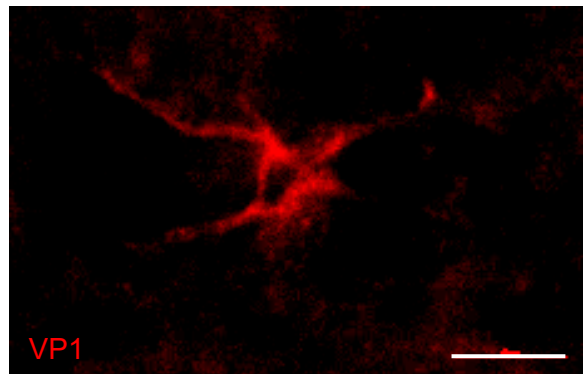
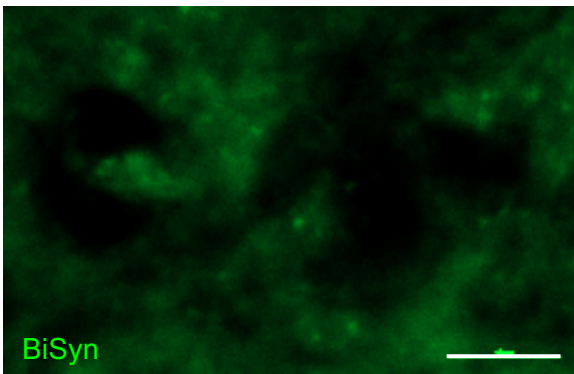
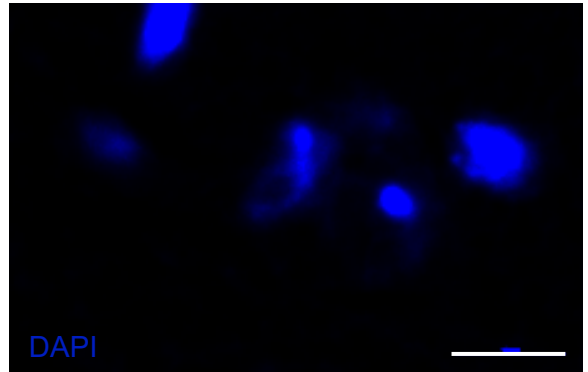
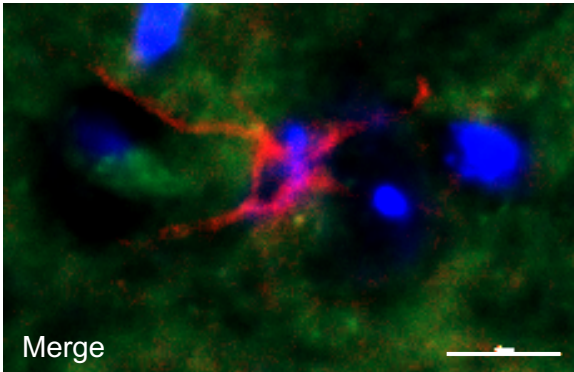


Figure 18: AAV capsid uptake into glia that neighbour BiSyn-containing axon termini in the SNr.

The structure of VP1+ cells (red) resembles microglia. These positively stained cells are located within a meshwork of axon termini that contain BiSyn aggregates.

Scale bar = 10µm.

both the CPu and SN. This suggests that microglia might play a role in AAV capsid degradation after deposition of target DNA into the neuronal nucleus.

4.0 Discussion

4.1 BiSyn/Cre transgenic mouse model

Although our BiSyn/Cre transgenic mice express BiSyn in a stochastic and mosaic fashion, and consequently cannot be used for future experimentation, this work reiterates the significance of position effect variegation. Expression in our mice demonstrate the dynamic nature of the boundary between eu- and heterochromatin. As well, our efforts to demonstrate patterns of silencing in development have uncovered the possibility of an earlier onset of position effect variegation (PEV) than was previously established.

4.1.1 *Re-evaluating the ubiquitous transgenic model*

The theory behind our ubiquitous transgenic system is quite appealing. Under the premise that α -syn possesses properties similar to PrP^{Sc}, a healthy cell becomes diseased when misfolded α -syn seeds the conversion of wildtype α -syn proteins to misfolded and aggregated species^{57,78,91,98,99}. It is therefore critical that the healthy cell expresses the native α -syn protein and therein, a ubiquitous system would seemingly be ideal. We demonstrated, however, that raw expression in the CNS was limited and therefore the ability of α -syn to seed misfolding and aggregation in healthy cells would have been inconsistent, not only between individuals but also within a single individual.

Should our transgenic system have been successful, α -syn overexpression would have occurred in parallel. Overexpression of α -syn alone is sufficient to stimulate its self-aggregation tendency, which occurs from familial *PARK4* mutations, and in particular *SNCA* trisomy^{66,67}. Therefore, distinguishing between propagated and spontaneous aggregates in a system that ubiquitously overexpresses α -syn may have been impractical. BiSyn was designed to target the earliest stages of initiation and propagation in order to identify mechanisms and pathways in the

ENS. For such purpose, a non-ubiquitous system may in fact be more ideal than we previously hypothesized. Although our novel AAV2/9-CMV-BiSyn system does not allow for recruitment of aggregate species in non-transduced cells, we are able to visualize aggregate propagation in its earliest stages.

4.1.2 Tamoxifen-inducible recombination efficiency

Our tamoxifen-inducible system was not entirely efficient in promoting recombination at the dose corresponding to our lab's protocol (180mg/kg body weight for 5 days) and therefore recombination was not occurring in all cells. Another study showed that recombination is dose-dependent wherein a higher tamoxifen dose (225mg/kg body weight for 5 days) was more successful at stimulating recombination in most tissues assessed including the hippocampus, cortex and intestines¹⁸⁵. Our observational assessment of recombination in testes, which were not assessed in the aforementioned study, revealed a highly mosaic phenotype post-recombination.

4.1.3 Zygotic genome activation

Single cell sequencing has discredited the longstanding notion that there is a specific developmental time point when maternal gene expression shifts to zygotic genome activation. A review published in *Developmental Cell* in 2017 describes instead a transition phase during which paternal zygotic alleles begin to sharply demethylate in the 1-cell stage, while maternal zygotic alleles are demethylated at a much slower rate. By the 8-cell stage, euchromatin is accessible, resembling that of somatic cells, and facilitating a drastic increase in gene expression [reviewed in 208]. We have demonstrated BiSyn silencing through the 1-, 2-, and 4-cell zygotic stages followed by an intriguing shift at the 8-cell stage when individuals began expressing our transgene. By the blastocyst stage, all individuals displayed mosaicism. The ability of some cells, but not others, to activate BiSyn expression renders transgene silencing in

the oocyte an unlikely cause of transgene silencing in zygotes. Rather, this observation suggests the source of silencing to stem from the site of transgene integration with respect to chromatin accessibility.

4.1.4 Mosaicism attributed to position effects

If transgene silencing was the result of a hypermethylated or deacetylated CAG promoter, as reported in other transgenic systems^{198,199}, treatments with 5-aza-dC and SAHA should have recovered expression^{200–203}. Since expression could not be restored, there are other factors to consider. We deliberated the leakiness of the Cre-lox system, however a previous study indicated that recombination in the absence of tamoxifen is minimal¹⁸⁵ and therefore could not be responsible for the high levels of silencing observed in our system. Further, tamoxifen-treated intestines in my assessment of ENS expression, which would have also accounted for recombination due to a leaky Cre-Lox system, showed a complete lack of expression.

Position effect variegation (PEV) describes the silencing of a gene in some somatic cells, but not others, resulting in a mosaic expression phenotype. An otherwise euchromatic gene can adopt a condensed heterochromatin-like structure with regularity in nucleosome array^{209,210}. This tightly packed arrangement reduces histone accessibility and thus diminishes gene expression. Our transgenic mouse expression data can be explained by PEV.

Drosophila melanogaster typically have red eye pigmentation; however, researchers observed some flies that display mosaicism. Herein, flies exhibited variegated expression of red and white pigmentation due to PEV. In 1989, Joel C. Eissenberg proposed a model for PEV, suggesting that chromosome rearrangement can alter the position of heterochromatic breakpoints (Figure 19A). When a rearrangement places a gene between a heterochromatic initiator and stop signal, the heterochromatin can extend into an otherwise euchromatic region (Figure 19B)²¹¹. Expression is therefore unstable at the interface between euchromatin and

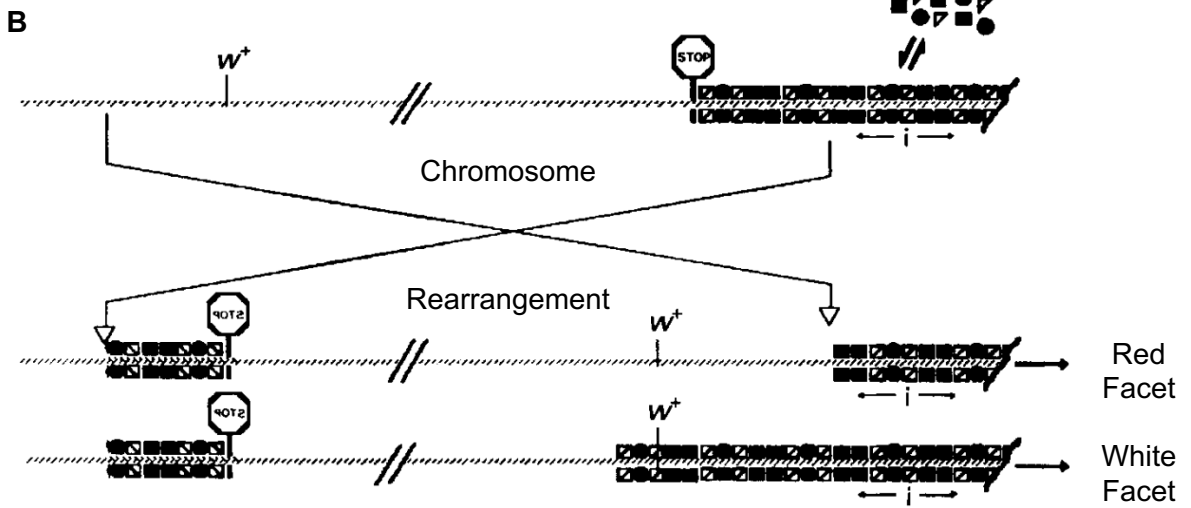
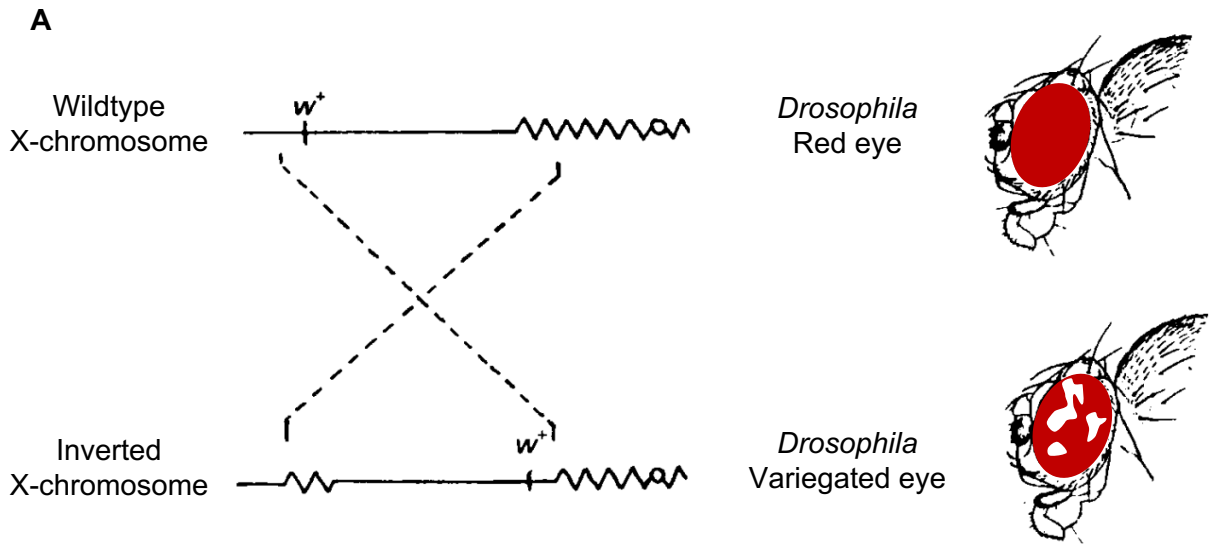


Figure 19: Position effect variegation in the *Drosophila* eye.

(A) The white locus (w^+) is critical for determining red pigment in the *Drosophila* eye. It is normally located in the euchromatic (straight line) region distal to heterochromatin (zig-zag line). In the case of the inverted X-chromosome, there is abnormal translocation of w^+ resulting from chromosomal breaks, which has moved w^+ between heterochromatic breakpoints. The corresponding flies have variegated eye pigmentation.

(B) Chromosome rearrangements that cause a heterochromatic breakpoint ($//$) to be located between initiator (i) and stop signals can cause heterochromatin to spread into an otherwise euchromatic region. In *Drosophila*, heterochromatin spreading into the region containing w^+ leads to its inactivation (bottom, white facet). The extent of heterochromatin spreading varies in each cell causing mosaic w^+ expression.

Adapted from ²¹¹. Permission to reproduce found in Appendix H.

heterochromatin²¹². In early development, genes that are included in the heterochromatic region become inactive. Each cell presents a varying degree of heterochromatin extension and thus the proportion of cells with consequent gene inactivation regulates the degree of mosaicism²¹¹. Rather than a designated boundary existing between hetero- and euchromatic domains, this region can be continuous, contributing to the expression variability between cells²¹².

Eissenberg's group later demonstrated that heterochromatic silencing, and thus the extent of PEV, is dependent on the developmental state²¹², as we have shown in our BiSyn/Cre transgenic mice. The highly mosaic phenotype presented a high degree of stochasticity between cells and individuals, consistent with PEV. Promoter strength cannot suppress PEV²¹². Therefore, the intrinsic efficiency of the CAG promoter¹⁹⁷ has no effect on heterochromatin spreading and mosaic expression phenotype in accordance with PEV. While Eissenberg and colleagues proposed that gastrulation marks the initiation of PEV²¹², we have shown that PEV can begin as early as the 8-cell stage and is prevalent in all individuals at the blastocyst stage.

In retrospect, it would have been worthwhile to breed progeny from more than one transgenic founder, which is typically the norm in our breeding schemes. Our original effort to generate 12 BiSyn chimeras resulted in only one that was able to produce transgenic offspring. Due to the extensive number of intercrosses that were anticipated to generate our BiSyn/Cre/SNCA mouse line by incorporating *Pac.4* in the absence of endogenous *Snca*, we chose to proceed with only one BiSyn founder. In accordance with the PEV hypothesis, multiple founders, and thus multiple transgene insertion sites, would likely have eliminated the observed mosaic phenotype and permitted ubiquitous BiSyn expression.

4.2 AAV2/9-CMV-BiSyn model

With a reputation for generating more ROS than any other cell type in the CNS²³⁻²⁶, nigral dopaminergic neurons have a heightened susceptibility to pathological α -syn and subsequent degeneration^{21,22}. We have provided evidence for viral uptake in striatal TH+ axon

terminals and have demonstrated that AAV2/9-CMV-BiSyn can transport both antero- and retrogradely, with BiSyn signal present in SNr axon termini and SNpc TH+ somas. We have also demonstrated intriguing evidence for the potential transduction of neural progenitor cells and provide insight into the interplay of inflammation, pathogenesis, and neurodegeneration in the olfactory bulb (OB).

4.2.1 Transduction specificity

Despite previous studies demonstrating the specificity for AAV9 to transduce almost entirely into neurons^{204,207}, further assessment for this specificity from our hybrid AAV2/9 is required. Our system expresses the capsid proteins associated with AAV9 and is therefore considered to act accordingly. We have, in fact, demonstrated the capacity for AAV2/9-CMV-BiSyn to transduce into neurons, however, additional staining is required to assess neuronal exclusivity. Future staining with PGP9.5, a neuronal marker, is expected to show colocalization with our BiSyn signal. Conversely, we anticipate mutual exclusivity of our BiSyn signal and staining with the glial marker GFAP. These experiments were in progress when laboratory work was suspended due to the COVID-19 pandemic.

4.2.2 Expression patterns

Our BiSyn signal presented differently in different neuronal structures and in distinct brain regions. At the injection site, entire somas and neurites displayed brilliant fluorescence, which is consistent with the previously mentioned study by McLean and colleagues⁷⁷ who used a similar approach to our AAV2/9-CMV-BiSyn. TH+ cell bodies in the SNpc displayed either the same fluorescence throughout as observed in the CPu, or punctate inclusion bodies in more caudal regions. Interestingly, we noticed a bead-like pattern in lengthy neurites, both in the CPu and SNpc. McLean's group demonstrated that this beading pattern is consistent with dystrophic neurites^{77,179}. Rather than our PBS injection as a control, their group uses a full-length Venus-

YFP cassette, enabling comparison between the pure fluorescent signal and fluorescence associated with α -syn pathology. While the Venus-YFP fluorescence is diffuse and supports healthy axons, the α -syn associated fluorescence precipitates puncta and corresponds to dystrophic neurites^{77,179}, consistent with an earlier report from 1998 in the *Journal of Neuropathology and Experimental Neurology*²¹³.

4.2.3 AAV propagation tendencies

The Braak hypothesis relies heavily on retrograde propagation of α -syn aggregates^{100,102–104} wherein these hypothesized prion-like species exploit axonal and transneuronal transport mechanisms¹¹³. In order to use our novel tool to study various aspects of the proposed dual-hit hypothesis^{103,104}, our AAV2/9-CMV-BiSyn system must propagate in a retrograde fashion. At 28dpi, we demonstrated the presence of both antero- and retrograde propagation from the CPu to the SNr and SNpc, respectively. The differentiation in expression level between the two SN parts, however, likely indicates that our system has a greater ability to travel in an anterograde rather than retrograde manner. The directional transport ability of AAVs is serotype dependent²¹⁴. Presentation of AAV9 capsid has been associated with bi-directional transport²⁰⁷, consistent with our results. The capacity for anterograde transport of AAV9 has a strong dose-dependence²⁰⁷. Our study's relatively high viral titer (4.9×10^{13} vg/mL) might account for this discrepancy in direction of propagation. In future endeavours, a 10-fold lower viral titer has been shown to be sufficient in its transduction capacity²⁰⁴ and also promotes lower levels of anterograde transport without disrupting retrograde transport²⁰⁷. Reducing the volume of injected substance should also prevent transduction in non-connected structures, which likely transported through CSF. Nonetheless, it would be negligent to disregard the vast divergence of dopaminergic SNpc axonal branching throughout the CPu^{215,216}, and in accordance we may

instead be observing signal dilution as only select terminals from any single neuron might be located near the injection site.

Regardless of antero- or retrograde transport tendencies, we observed finite evidence supporting cell-to-cell spread of BiSyn signal. AAVs have an innate inability to self-propagate²¹⁷. Once internalized, AAVs undergo one of two fates: proteolysis by the proteasome or nuclear transport via nuclear pores. In the nucleus, our single-stranded vector DNA encoding BiSyn is converted to double-stranded DNA by the action of mouse DNA polymerases. The inverted terminal repeats that flank our BiSyn cassette stimulate recombination, which can either enable BiSyn to incorporate into the mouse genome, which is unsustainable and occurs at low frequencies, or recombination can convert BiSyn into a circular episomal genome, which persists in the nucleus and offers sustained transgene expression (Figure 20) [reviewed in ²¹⁸]. With the mechanism of AAV transduction in mind, it is conceivable that any BiSyn signal residing outside the neurons directly connecting the CPu and SNpc could therefore only exist in adjacent cells owing to cell-to-cell propagation of BiSyn. Further investigation is required to verify whether this hypothesized prion-like spread of BiSyn is, in fact, occurring.

4.2.4 Adult neurogenesis and Parkinson's disease

We have demonstrated that AAV2/9-CMV-BiSyn transduced neurons in the subventricular zone (SVZ), a narrow region located along the outer wall of the lateral ventricles, adjacent to the CPu. Mammalian adult neurogenesis, first described by Joseph Altman in 1962²¹⁹, occurs in two CNS locations: the SVZ and the subgranular zone in the hippocampus. Neuronal progenitors that are produced in the SVZ migrate along the rostral migratory stream (RMS) to the olfactory bulb (Figure 21)^{220,221}. As the cells travel through the RMS, they differentiate into olfactory periglomerular and granule GABAergic interneurons²²¹⁻²²³. Intriguingly, we found BiSyn signal in a compact region of the medial nucleus accumbens, which we postulate to be the RMS. The cells that presented BiSyn signal in this region were small and

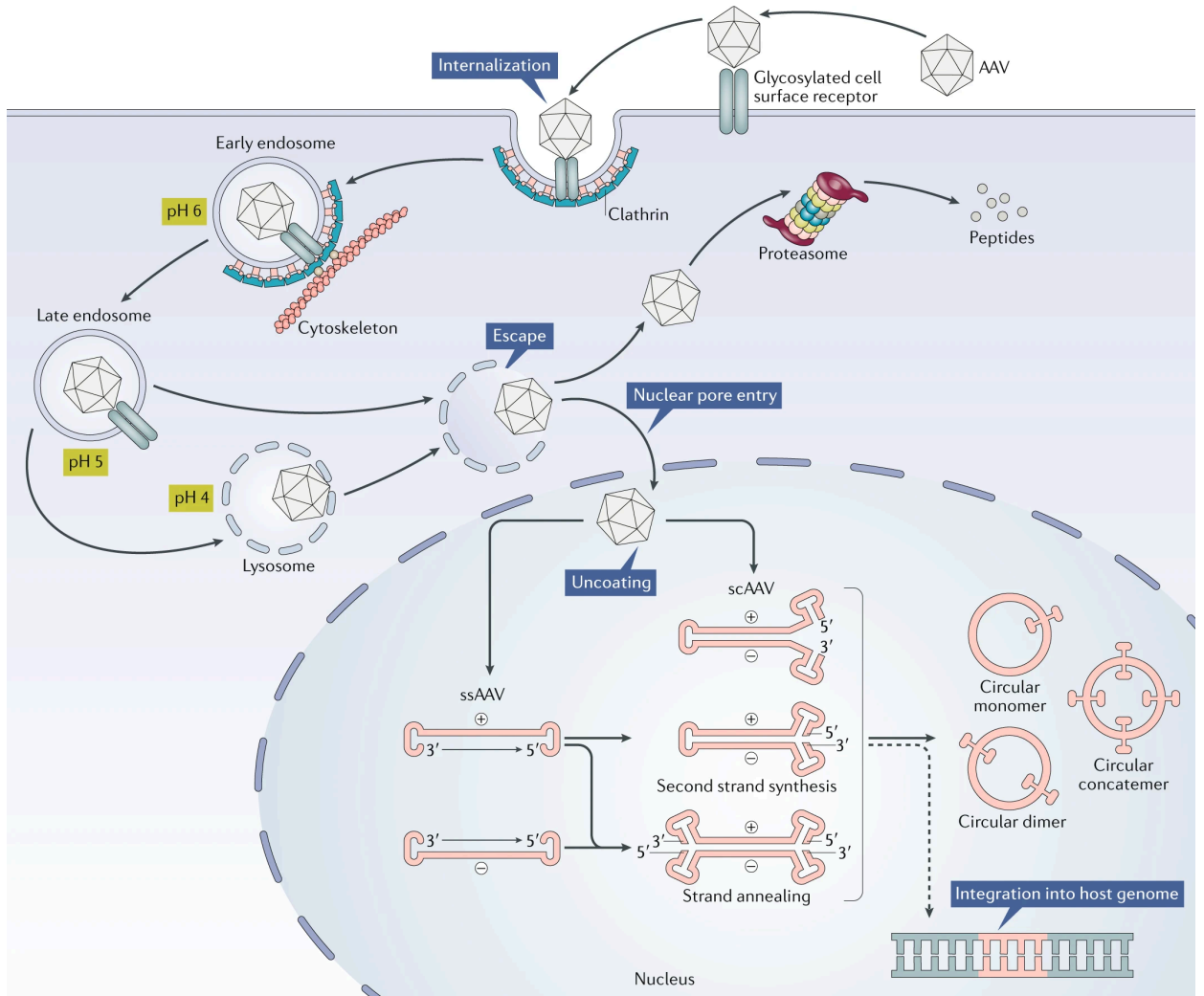


Figure 20: Mechanism of rAAV transduction.

Glycosylated cell surface receptors bind AAV, stimulating clathrin-mediated endocytosis. This process is called internalization. The capsid proteins change conformation in the endosome due to the altered pH. This facilitates endosomal escape. The AAV can then follow one of two pathways: proteolysis by the proteasome or nuclear transport via nuclear pores. Once in the nucleus, the AAV undergoes uncoating, wherein the capsid proteins are removed, enabling access to the target DNA. Once in a double-stranded form either by means of self-complimentary AAV or conversion of single-stranded DNA via synthesis of the second strand by DNA polymerases from the host cell. Recombination is stimulated by the viral inverted terminal repeats that flank the target gene. This converts the target DNA into a circular episomal genome that persists independently in the nucleus or, less commonly can be incorporated into the host genome.

From ²¹⁸. Permission to reproduce found in Appendix I.

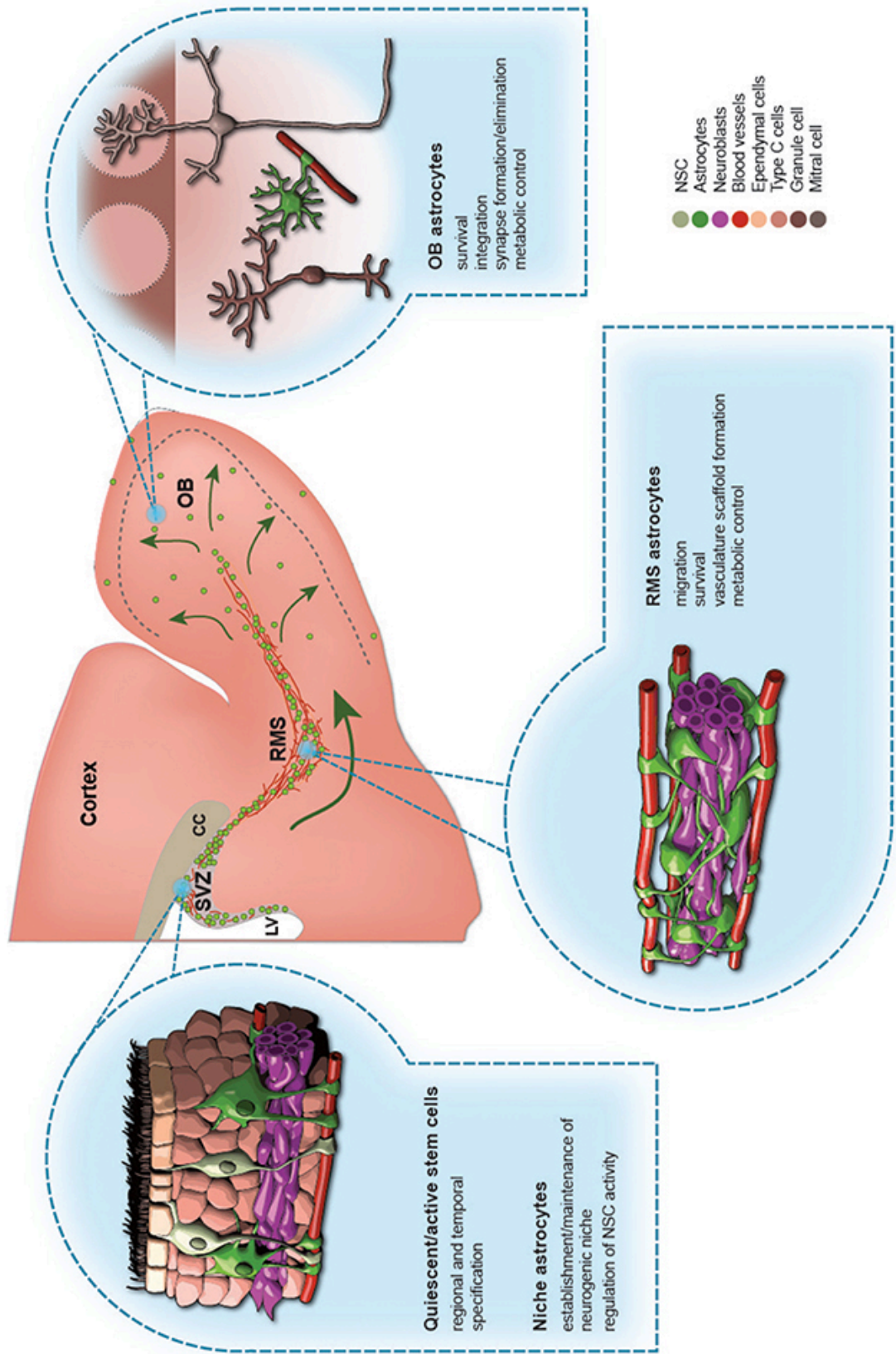


Figure 21: The rostral migratory stream.

Neural progenitors are produced in the SVZ. They travel along the RMS to reach the OB. The RMS is sheathed in an astroglial tube, which provides scaffolding for the vasculature system. Astrocytes have many important functions throughout this network, which are highlighted in the schematic.

From ²²⁴. Permission to reproduce under the Creative Commons Attributions License.

round with BiSyn signal evident in surrounding cell processes, appearing much like the morphology presented in a *BMC Neuroscience* article in 2005 depicting migrating neural progenitors through the RMS²²⁵. Since differentiated neurons from the RMS incorporate into the granule cell layer in the OB, we propose that neural stem cells were transduced in the SVZ and began migrating to the olfactory bulb via the RMS. Transgene overexpression led to the visualization of α -syn aggregates, enabling detection in the RMS. Further studies, including immunostaining for neural stem cell markers (e.g., neural cell adhesion molecule, nestin, etc.), are required to elucidate this intriguing possibility.

Interestingly, olfaction is seldom considered in a routine clinical examination despite its relevance in a number of neurological diseases [reviewed in ²²⁶]. Early loss of odor discrimination is common in 90% of PD patients²²⁷. Accordingly, impaired SVZ neuronal progenitor proliferation and subsequent migration to OB regions has been observed in both PD patients and animal models^{228,229}, which has been specifically correlated with compromised odor discrimination in rodents²²². Zapiec and colleagues recently described a novel 3-dimensional approach, demonstrating that higher phosphorylated-serine-129- α -syn concentrations are correlated with lower glomerular voxel volume (i.e., the 3-dimensional volume within the olfactory bulb that is immunohistochemically positive for glomeruli)²³⁰. Compared to controls, the glomerular voxel volume is reduced by approximately 50% in PD patients²³⁰. Although age-related reductions in progenitor proliferation have been established²²⁹, this compounding loss in PD patients is at the consequence of dopaminergic denervation^{228,229}. Similar to the projections from SNpc to CPU₁₈, dopaminergic fibers from the SNpc project topographically to the SVZ²²⁹. Therefore, nigral dopaminergic atrophy reduces DA release at the SVZ, and in particular reduced D2 receptor binding is associated with impaired progenitor proliferation²²⁸. Various PD rodent models have shown distinct alterations in neurogenesis, including reduced proliferation, altered stem cell fate, and altered migration patterns [reviewed in ²³¹]. In the hippocampal

subgranular zone, aberrant and aggregated α -syn mediates repression of Notch1 signalling, which in turn prevents neural progenitor proliferation, maturation and survival²³².

Transduction in regions that generate neural progenitors creates possibilities for regenerative therapeutics using rAAV. For example, Yu and colleagues showed that transduction of SVZ neural progenitors with AAV serotype 1 containing brain derived neurotrophic factor (BDNF) significantly helped with progenitor migration in a rodent stroke model, corresponding to significant functional recovery²³³. More relevant to PD, a similar AAV approach delivering vector BDNF promoted recruitment of SVZ progenitors to the CPu of lesioned rodents and facilitated neuronal differentiation²³⁴. If researchers can manipulate the chemoattractive signals that guide migration of neural progenitors, which was revolutionized in these rodent models, we can guide neural progenitors specifically to the SNpc. Thereafter, a mechanism to stimulate synaptogenesis into CPu regions could offer functional recovery in Parkinson's disease. In this respect, it is critical to understand neurodevelopmental chemokine signalling to innovate regenerative therapeutics.

In combination with the prion-like propagation of α -syn aggregates^{57,78,91,98,99} and the presence of SNpc axon terminals within the SVZ²²⁹, our data suggest a potential alternative route from that suggested by Braak and colleagues. Since SVZ neural progenitors can acquire BiSyn signal and migrate to the OB via the RMS, it is conceivable that α -syn aggregates could travel in a retrograde fashion from the OB to SNpc regions using the RMS as a means for transport. In addition to their established ability to transmit via transneuronal mechanisms, prions have also been shown to capitalize on hematogenous routes [^{235–237}, reviewed in ²³⁸]. Considering α -syn to have prion-like properties, the pathogenic protein could exploit the vasculature that courses through the RMS and accumulate in neural progenitors that lie in the SVZ. Moreover, the RMS is critical for the intranasal administration of drugs to the CNS²³⁹, linking the permeability of its blood-brain barrier. Nigral dopaminergic axons might then acquire toxic α -syn oligomers via transneuronal means. In a similar way, the DMV might be indirectly

vulnerable to hematogenic neuroinvasion. Circumventricular organs act as communication pathways between the CNS and periphery. They have the ability to exchange large molecules through their fenestrated capillaries and are characterized by their inherent lack of blood-brain barrier [reviewed in ²⁴⁰]. One of these organs, the area postrema, is part of the dorsal vagal complex, which also comprises the DMV. Since they are in such close proximity, the leaky vasculature of the area postrema may permit entry of prion-like particles that are able to transmit to the DMV via transneuronal mechanisms, thereby bypassing the slower vagal propagation route from gut to brain. This might also be a clue as to why vagotomy and appendectomy procedures are not more effective in reducing sporadic PD risk.

Alternatively, or perhaps aggravatingly, misfolded α -syn can cause a non-classical stress-induced exocytosis response where the toxic α -syn species are released from the neuron and taken up by neighbouring astrocytes through endocytosis, where they form inclusion bodies^{241,242}. The RMS is comprised of an astroglial tube²⁴³, which encases CSF through which neural progenitors migrate [reviewed in ²²⁴]. Astrocytic exposure to α -syn causes a microglial-induced inflammatory response²⁴², which could instigate pathogenesis. Further studies are required to elucidate these intriguing propositions, which may provide further support for a dual-hit hypothesis, proposed by Braak and colleagues. AAV4 has been shown to selectively transduce astrocytes and ependymal cells in the SVZ and RMS²⁴⁴, and therefore packaging the BiSyn cassette in this AAV serotype rather than the current AAV2/9 hybrid could help to elucidate this proposed mechanism.

4.2.5 Inflammation at the epicentre of PD pathogenesis

The dual-hit hypothesis, proposed by Braak and colleagues^{100,102–104}, implies gastrointestinal and olfactory origins for PD pathogenesis. The olfactory derivation was reviewed in further detail by Rey and colleagues in 2018²⁴⁵. Just as the ENS is highly intertwined with the immune system, the OB is heavily protected by microglia and macrophages,

which instigate inflammatory responses²⁴⁶. The relation between macrophages and PD was discussed in section 1.4.3, highlighting their elevated LRRK2 expression and functional importance in maintaining ENS homeostasis^{155,162–165}. Since the OB is a region with similar environmental exposure to the GI tract, it would be reasonable to suggest a similar inflammatory role in OB pathogenesis. Despite an abundance of protection factors secreted in the olfactory mucosa [reviewed in ²⁴⁷], the nerve bundles that extend into the OB from the olfactory epithelium are in close contact with an abundance of microglia and macrophages, which can sense inflammation in regions distal to the OB²⁴⁶. Despite the robust regenerative capacity of the olfactory epithelium, chronic inflammation can shift the fate of migrating neural progenitors to a fixed undifferentiated state for enhancing immune defence²⁴⁸. Additionally, non-steroidal anti-inflammatory drugs (NSAIDs) have a protective benefit in PD^{249–251}. Together these studies suggest inflammation to be central to PD pathogenesis, wherein it is entirely plausible to propose a role for a hyperactive microglia and macrophage-mediated inflammatory response in reducing neuroregeneration, triggering initial α -syn oligomerization and facilitating pathological propagation. Going forward, it will be important for our group to consider inflammatory changes as we use our novel BiSyn approach to assess initial mechanisms that drive PD pathology.

By shifting from transgenic to viral systems, BiSyn can now be used to assess discrete regions rather than the individual as a whole. With this in mind, we can inject AAV2/9-CMV-BiSyn into the olfactory bulb with confidence that pathology does not initially exist in any other region. While overexpression of BiSyn alone is sufficient to stimulate α -syn aggregation, the punctate inclusion bodies typical of PD were not dominant. It is likely that an additional stimulus or prolonged duration will shift aggregates to the ultimate inclusion body fate. For example, McLean's group showed a nonsignificant 8% reduction in dopaminergic neurons at 28dpi, but a significant 29% loss after 12 weeks when degeneration essentially plateaued⁷⁷. Considering the ideal investigation of initial aggregates, a shorter duration would be favourable. We can use a

compressed end point with additional insult to reveal early deficits. Preformed fibrils have been shown to induce pathology and degeneration^{98,99,252}, and aberrant α -syn species from vertebrate food products are hypothesized to induce seeding of pathogenic species in the GI tract⁹¹. In accord, our group hypothesizes that inhalation of these preformed fibrils can induce pathology in the olfactory epithelium where nerve fibers are exposed to environmental stimuli. With this model in mind, we can then ask questions regarding factors that exacerbate or preclude pathology accumulation and denervation. For example, inflammation appears to be a critical feature in disease pathogenesis. The lymphocyte-activation gene 3 (LAG3), an immune checkpoint receptor, has a high affinity for α -syn fibrils and facilitates its prion-like transmission between cells. Further, LAG3 knockout models diminish pathological α -syn transmission (Figure 22)²⁵³. In the discrete region of the OB, we can assess whether depletion of this immune checkpoint receptor can ameliorate α -syn propagation and PD onset. Alternatively, mass generation of ROS is another prominent feature in PD^{9,27} and the natural antioxidant glutathione has reduced concentrations in diseased individuals^{26,28–30}. As previously mentioned, our lab has generated UCHL1 knockout mice that are glutathione deficient²⁰⁵. These mice display a progressive neurodegenerative phenotype and show morphological alterations in the ENS. We can use our knockout mice to assess whether the PD phenotype is exacerbated in the absence of glutathione. Clinical trials administering glutathione orally, intranasally, and intravenously have proven to be safe and offer promising increases in brain glutathione levels^{254,255}, however, a significant improvement after 3-months compared to placebo was not observed in a recent Phase IIb study²⁵⁶.

4.2.6 Future use of AAV2/9-CMV-BiSyn in the appendix

The human appendix is equipped with a robust population of nerve endings that contain α -syn, implicating it as a possible site for enteric PD pathogenesis. Although once considered to

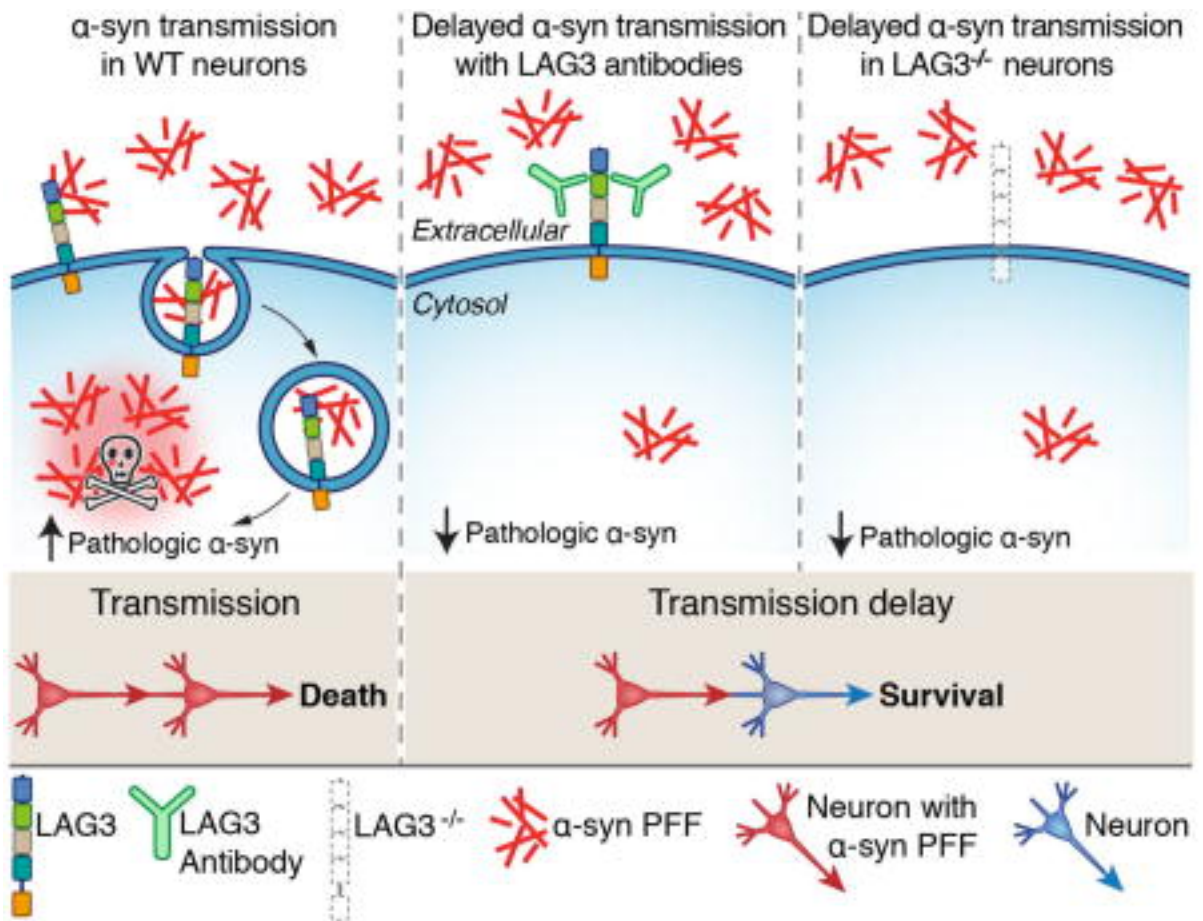


Figure 22: LAG3 facilitates α -syn fibril transmission and toxicity.

The high affinity of LAG3 for α -syn fibrils facilitates prion-like endocytosis. Antibodies against LAG3 and LAG3 knockout models significantly reduces the rate of α -syn fibril transmission, which reduces toxicity and promotes survival.

From ²⁵³. Permission to reproduce found in Appendix J.

be a vestigial organ with no defined function, recent evidence indicates that the appendix plays an important role in regulating the composition of intestinal microbiota^{142,145}. The evolutionarily equivalent cecal cavity in the mouse is also host to extensive flora, which produce vitamins B and K as well as free fatty acids²⁵⁷. There is limited data in reference to the immunological role of the mouse cecum, however, the chicken cecum has been shown to instigate an immune response when challenged with *Salmonella enterica*^{258,259}. The novel AAV2/9-CMV-BiSyn provides opportunity to assess the cecal role in PD pathogenesis. Benskey and colleagues demonstrated that injecting 5 μ L of AAV9 at a titer of 1.2x10¹³vg/mL transduced an area of nearly 50mm² in both the myenteric and submucosal plexuses of the colon²⁰⁴. Extending our hypothesis that a lower volume will prevent spreading through CSF, we can also deduce that a reduced volume injected into the cecum will transduce a smaller area of the ENS. Beyond the defined viral transduction radius, we can presume that aggregates propagate in a prion-like manner. Going forward, it will be critical to quantify the amount of aggregated species at specific time points, perhaps using flow cytometry in segments of tissue adjacent to those that will be used for IF application. This will enable a time-dependent analysis of aggregate propagation.

Our AAV system broadens our research potential, ceasing to constrain our investigations to mice. Since the appendix is of significant interest in our group, shifting to a species that has an appendix rather than cecum would be revolutionary. Not only do laboratory rabbits have an appendix, their appendiceal environment is the only virtual equivalent to that of humans due to our excessively hygienic nature¹⁴⁶.

4.3 Conclusion

Despite the prominence of stochastic mosaicism in our BiSyn/Cre transgenic mice, our system is an excellent representation of PEV. We have provided evidence for an earlier developmental onset of heterochromatic variegation than previously reported, and the high

degree of stochasticity observed in our model confirms the dynamic nature of the heterochromatic boundary.

Our AAV2/9-CMV-BiSyn system transduces neurons and can travel in both antero- and retrograde directions in accordance with AAV9 capsid presentation. We have demonstrated a limited, yet powerful, body of evidence for the cell-to-cell propagation of BiSyn that requires further exploration. Our data also suggests that neural progenitors in the SVZ were transduced and acquired α -syn oligomers, and thereafter migrated through the RMS toward the olfactory epithelium. Further validation is required for this intriguing possibility. The novel AAV2/9-CMV-BiSyn system breeds potential for uncovering the key initial steps in PD pathogenesis. In accordance with the Braak “dual-hit” hypothesis, we aim to target the appendix and olfactory epithelium using our novel AAV2/9-CMV-BiSyn system to visualize the most premature steps in α -syn aggregation and propagation.

References

- (1) Marras, C., Beck, J. C., Bower, J. H., Roberts, E., Ritz, B., Ross, G. W., Abbott, R. D., Savica, R., Van Den Eeden, S. K., Willis, A. W., and Tanner, C. M. (2018) Prevalence of Parkinson's disease across North America. *npjParkinson's Dis.* 4, 21.
- (2) Rossi, A., Berger, K., Chen, H., Leslie, D., Mailman, R., and Huang, X. (2018) Projection of the prevalence of Parkinson's disease in the coming decades: revisited. *Mov. Disord.* 33, 156–159.
- (3) Neurological Health Charities Canada, Health Canada, Public Health Agency of Canada, and Canadian Institute of Health Research. (2014) MAPPING CONNECTIONS: An understanding of neurological conditions in Canada.
- (4) Pringsheim, T., Jette, N., Frolkis, A., and Steeves, T. D. L. (2014) The prevalence of Parkinson's disease: a systematic review and meta-analysis. *Mov. Disord.* 29, 1583–1590.
- (5) Gordon, P. H., Mehal, J. M., Holman, R. C., Bartholomew, M. L., Cheek, J. E., and Rowland, A. S. (2015) Incidence and prevalence of Parkinson's disease among Navajo people living in the Navajo nation. *Mov. Disord.* 30, 714–720.
- (6) Bauso, D. J., Tartari, J. P., Stefani, C. V., Rojas, J. I., Giunta, D. H., and Cristiano, E. (2012) Incidence and prevalence of Parkinson's disease in Buenos Aires City, Argentina. *Eur. J. Neurol.* 19, 1108–1113.
- (7) Riedel, O., Bitters, D., Amann, U., Garbe, E., and Langner, I. (2016) Estimating the prevalence of Parkinson's disease (PD) and proportions of patients with associated dementia and depression among the older adults based on secondary claims data. *Int. J. Geriatr. Psychiatry* 31, 938–943.
- (8) Moisan, F., Spinosi, J., Dupupet, J.-L., Delabre, L., Mazurie, J.-L., Goldberg, M., Imbernon, E., Tzourio, C., and Elbaz, A. (2011) The Relation Between Type of Farming and Prevalence of Parkinson's Disease Among Agricultural Workers in Five French Districts. *Mov. Disord.* 26, 271–279.
- (9) Glatt, C. E., Wahner, A. D., White, D. J., Ruiz-Linares, A., and Ritz, B. (2006) Gain-of-function haplotypes in the vesicular monoamine transporter promoter are protective for Parkinson disease in women. *Hum. Mol. Genet.* 15, 299–305.
- (10) Haaxma, C. A., Bloem, B. R., Borm, G. F., Oyen, W. J., Leenders, K. L., Eshuis, S., Dluzen, D. E., and Horstink, M. W. I. M. (2007) Gender differences in Parkinson's disease. *J Neurol Neurosurg Psychiatry* 78, 819–824.
- (11) Green, P. S., and Simpkins, J. W. (2000, July 1) Neuroprotective effects of estrogens: Potential mechanisms of action. *Int. J. Dev. Neurosci.*
- (12) Dubal, D. B., and Wise, P. M. (2001) Neuroprotective effects of estradiol in middle-aged female rats. *Endocrinology* 142, 43–48.
- (13) Dluzen, D. E. (2000) Neuroprotective effects of estrogen upon the nigrostriatal dopaminergic system. *J. Neurocytol.* 29, 387–399.
- (14) Roof, R. L., and Hall, E. D. (2000) Gender differences in acute CNS trauma and stroke: Neuroprotective effects of estrogen and progesterone. *J. Neurotrauma* 17, 367–388.
- (15) Yang, S.-H., Shi, J., Day, A. L., and Simpkins, J. W. (2000) Estradiol exerts neuroprotective effects when administered after ischemic insult. *Stroke* 31, 745–750.
- (16) Lichtesteiger, W., Felix, D., Lienhart, R., and Hefti, F. (1976) A quantitative correlation between single unit activity and fluorescence intensity of dopamine neurones in zona compacta of substantia nigra, as demonstrated under the influence of nicotine and physostigmine. *Brain Res.* 117, 85–103.
- (17) Lichtensteiger, W., Hefti, F., Felix, D., Huwyler, T., Melamed, E., and Schlumpf, M. (1982) Stimulation of nigrostriatal dopamine neurones by nicotine. *Neuropharmacology* 21, 963–968.

- (18) Bédard, P., Larochelle, L., Parent, A., and Poirier, L. J. (1969) The nigrostriatal pathway: A correlative study based on neuroanatomical and neurochemical criteria in the cat and the monkey. *Exp. Neurol.* 25, 365–377.
- (19) Vallone, D., Picetti, R., and Borrelli, E. (2000) Structure and function of dopamine receptors. *Neurosci. Biobehav. Rev.* 24, 125–132.
- (20) Bjarkam, C. R., Sørensen, J. C., Sunde, N. Å., Geneser, F. A., and Østergaard, K. (2001) New strategies for the treatment of Parkinson's disease hold considerable promise for the future management of neurodegenerative disorders. *Biogerontology* 2, 193–207.
- (21) McRitchie, D. A., Cartwright, H. R., and Halliday, G. M. (1997) Specific A10 dopaminergic nuclei in the midbrain degenerate in Parkinson's disease. *Exp. Neurol.* 144, 202–213.
- (22) Mosharov, E. V., Larsen, K. E., Kanter, E., Phillips, K. A., Wilson, K., Schmitz, Y., Krantz, D. E., Kobayashi, K., Edwards, R. H., and Sulzer, D. (2009) Interplay between cytosolic dopamine, calcium, and α -synuclein causes selective death of substantia nigra neurons. *Neuron* 62, 218–229.
- (23) Berman, S. B., and Hastings, T. G. (2001) Dopamine oxidation alters mitochondrial respiration and induces permeability transition in brain mitochondria. *J. Neurochem.* 73, 1127–1137.
- (24) Montine, T. J., Picklo, M. J., Amarnath, V., Whetsell, W. O., and Graham, D. G. (1997) Neurotoxicity of endogenous cysteinylcatechols. *Exp. Neurol.* 148, 26–33.
- (25) Tomita, Y., Hariu, A., Kato, C., and Seiji, M. (1984) Radical production during tyrosinase reaction, dopa-melanin formation, and photoirradiation of dopa-melanin. *J. Invest. Dermatol.* 82, 573–576.
- (26) Perry, T. L., Godin, D. V., and Hansen, S. (1982) Parkinson's disease: a disorder due to nigral glutathione deficiency. *Neurosci. Lett.* 33, 305–310.
- (27) Lohr, K. M., and Miller, G. W. (2014) VMAT2 and Parkinson's disease: harnessing the dopamine vesicle. *Expert Rev. Neurother* 14, 1115–1117.
- (28) Perry, T. L., and Yong, V. W. (1986) Idiopathic Parkinson's disease, progressive supranuclear palsy and glutathione metabolism in the substantia nigra of patients. *Neuroscience Lett.*
- (29) Kish, S. J., Morito, C., and Hornykiewicz, O. (1985) Glutathione peroxidase activity in Parkinson's disease brain. *Neurosci. Lett.* 58, 343–346.
- (30) Sofic, E., Lange, K. W., Jellinger, K., and Riederer, P. (1992) Reduced and oxidized glutathione in the substantia nigra of patients with Parkinson's disease. *Neurosci. Lett.* 142, 128–130.
- (31) Filion, M. (1979) Effects of interruption of the nigrostriatal pathway and of dopaminergic agents on the spontaneous activity of globus pallidus neurons in the awake monkey. *Brain Res.* 178, 425–441.
- (32) Pan, H. S., and Walters, J. R. (1988) Unilateral lesion of the nigrostriatal pathway decreases the firing rate and alters the firing pattern of globus pallidus neurons in the rat. *Synapse* 2, 650–656.
- (33) Bjarkam, C. R., and Sørensen, J. C. (2004) Therapeutic strategies for neurodegenerative disorders: Emerging clues from Parkinson's disease. *Neurosci. Perspect.* 56, 213–216.
- (34) Maroteaux, L., Campanelli, J. T., and Scheller, R. H. (1988) Synuclein: A neuron-specific protein localized to the nucleus and presynaptic nerve terminal. *J. Neurosci.* 8, 2804–2815.
- (35) Huang, Z., Xu, Z., Wu, Y., and Zhou, Y. (2011) Determining nuclear localization of alpha-synuclein in mouse brains. *Neuroscience* 199, 318–332.
- (36) George, J. M., Jin, H., Woods, W. S., and Clayton, D. F. (1995) Characterization of a novel protein regulated during the critical period for song learning in the zebra finch. *Neuron*

15, 361–372.

(37) Clayton, D. F., and George, J. M. (1998) The synucleins: a family of proteins involved in synaptic function, plasticity, neurodegeneration and disease. *Trends Neurosci.* 21, 249–254.

(38) Spillantini, M. G., Divane, A., and Goedert, M. (1995) Assignment of human alpha-synuclein (SNCA) and beta-synuclein (SNCB) genes to chromosomes 4q21 and 5q35. *Genomics* 27, 379–381.

(39) Jakes, R., Spillantini, M. G., and Goedert, M. (1994) Identification of two distinct synucleins from human brain. *Fed. Eur. Biochem. Soc. Lett.* 345, 27–32.

(40) Ueda, K., Fukushima, H., Masliah, E., Xia, Y., Iwai, A., Yoshimoto, M., Otero, D. A. C., Kondo, J., Ihara, Y., and Saitoh, T. (1993) Molecular Cloning of cDNA Encoding an Unrecognized Component of Amyloid in. *Proc. Natl. Acad. Sci. USA* 90, 11282–11286.

(41) Chandra, S., Gallardo, G., Fernández-Chacón, R., Schlüter, O. M., and Südhof, T. C. (2005) α -synuclein cooperates with CSP α in preventing neurodegeneration. *Cell* 123, 383–396.

(42) Burré, J., Sharma, M., Tsetsenis, T., Buchman, V., Etherton, M. R., and Südhof, T. C. (2010) α -synuclein promotes SNARE-complex assembly in vivo and in vitro. *Science* (80-.). 329, 1663–1667.

(43) Nemani, V. M., Lu, W., Berge, V., Nakamura, K., Onoa, B., Lee, M. K., Chaudhry, F. A., Nicoll, R. A., and Edwards, R. H. (2010) Increased expression of α -synuclein reduces neurotransmitter release by inhibiting synaptic vesicle reclustering after endocytosis. *Neuron* 65, 66–79.

(44) Senior, S. L., Ninkina, N., Deacon, R., Bannerman, D., Buchman, V. L., Cragg, S. J., and Wade-Martins, R. (2008) Increased striatal dopamine release and hyperdopaminergic-like behaviour in mice lacking both alpha-synuclein and gamma-synuclein. *Eur. J. Neurosci.* 27, 947–957.

(45) Swant, J., Goodwin, J. S., North, A., Ali, A. A., Gamble-George, J., Chirwa, S., and Khoshbouei, H. (2011) α -synuclein stimulates a dopamine transporter-dependent chloride current and modulates the activity of the transporter. *J. Biol. Chem.* 286, 43933–43943.

(46) Butler, B., Saha, K., Rana, T., Becker, J. P., Sambo, D., Davari, P., Goodwin, J. S., and Khoshbouei, H. (2015) Dopamine transporter activity is modulated by α -synuclein. *J. Biol. Chem.* 290, 29542–29554.

(47) Guo, J. T., Chen, A. Q., Kong, Q., Zhu, H., Ma, C. M., and Qin, C. (2008) Inhibition of vesicular monoamine transporter-2 activity in α -synuclein stably transfected SH-SY5Y cells. *Cell. Mol. Neurobiol.* 28, 35–47.

(48) Perez, R. G., Waymire, J. C., Lin, E., Liu, J. J., Guo, F., and Zigmond, M. J. (2002) A role for α -synuclein in the regulation of dopamine biosynthesis. *J. Neurosci.* 22, 3090–3099.

(49) Baptista, M. J., O'Farrell, C., Daya, S., Ahmad, R., Miller, D. W., Hardy, J., Farrer, M. J., and Cookson, M. R. (2003) Co-ordinate transcriptional regulation of dopamine synthesis genes by α -synuclein in human neuroblastoma cell lines. *J. Neurochem.* 85, 957–968.

(50) Yu, S., Zuo, X., Li, Y., Zhang, C., Zhou, M., Zhang, Y. A., Ueda, K., and Chan, P. (2004) Inhibition of tyrosine hydroxylase expression in-synuclein-transfected dopaminergic neuronal cells. *Neurosci. Lett.* 367, 34–39.

(51) Nakajo, S., Omata, K., Aiuchi, T., Shibayama, T., Okahashi, I., Ochiai, H., Nakai, Y., Nakaya, K., and Nakamura, Y. (1990) Purification and characterization of a novel brain-specific 14-kDa protein. *J. Neurochem.* 55, 2031–2038.

(52) Shibayama-Imazu, T., Okahashi, I., Omata, K., Nakajo, S., Ochiai, H., Nakai, Y., Hama, T., Nakamura, Y., and Nakaya, K. (1993) Cell and tissue distribution and developmental change of neuron specific 14 kDa protein (phosphoneuroprotein 14). *Brain Res.* 622, 17–25.

(53) Spillantini, M. G., Schmidt, M. L., Lee, V. M.-Y., Trojanowski, J. Q., Jakes, R., and Goedert, M. (1997) α -synuclein in Lewy bodies. *Nature* 388, 839–840.

- (54) Hashimoto, M., Rockenstein, E., Mante, M., Mallory, M., and Masliah, E. (2001) Beta-synuclein inhibits alpha-synuclein aggregation: A possible role as an anti-Parkinsonian factor. *Neuron* 32, 213–223.
- (55) Akopian, A. N., and Wood, J. N. (1995) Peripheral nervous system-specific genes identified by subtractive cDNA cloning. *J. Biol. Chem.* 270, 21264–21270.
- (56) Ji, H., Liu, Y. E., Jia, T., Wang, M., Liu, J., Xiao, G., Joseph, B. K., Rosen, C., and Shi, Y. E. (1997) Identification of a breast cancer-specific gene, BCSG1, by direct differential cDNA sequencing. *Cancer Res.* 57, 759–764.
- (57) Polymeropoulos, M. H., Lavedan, C., Leroy, E., Ide, S. E., Dehejia, A., Dutra, A., Pike, B., Root, H., Rubenstein, J., Boyer, R., Stenroos, E. S., Chandrasekharappa, S., Athanassiadou, A., Papapetropoulos, T., Johnson, W. G., Lazzarini, A. M., Duvoisin, R. C., Di Iorio, G., Golbe, L. I., and Nussbaum, R. L. (1997) Mutation in the α -synuclein gene identified in families with Parkinson's disease. *Science* (80-). 276, 2045–2047.
- (58) Krüger, R., Kuhn, W., Müller, T., Woitalla, D., Graeber, M., Kösel, S., Przuntek, H., Eppelen, J. T., Schöls, L., and Riess, O. (1998) Ala30Pro mutation in the gene encoding α -synuclein in Parkinson's disease. *Nat. Genet.* 18, 106–108.
- (59) Spillantini, M. G., Crowther, R. A., Jakes, R., Hasegawa, M., and Goedert, M. (1998) Synuclein in filamentous inclusions of Lewy bodies from Parkinson's disease and dementia with Lewy bodies. *Neurobiology* 95, 6469–6473.
- (60) Lewy, F. H. (1912) Paralysis agitans, in *Pathologische Anatomie. Handbuch der Neurologie* (Lewandowsky, M., Ed.), pp 920–933. Julius Springer, Berlin.
- (61) Lafora, G. R. (1913) Contribución a la histopatología de la parálisis agitante.
- (62) Trétiakoff, K. (1919) Contribution a l'Etude de L'Anatomie pathologique du Locus Niger de Soemmering avec quelques déductions relatives à la pathogénie des troubles du tonus musculaire et De La Maladie de Parkinson. Paris.
- (63) Kuzuhara, S., Mori, H., Izumiyama, N., Yoshimura, M., and Ihara, Y. (1988) Lewy bodies are ubiquitinated. A light and electron microscopic immunocytochemical study. *Acta Neuropathol.* 75, 345–353.
- (64) Dinner, A. R., Sali, A., Smith, L. J., Dobson, C. M., and Karplus, M. (2000) Understanding protein folding via free-energy surfaces from theory and experiment. *Trends Biochem. Sci.* 25, 331–339.
- (65) Ellisdon, A., and Bottomley, S. (2004) The role of protein misfolding in the pathogenesis of human diseases. *International Union Biochem. Mol. Biol. Life* 56, 119–123.
- (66) Singleton, A. B., Farrer, M., Johnson, J., Singleton, A., Hague, S., Kachergus, J., Hulihan, M., Peuralinna, T., Dutra, A., Nussbaum, R., Lincoln, S., Crawley, A., Hanson, M., Maraganore, D., Adler, C., Cookson, M. R., Muenter, M., Baptista, M., Miller, D., Blancato, J., Hardy, J., and Gwinn-Hardy, K. (2003) Alpha-synuclein locus triplication causes Parkinson's disease. *Science* (80-). 302, 841.
- (67) Muenter, M. D., Forno, L. S., Hornykiewicz, O., Kish, S. J., Maraganore, D. M., Caselli, R. J., Okazaki, H., Howard, F. M., Snow, B. J., and Calne, D. B. (1998) Hereditary form of parkinsonism-dementia. *Ann. Neurol.* 43, 781.
- (68) Fuchs, J., Nilsson, C., Kachergus, J., Munz, M., Larsson, E. M., Schüle, B., Langston, J. W., Middleton, F. A., Ross, O. A., Hulihan, M., Gasser, T., and Farrer, M. J. (2007) Phenotypic variation in a large Swedish pedigree due to SNCA duplication and triplication. *Neurology* 68, 916–922.
- (69) Chartier-Harlin, M.-C., Kachergus, J., Roumier, C., Mouroux, V., Douay, X., Lincoln, S., Levecque, C., Larvor, L., Andrieux, J., Hulihan, M., Waucquier, N., Defebvre, L., Amouyel, P., Farrer, M., and Destée, A. (2004) Alpha-synuclein locus duplication as a cause of familial Parkinson's disease. *Lancet* 364, 1167–1169.
- (70) Ibáñez, P., Bonnet, A.-M., Débarges, B., Lohmann, E., Tison, F., Poliak, P., Agrid, Y., Dürr, A., Brice, A., and French Parkinson's Disease Genetics Study Group. (2004) Causal

relation between alpha-synuclein gene duplication and familial Parkinson's disease. *Lancet* 364, 1169–1171.

(71) Cabin, D. E., Shimazu, K., Murphy, D., Cole, N. B., Gottschalk, W., McIlwain, K. L., Orrison, B., Chen, A., Ellis, C. E., Paylor, R., Lu, B., and Nussbaum, R. L. (2002) Synaptic vesicle depletion correlates with attenuated synaptic responses to prolonged repetitive stimulation in mice lacking α -synuclein. *J. Neurosci.* 22, 8797–8807.

(72) Ellis, C. E., Murphy, E. J., Mitchell, D. C., Golovko, M. Y., Scaglia, F., Barceló-Coblijn, G. C., and Nussbaum, R. L. (2005) Mitochondrial lipid abnormality and electron transport chain impairment in mice lacking α -synuclein. *Mol. Cell. Biol.* 25, 10190–10201.

(73) Ryan, T., Bamm, V. V., Stykel, M. G., Coackley, C. L., Humphries, K. M., Jamieson-Williams, R., Ambasudhan, R., Mosser, D. D., Lipton, S. A., Harauz, G., and Ryan, S. D. (2018) Cardiolipin exposure on the outer mitochondrial membrane modulates α -synuclein. *Nat. Commun.* 9, 817.

(74) Zhu, M., and Fink, A. L. (2003) Lipid binding inhibits alpha-synuclein fibril formation. *J. Biol. Chem.* 278, 16873–16877.

(75) Klucken, J., Outeiro, T. F., Nguyen, P., Mclean, P. J., and Hyman, B. T. (2006) Detection of novel intracellular-synuclein oligomeric species by fluorescence lifetime imaging. *FASEB J.* 20, 2050–2057.

(76) Outeiro, T. F., Putcha, P., Tetzlaff, J. E., Spoelgen, R., Koker, M., Carvalho, F., Hyman, B. T., and Mclean, P. J. (2008) Formation of toxic oligomeric α -synuclein species in living cells. *PLoS One* 3, e1867.

(77) Cai, W., Feng, D., Schwarzschild, M. A., Mclean, P. J., and Chen, X. (2018) Bimolecular fluorescence complementation of alpha-synuclein demonstrates its oligomerization with dopaminergic phenotype in mice. *EBioMedicine* 29, 13–22.

(78) Roostae, A., Beaudoin, S., Staskevicius, A., and Roucou, X. (2013) Aggregation and neurotoxicity of recombinant α -synuclein aggregates initiated by dimerization. *Mol. Neurodegener.* 8, 5.

(79) Lücking, C. B., Dürr, A., Bonifati, V., Vaughan, J., De Michele, G., Gasser, T., Harhangi, B. S., Meo, G., Denèfle, P., Wood, N. W., Agid, Y., and Brice, A. (2000) Association between early-onset Parkinson's disease and mutations in the Parkin gene. *N. Engl. J. Med.* 342, 1560–1567.

(80) Dodson, M. W., and Guo, M. (2007) Pink1, Parkin, DJ-1 and mitochondrial dysfunction in Parkinson's disease. *Curr. Opin. Neurobiol.* 17, 331–337.

(81) Ariga, H., Takahashi-Niki, K., Kato, I., Maita, H., Niki, T., and Iguchi-Ariga, S. M. M. (2013) Neuroprotective function of DJ-1 in Parkinson's disease. *Oxid. Med. Cell. Longev.* 2013, 1–9.

(82) Maita, C., Maita, H., Iguchi-Ariga, S. M. M., and Ariga, H. (2013) Monomer DJ-1 and its N-Terminal sequence are necessary for mitochondrial localization of DJ-1 mutants. *PLoS One* 8, e54087.

(83) Prusiner, S. B. (2013) Biology and genetics of prions causing neurodegeneration. *Annu Rev Genet* 47, 601–623.

(84) Barbeau, A., Roy, M., Bernier, G., Campanella, G., and Paris, S. (1987) Ecogenetics of Parkinson's disease: prevalence and environmental aspects in rural areas. *Can. J. Neurol. Sci.* 14, 36–41.

(85) Yuan, Y.-H., Yan, W.-F., Sun, J.-D., Huang, J.-Y., Mu, Z., and Chen, N.-H. (2015) The molecular mechanism of rotenone-induced α -synuclein aggregation: Emphasizing the role of the calcium/GSK3 β pathway. *Toxicol. Lett.* 233, 163–171.

(86) Drolet, R. E., Cannon, J. R., Montero, L., and Timothy Greenamyre, J. (2009) Chronic rotenone exposure reproduces Parkinson's disease gastrointestinal neuropathology. *Neurobiol. Dis.* 36, 96–102.

(87) Dodiya, H. B., Forsyth, C. B., Voigt, R. M., Engen, P. A., Patel, J., Shaikh, M.,

- Green, S. J., Naqib, A., Roy, A., Kordower, J. H., Pahan, K., Shannon, K. M., and Keshavarzian, A. (2018) Chronic stress-induced gut dysfunction exacerbates Parkinson's disease phenotype and pathology in a rotenone-induced mouse model of Parkinson's disease. *Neurobiol. Dis.*
- (88) Langston, J. W., Ballard, P., Tetrud, J. W., and Irwin, I. (1983) Chronic Parkinsonism in humans due to a product of meperidine-analog synthesis. *Science (80-)*. 219, 979–980.
- (89) Ballard, P. A., Tetrud, J. W., and Langston, J. W. (1985) Permanent human parkinsonism due to 1-methyl-4-phenyl-1,2,3,6-tetrahydropyridine (MPTP): Seven cases. *Neurology* 35, 949–956.
- (90) Nonnekes, J., Post, B., Tetrud, J. W., Langston, J. W., and Bloem, B. R. (2018) MPTP-induced parkinsonism: an historical case series. *Lancet Neurol.* 17, 300–301.
- (91) Killinger, B. A., and Labrie, V. (2017) Vertebrate food products as a potential source of prion-like α -synuclein. *Nat. Partn. Journals Park. Dis.* 3.
- (92) Siddiqui, I. J., Pervaiz, N., and Abbasi, A. A. (2016) The Parkinson disease gene SNCA: Evolutionary and structural insights with pathological implication. *Sci. Rep.* 6, 24475.
- (93) Prusiner, S. B. (1982) Novel proteinaceous infectious particles cause scrapie. *Science (80-)*. 216, 136–144.
- (94) Pan, K.-M., Baldwin, M., Nguyen, J., Gasset, M., Serban, A., Groth, D., Mehlhorn, I., Huang, Z., Fletterick, R. J., Cohen, F. E., and Prusiner, S. B. (1993) Conversion of alpha-helices into beta-sheets features in the formation of the scrapie prion proteins. *Proc. Natl. Acad. Sci. USA* 90, 10962–10966.
- (95) Nguyen, J., Baldwin, A., Cohen, F. E., and Prusiner, S. B. (1995) Prion protein peptides induce alpha-helix to beta-sheet conformational transitions. *Biochemistry* 34, 4186–4192.
- (96) Morillas, M., Vanik, D. L., and Surewicz, W. K. (2001) On the mechanism of alpha-helix to beta-sheet transition in the recombinant prion protein. *Biochemistry* 40, 6982–6987.
- (97) Prusiner, S. B. (2012) A unifying role for prions in neurodegenerative diseases. *Science (80-)*. 336, 1511–1513.
- (98) Luk, K. C., Kehm, V., Carroll, J., Zhang, B., O'Brien, P., Trojanowski, J. Q., and Lee, V. M.-Y. (2012) Pathological α -synuclein transmission initiates Parkinson-like neurodegeneration in nontransgenic mice. *Science (80-)*. 338, 949–953.
- (99) Paumier, K. L., Luk, K. C., Manfredsson, F. P., Kanaan, N. M., Lipton, J. W., Collier, T. J., Steece-Collier, K., Kemp, C. J., Celano, S., Schulz, E., Sandoval, I. M., Fleming, S., Dirr, E., Polinski, N. K., Trojanowski, J. Q., Lee, V. M., and Sortwell, C. E. (2015) Intrastratial injection of pre-formed mouse α -synuclein fibrils into rats triggers α -synuclein pathology and bilateral nigrostriatal degeneration. *Neurobiol. Dis.* 82, 185–199.
- (100) Braak, H., Tredici, K. Del, Rüb, U., De Vos, R. A. I., Jansen Steur, E. N. H., and Braak, E. (2003) Staging of brain pathology related to sporadic Parkinson's disease. *Neurobiol. Aging* 24, 197–211.
- (101) Braak, H., de Vos, R. A. I., Bohl, J., and Del Tredici, K. (2006) Gastric alpha-synuclein immunoreactive inclusions in Meissner's and Auerbach's plexuses in cases staged for Parkinson's disease-related brain pathology. *Neurosci. Lett.* 396, 67–72.
- (102) Braak, H., Rüb, U., Gai, W. P., and Tredici, K. Del. (2003) Idiopathic Parkinson's disease: possible routes by which vulnerable neuronal types may be subject to neuroinvasion by an unknown pathogen. *J Neural Transm* 110, 517–536.
- (103) Hawkes, C. H., Del Tredici, K., and Braak, H. (2007) Review: Parkinson's disease: a dual-hit hypothesis. *Neuropathol. Appl. Neurobiol.* 33, 599–614.
- (104) Hawkes, C. H., Del Tredici, K., and Braak, H. (2009) Parkinson's disease: the dual hit theory revisited. *Int. Symp. Olfaction Tast.* 1170, 615–622.
- (105) Attems, J., and Jellinger, K. A. (2008) The dorsal motor nucleus of the vagus is not an obligatory trigger site of Parkinson's disease. *Neuropathol. Appl. Neurobiol.* 34, 466–467.

- (106) Zaccai, J., Brayne, C., McKeith, I., Matthews, F., and Ince, P. G. (2008) Patterns and stages of α -synucleinopathy: Relevance in a population-based cohort. *Neurology* 70, 1042–1048.
- (107) Dickson, D. W., Fujishiro, H., DelleDonne, A., Menke, J., Ahmed, Z., Klos, K. J., Josephs, K. A., Frigerio, R., Burnett, M., Parisi, J. E., and Ahlskog, J. E. (2008) Evidence that incidental Lewy body disease is pre-symptomatic Parkinson's disease. *Acta Neuropathol.* 115, 437–444.
- (108) Jellinger, K. A. (2008) A critical reappraisal of current staging of Lewy-related pathology in human brain. *Acta Neuropathol.* 116, 1–16.
- (109) Rietdijk, C. D., Perez-Pardo, P., Garssen, J., van Wezel, R. J. A., and Kraneveld, A. D. (2017) Exploring Braak's hypothesis of parkinson's disease. *Front. Neurol.* 8, 37.
- (110) Braak, H., and Del Tredici, K. (2017) Neuropathological staging of brain pathology in sporadic Parkinson's disease: separating the wheat from the chaff. *J. Parkinsons. Dis.* 7, S71–S85.
- (111) Clairembault, T., Leclair-Visonneau, L., Coron, E., Bourreille, A., Le Dily, S., Vavasseur, F., Heymann, M.-F., Neunlist, M., and Derkinderen, P. (2015) Structural alterations of the intestinal epithelial barrier in Parkinson's disease. *Acta Neuropathol. Commun.* 3, 1–9.
- (112) Devos, D., Lebouvier, T., Lardeux, B., Biraud, M., Rouaud, T., Pouclet, H., Coron, E., Bruley des Varannes, S., Naveilhan, P., Nguyen, J.-M., Neunlist, M., and Derkinderen, P. (2013) Colonic inflammation in Parkinson's disease. *Neurobiol. Dis.* 50, 42–48.
- (113) Saper, C. B., Wainer, B. H., and German, D. C. (1987) Axonal and transneuronal transport in the transmission of neurological disease: potential role in system degenerations, including Alzheimer's disease. *Neuroscience* 23, 389–398.
- (114) Svensson, E., Horvath-Puho, E., Thomsen, R. W., Djurhuus, J. C., Pedersen, L., Borghammer, P., and Sørensen, H. T. (2015) Vagotomy and Subsequent Risk of Parkinson's Disease. *Ann Neurol* 78, 522–529.
- (115) Liu, B., Fang, F., Pedersen, N. L., Tillander, A., Ludvigsson, J. F., Ekbo, A., Svenningsson, P., Chen, H., and Wirdefeldt, K. (2017) Vagotomy and Parkinson disease: A Swedish register-based matched-cohort study. *Neurology* 88, 1996–2002.
- (116) Pan-Montojo, F., Anichtchik, O., Dening, Y., Knels, L., and Pursche, S. (2010) Progression of Parkinson's Disease Pathology Is Reproduced by Intragastric Administration of Rotenone in Mice. *PLoS One* 5, e8762.
- (117) Pan-Montojo, F., Schwarz, M., Winkler, C., Arnhold, M., O'sullivan, G. A., Pal, A., Said, J., Marsico, G., Verbavatz, J.-M., Rodrigo-Angulo, M., Gille, G., Funk, R. H. W., and Reichmann, H. (2012) Environmental toxins trigger PD-like progression via increased alpha-synuclein release from enteric neurons in mice. *Sci. Rep.* 2, 898.
- (118) Langley, J. N. (1903) The autonomic nervous system: Part I. *Brain* 26, 1–26.
- (119) Furness, J. B. (2006) Structure of the enteric nervous system, in *The Enteric Nervous System* (Brown, A., Van der Linden, S., Blundell, R., and Charman, K., Eds.), pp 1–28. Blackwell Publishing.
- (120) Bayliss, W. M., and Starling, E. H. (1899) The movements and innervation of the small intestine. *J. Physiol.* 24, 99–143.
- (121) Costa, M., and Furness, J. B. (1976) The peristaltic reflex: An analysis of the nerve pathways and their pharmacology. *Naunyn. Schmiedeberg's Arch. Pharmacol.* 294, 47–60.
- (122) Furness, J. B., Callaghan, B. P., Rivera, L. R., and Cho, H. J. (2014) The enteric nervous system and gastrointestinal innervation: Integrated local and central control. *Adv. Exp. Med. Biol.* 817, 39–71.
- (123) Fox, E. A., and Powley, T. L. (1985) Longitudinal columnar organization within the dorsal motor nucleus represents separate branches of the abdominal vagus. *Brain Res.* 341, 269–282.
- (124) Schemann, M., and Grundy, D. (1992) Electrophysiological identification of vagally

- innervated enteric neurons in guinea pig stomach. *Am. J. Physiol.* 263, G709–G718.
- (125) Holst, M.-C., Kelly, J. B., and Powley, T. L. (1997) Vagal preganglionic projections to the enteric nervous system characterized with Phaseolus vulgaris-leucoagglutinin. *J. Comp. Neurol.* 381, 81–100.
- (126) Kuntz, A. (1922) On the occurrence of reflex arcs in the myenteric and submucous plexuses. *Anat. Rec.* 24, 192–210.
- (127) Schrag, A., Horsfall, L., Walters, K., Noyce, A., and Petersen, I. (2014) Prediagnostic presentations of Parkinson's disease in primary care: a case-control study. *Lancet Neurol.* 14, 57–64.
- (128) Ross, G. W., Abbott, R. D., Petrovitch, H., Tanner, C. M., and White, L. R. (2012) Pre-motor features of Parkinson's disease: The Honolulu-Asia aging study experience. *Park. Relat. Disord.* 18, S199–S202.
- (129) Savica, R., Carlin, J. M., Grossardt, B. R., Bower, J. H., Ahlskog, J. E., Maraganore, D. M., Bharucha, A. E., and Rocca, W. A. (2009) Medical records documentation of constipation preceding Parkinson disease: A case-control study. *Neurology* 73, 1752–1758.
- (130) Gao, X., Chen, H., Schwarzschild, M. A., and Ascherio, A. (2011) A prospective study of bowel movement frequency and risk of Parkinson's disease. *Am. J. Epidemiol.* 174, 546–551.
- (131) Postuma, R. B., Gagnon, J.-F., Pelletier, A., and Montplaisir, J. (2013) Prodromal autonomic symptoms and signs in Parkinson's disease and dementia with Lewy bodies. *Mov. Disord.* 28, 597–604.
- (132) Furness, J. B., Alex, G., Clark, M. J., and Lal, V. V. (2003) Morphologies and projections of defined classes of neurons in the submucosa of the guinea-pig small intestine. *Anat. Rec.* 272A, 475–483.
- (133) Banks, M. R., Farthing, M. J. G., Robberecht, P., and Burleigh, D. E. (2005) Antisecretory actions of a novel vasoactive intestinal polypeptide (VIP) antagonist in human and rat small intestine. *Br. J. Pharmacol.* 144, 994–1001.
- (134) Schwartz, C. J., Kimberg, D. V., Sheerin, H. E., Field, M., and Said, S. I. (1974) Vasoactive intestinal peptide stimulation of adenylate cyclase and active electrolyte secretion in intestinal mucosa. *J. Clin. Invest.* 54, 536–544.
- (135) Qualman, S. J., Haupt, H. M., Yang, P., and Hamilton, S. R. (1984) Esophageal Lewy bodies associated with ganglion cell loss in Achalasia: Similarity to Parkinson's disease. *Gastroenterology* 87, 848–856.
- (136) Wakabayashi, K., Takahashi, H., Ohama, E., and Ikuta, F. (1990) Parkinson's disease: An immunohistochemical study of Lewy body-containing neurons in the enteric nervous system. *Acta Neuropathol.* 79, 581–583.
- (137) Singaram, C., Gaumnitz, E. A., Torbey, C., Ashraf, W., Quigley, E. M. M., Sengupta, A., and Pfeiffer, R. (1995) Dopaminergic defect of enteric nervous system in Parkinson's disease patients with chronic constipation. *Lancet* 346, 861–864.
- (138) Anderson, G., Noorian, A. R., Taylor, G., Anitha, M., Bernhard, D., Srinivasan, S., and Greene, J. G. (2007) Loss of enteric dopaminergic neurons and associated changes in colon motility in an MPTP mouse model of Parkinson's disease. *Exp. Neurosci.* 207, 4–12.
- (139) Zhi, S. L., Schmauss, C., Cuenca, A., Ratcliffe, E., and Gershon, M. D. (2006) Physiological modulation of intestinal motility by enteric dopaminergic neurons and the D2 receptor: Analysis of dopamine receptor expression, location, development, and function in wild-type and knock-out mice. *J. Neurosci.* 26, 2798–2807.
- (140) Ansaloni, L., Catena, F., and Pinna, A. D. (2009) What is the function of the human vermiform appendix? *Eur. Surg. Res.* 43, 67–71.
- (141) Kardong, K. V. (1995) *Vertebrates: Comparative anatomy, function, evolution* 5th ed. McGraw-Hill Higher Education, Boston.
- (142) Smith, H. F., Parker, W., Kotzé, S. H., and Laurin, M. (2013) Multiple independent

appearances of the cecal appendix in mammalian evolution and an investigation of related ecological and anatomical factors. *Comptes rendus - Palevol* 12, 339–354.

(143) Matsushita, M., Uchida, K., and Okazaki, K. (2007) Role of the appendix in the pathogenesis of ulcerative colitis. *Inflammopharmacology* 15, 154–157.

(144) Hardin, D. M. (1999) Acute appendicitis: Review and update. *Am. Fam. Physician* 60, 2027–2034.

(145) Bollinger, R. R., Barbas, A. S., Bush, E. L., Lin, S. S., and Parker, W. (2007) Biofilms in the large bowel suggest an apparent function of the human vermiform appendix. *J. Theor. Biol.* 249, 826–831.

(146) Laurin, M., Everett, M. Lou, and Parker, W. (2011) The cecal appendix: One more immune component with a function disturbed by post-industrial culture. *Anat. Rec.* 294, 567–579.

(147) Reshetnikov, O. V, Kurilovich, S. A., Denisova, D. V, Zav'ialova, L. G., Svetlova, I. O., Tereshonok, I. N., Krivenchuk, N. A., and Eremeeva, L. I. (2001) [Prevalence and risk factors of the development of irritable bowel syndrome in adolescents: a population study]. *Ter. arkhiv* 73, 24–9.

(148) Sleator, R. D., Cronin, M., and Hill, C. (2008) Why appendectomies may lead to an increased risk of functional gastrointestinal disorders. *Med. Hypotheses* 71, 814–816.

(149) Brender, J. D., Weiss, N. S., Koepsell, T. D., and Marcuse, E. K. (1985) Fiber intake and childhood appendicitis. *Am. J. Public Health* 75, 399–400.

(150) Adamidis, D., Roma-Giannikou, E., Karamolegou, K., Tselalidou, E., and Constantopoulos, A. (2000) Fiber intake and childhood appendicitis. *Int. J. Food Sci. Nutr.* 51, 153–157.

(151) Barker, D. J. P., Osmond, C., Golding, J., and Wadsworth, M. E. J. (1988) Acute appendicitis and bathrooms in three samples of British children. *Br. Med. J.* 296, 956–958.

(152) Sutherland, D. E. R., Archer, O. K., and Good, R. A. (1964) Role of the appendix in development of immunologic capacity. *Exp. Biol. Med.* 115, 673–676.

(153) Wong, S. H., Hill, A., Vannberg, F. O., Netea, M. G., and Kullberg, B. J. (2010) Genomewide association study of leprosy. *N. Engl. J. Med.* 362, 1446–1448.

(154) Barrett, J. C., Hansoul, S., Nicolae, D. L., Cho, J. H., Duerr, R. H., Rioux, J. D., Brant, S. R., Silverberg, M. S., Taylor, K. D., Barmada, M. M., Bitton, A., Dassopoulos, T., Datta, L. W., Green, T., Griffiths, A. M., Kistner, E. O., Murtha, M. T., Regueiro, M. D., Rotter, J. I., Schumm, L. P., Steinhardt, A. H., Targan, S. R., Xavier, R. J., Libioulle, C., Sandor, C., Lathrop, M., Belaiche, J., Dewit, O., Gut, I., Heath, S., Laukens, D., Mni, M., Rutgeerts, P., Van Gossum, A., Zelenika, D., Franchimont, D., Hugot, J. P., De Vos, M., Vermeire, S., Louis, E., Cardon, L. R., Anderson, C. A., Drummond, H., Nimmo, E., Ahmad, T., Prescott, N. J., Onnie, C. M., Fisher, S. A., Marchini, J., Ghori, J., Bumpstead, S., Gwilliam, R., Tremelling, M., Deloukas, P., Mansfield, J., Jewell, D., Satsangi, J., Mathew, C. G., Parkes, M., Georges, M., and Daly, M. J. (2008) Genome-wide association defines more than 30 distinct susceptibility loci for Crohn's disease. *Nat. Genet.* 40, 955–962.

(155) Rioux, P., Daly, M. J., Xavier, R. J., Ballester, D. K., Stevens, C., Korzenik, J. R., Agnès Gardet, J. D., Benita, Y., Li, C., and Sands, B. E. (2010) LRRK2 is involved in the IFN- γ response and host response to pathogens. *J. Immunol.* 185, 5577–5585.

(156) Lesage, S., Dürr, A., Tazir, M., Lohmann, E., and Leutenegger, A.-L. (2006) LRRK2 G2019S as a cause of Parkinson's disease in North African Arabs. *N. Engl. J. Med.* 354, 422–423.

(157) Zimprich, A., Biskup, S., Leitner, P., Lichtner, P., Farrer, M., Lincoln, S., Kachergus, J., Hulihan, M., Uitti, R. J., Calne, D. B., Stoessl, A. J., Pfeiffer, R. F., Patenge, N., Carbajal, I. C., Vieregge, P., Asmus, F., Müller-Myhsok, B., Dickson, D. W., Meitinger, T., Strom, T. M., Wszolek, Z. K., and Gasser, T. (2004) Mutations in LRRK2 cause autosomal-dominant parkinsonism with pleomorphic pathology. *Neuron* 44, 601–607.

- (158) Krüger, R. (2008) LRRK2 in Parkinson's disease - drawing the curtain of penetrance: A commentary. *BMC Med.* 6, 33.
- (159) Gasser, T. (2005) Genetics of Parkinson's disease. *Curr. Opinon Neurol.* 18, 363–369.
- (160) Shutinoski, B., Hakimi, M., Harmsen, I. E., Lunn, M., Rocha, J., Lengacher, N., Yuan Zhou, Y., Khan, J., Nguyen, A., Hake-Volling, Q., El-Kodsi, D., Li, J., Alikashani, A., Beauchamp, C., Majithia, J., Coombs, K., Shimshek, D., Marcogliese, P. C., Park, D. S., Rioux, J. D., Philpott, D. J., Woulfe, J. M., Hayley, S., Sad, S., Tomlinson, J. J., Brown, E. G., and Schlossmacher, M. G. (2019) Lrrk2 alleles modulate inflammation during microbial infection of mice in a sex-dependent manner. *Sci. Transl. Med.* 11, eaas9292.
- (161) Moehle, M. S., Lima Daher, J. P., Hull, T. D., Boddu, R., Abdelmotilib, H. A., Mobley, J., Kannarkat, G. T., Tansey, M. G., and West, A. B. (2015) The G2019S LRRK2 mutation increases myeloid cell chemotactic responses and enhances LRRK2 binding to actin-regulatory proteins. *Hum. Mol. Genet.* 24, 4250–4267.
- (162) Muller, P. A., Koscsó, B., Rajani, G. M., Stevanovic, K., Berres, M.-L., Hashimoto, D., Mortha, A., Leboeuf, M., Li, X.-M., Mucida, D., Stanley, E. R., Dahan, S., Margolis, K. G., Gershon, M. D., Merad, M., and Bogunovic, M. (2014) Crosstalk between muscularis macrophages and enteric neurons regulates gastrointestinal motility. *Cell* 158, 300–313.
- (163) Mikkelsen, H. B., Thuneberg, L., Rumessen, J. J., and Thorball, N. (1985) Macrophage-like cells in the muscularis externa of mouse small intestine. *Anat. Rec.* 213, 77–86.
- (164) Gabanyi, I., Muller, P. A., Feighery, L., Oliveira, T. Y., Costa-Pinto, F. A., and Mucida, D. (2016) Neuro-immune interactions drive tissue programming in intestinal macrophages. *Cell* 164, 378–391.
- (165) Kulkarni, S., Micci, M. A., Leser, J., Shin, C., Tang, S. C., Fu, Y. Y., Liu, L., Li, Q., Saha, M., Li, C., Enikolopov, G., Becker, L., Rakhilin, N., Anderson, M., Shen, X., Dong, X., Butte, M. J., Song, H., Southard-Smith, E. M., Kapur, R. P., Bogunovic, M., and Pasricha, P. J. (2017) Adult enteric nervous system in health is maintained by a dynamic balance between neuronal apoptosis and neurogenesis. *Proc. Natl. Acad. Sci. U. S. A.* 114, E3709–E3718.
- (166) Kulkarni, S., Ganz, J., Bayrer, J., Laren Becker, X., Bogunovic, M., and Rao, X. M. (2018) Advances in enteric neurobiology: The “brain” in the gut in health and disease. *J. Neurosci.* 38, 9346–9354.
- (167) Berthoud, H. -R, Jedrzejewska, A., and Powley, T. L. (1990) Simultaneous labeling of vagal innervation of the gut and afferent projections from the visceral forebrain with Dil injected into the dorsal vagal complex in the rat. *J. Comp. Neurol.* 301, 65–79.
- (168) Berthoud, H. R., Carlson, N. R., and Powley, T. L. (1991) Topography of efferent vagal innervation of the rat gastrointestinal tract. *Am. J. Physiol.* 260, R200–R207.
- (169) Gray, M. T., Munoz, D. G., Gray, D. A., Schlossmacher, M. G., and Woulfe, J. M. (2014) Alpha-synuclein in the appendiceal mucosa of neurologically intact subjects. *Mov. Disord.* 29, 991–998.
- (170) Killinger, B. A., Madaj, Z., Sikora, J. W., Rey, N., Haas, A. J., Vepa, Y., Lindqvist, D., Chen, H., Thomas, P. M., Brundin, P., Brundin, L., and Labrie, V. (2018) The vermiform appendix impacts the risk of developing Parkinson's disease. *Sci. Transl. Med.* 10, eaar5280.
- (171) Scheperjans, F., Aho, V., Pereira, P. A. B., Koskinen, K., Paulin, L., Pekkonen, E., Haapaniemi, E., Kaakkola, S., Eerola-Rautio, J., Pohja, M., Kinnunen, E., Murros, K., and Auvinen, P. (2015) Gut microbiota are related to Parkinson's disease and clinical phenotype. *Mov. Disord.* 30, 350–358.
- (172) Keshavarzian, A., Green, S. J., Engen, P. A., Voigt, R. M., Naqib, A., Forsyth, C. B., Mutlu, E., and Shannon, K. M. (2015) Colonic bacterial composition in Parkinson's disease. *Mov. Disord.* 30, 1351–1360.
- (173) Unger, M. M., Spiegel, J., Dillmann, K.-U., Grundmann, D., Philippeit, H.,

Bürmann, J., Fabbender, K., Schwierz, A., and Schäfer, K.-H. (2016) Short chain fatty acids and gut microbiota differ between patients with Parkinson's disease and age-matched controls. *Park. Relat. Disord.* 32, 66–72.

(174) Sampson, T. R., Debelius, J. W., Thron, T., Wittung-Stafshede, P., Knight, R., and Mazmanian, S. K. (2016) Gut microbiota regulate motor deficits and neuroinflammation in a model of Parkinson's disease. *Cell* 167, 1469–1480.

(175) Ananthaswamy, A. (2011) Faecal transplant eases symptoms of Parkinson's disease. *New Sci.* 209, 8–9.

(176) Ghosh, I., Hamilton, A. D., and Regan, L. (2000) Antiparallel leucine zipper-directed protein reassembly: Application to the green fluorescent protein. *J. Am. Chem. Soc.* 122, 5658–5659.

(177) Hu, C.-D., Chinenov, Y., and Kerppola, T. K. (2002) Visualization of interactions among bZIP and Rel family proteins in living cells using bimolecular fluorescence complementation. *Mol. Cell* 9, 789–798.

(178) McLean, P. J., Kawamata, H., and Hyman, B. T. (2001) α -Synuclein-enhanced green fluorescent protein fusion proteins form proteasome sensitive inclusions in primary neurons. *Neuroscience* 104, 901–912.

(179) Dimant, H., Kalia, S. K., Kalia, L. V., Zhu, L. N., Kibuuka, L., Ebrahimi-Fakhari, D., McFarland, N. R., Fan, Z., Hyman, B. T., and McLean, P. J. (2013) Direct detection of alpha synuclein oligomers in vivo. *Acta Neuropathol. Commun.* 1, 6.

(180) Sauer, B. (1987) Functional expression of the cre-lox site-specific recombination system in the yeast *Saccharomyces cerevisiae*. *Mol. Cell. Biol.* 7, 2087–2096.

(181) Sauer, B., and Henderson, N. (1988) Site-specific DNA recombination in mammalian cells by the Cre recombinase of bacteriophage P1. *Proc. Natl. Acad. Sci. U. S. A.* 85, 5166–5170.

(182) Picard, D. (1994) Regulation of protein function through expression of chimaeric proteins. *Curr. Opin. Biotechnol.* 5, 511–515.

(183) Metzger, D., and Chambon, P. (2001) Site- and time-specific gene targeting in the mouse. *Methods* 24, 71–80.

(184) Johnson, M. D., Zuo, H., Lee, K. H., Trebley, J. P., Rae, J. M., Weatherman, R. V., Desta, Z., Flockhart, D. A., and Skaar, T. C. (2004) Pharmacological characterization of 4-hydroxy-N-desmethyl tamoxifen, a novel active metabolite of tamoxifen. *Breast Cancer Res. Treat.* 85, 151–159.

(185) Hayashi, S., and McMahon, A. P. (2002) Efficient recombination in diverse tissues by a tamoxifen-inducible form of cre: A tool for temporally regulated gene activation/inactivation in the mouse. *Dev. Biol.* 244, 305–318.

(186) Raghavan, R., Kruijff, L. de, Sterrenburg, M. D., Rogers, B. B., Hladik, C. L., and White, C. L. (2004) Alpha-synuclein expression in the developing human brain. *Pediatr. Dev. Pathol.* 7, 506–516.

(187) Zhong, S. C., Luo, X., Chen, X. S., Cai, Q. Y., Liu, J., Chen, X. H., and Yao, Z. X. (2010) Expression and subcellular location of alpha-synuclein during mouse-embryonic development. *Cell. Mol. Neurobiol.* 30, 469–482.

(188) Lobe, C. G., Koop, K. E., Kreppner, W., Lomeli, H., Gertsenstein, M., and Nagy, A. (1999) Z/AP, a Double Reporter for Cre-Mediated Recombination. *Dev. Biol.* 208, 281–292.

(189) Ruzankina, Y., Pinzon-Guzman, C., Asare, A., Ong, T., Pontano, L., Cotsarelis, G., Zediak, V. P., Velez, M., Bhandoola, A., and Brown, E. J. (2007) Deletion of the developmentally essential gene ATR in adult mice leads to age-related phenotypes and stem cell loss. *Cell Stem Cell* 1, 113–126.

(190) Goodwin, L. O., Splinter, E., Davis, T. L., Urban, R., He, H., Braun, R. E., Chesler, E. J., Kumar, V., Van Min, M., Ndikum, J., Philip, V. M., Reinholdt, L. G., Svenson, K., White, J. K., Sasner, M., Lutz, C., and Murray, S. A. (2019) Large-scale discovery of mouse transgenic

integration sites reveals frequent structural variation and insertional mutagenesis. *Genome Res.* 29, 494–505.

(191) Kuo, Y. M., Li, Z., Jiao, Y., Gaborit, N., Pani, A. K., Orrison, B. M., Bruneau, B. G., Giasson, B. I., Smeyne, R. J., Gershon, M. D., and Nussbaum, R. L. (2010) Extensive enteric nervous system abnormalities in mice transgenic for artificial chromosomes containing Parkinson disease-associated α -synuclein gene mutations precede central nervous system changes. *Hum. Mol. Genet.* 19, 1633–1650.

(192) Haworth, S., Grynspan, D., and Schock, S. (2018) Gastrointestinal whole mount methods. Ottawa.

(193) Lowery, R. L., and Majewska, A. K. (2010) Intracranial injection of adeno-associated viral vectors. *J. Vis. Exp.* 45, 14–16.

(194) Djureinovic, D., Fagerberg, L., Hallström, B., Danielsson, A., Lindskog, C., Uhlén, M., and Pontén, F. (2014) The human testis-specific proteome defined by transcriptomics and antibody-based profiling. *Mol. Hum. Reprod.* 20, 476–488.

(195) Smith, M. W., and Lloyd, S. (1989) Intestinal infection with *Nematospiroides dubius* selectively increases lactase expression by mouse jejunal enterocytes. *Clin. Sci.* 77, 139–144.

(196) Okabe, M., Ikawa, M., Kominami, K., Nakanishi, T., and Nishimune, Y. (1997) 'Green mice' as a source of ubiquitous green cells. *Fed. Eur. Biochem. Soc. Lett.* 407, 313–319.

(197) Liu, Y., Okada, T., Nomoto, T., Ke, X., Kume, A., Ozawa, K., and Xiao, S. (2007) Promoter effects of adeno-associated viral vector for transgene expression in the cochlea in vivo. *Exp. Mol. Med.* 39, 170–175.

(198) Zhou, Y., Zhang, T., Zhang, Q.-K., Jiang, Y., Xu, D.-G., Zhang, M., Shen, W., and Pan, Q.-J. (2014) Unstable expression of transgene is associated with the methylation of CAG promoter in the offspring from the same litter of homozygous transgenic mice. *Mol Biol Rep* 41, 5177–5186.

(199) Yang, C., Shang, X., Cheng, L., Yang, L., Liu, X., Bai, C., Wei, Z., Hua, J., and Li, G. (2017) DNMT 1 maintains hypermethylation of CAG promoter specific region and prevents expression of exogenous gene in fat-1 transgenic sheep. *PLoS One* 12, e0171442.

(200) Pali, S. S., Van Emburgh, B. O., Sankpal, U. T., Brown, K. D., and Robertson, K. D. (2008) DNA methylation inhibitor 5-aza-2-deoxycytidine induces reversible genome-wide DNA damage that is distinctly influenced by DNA methyltransferases 1 and 3b. *Mol. Cell. Biol.* 28, 752–771.

(201) Grassi, G., Maccaroni, P., Meyer, R., Kaiser, H., D'Ambrosio, E., Pascale, E., Grassi, M., Kuhn, A., Di Nardo, P., Kandolf, R., and Küpper, J.-H. (2003) Inhibitors of DNA methylation and histone deacetylation activate cytomegalovirus promoter-controlled reporter gene expression in human glioblastoma cell line U87. *Carcinogenesis* 24, 1625–1635.

(202) Lai, M. D., Chen, C. S., Yang, C. R., Yuan, S. Y., Tsai, J. J., Tu, C. F., Wang, C. C., Yen, M. C., and Lin, C. C. (2010) An HDAC inhibitor enhances the antitumor activity of a CMV promoter-driven DNA vaccine. *Cancer Gene Ther.* 17, 203–211.

(203) Bubna, A. K. (2015, July 1) Vorinostat-An overview. *Indian J. Dermatol.* Medknow Publications.

(204) Benskey, M. J., Kuhn, N. C., Galligan, J. J., Garcia, J., Boye, S. E., Hauswirth, W. W., Mueller, C., Boye, S. L., and Manfredsson, F. P. (2015) Targeted Gene Delivery to the Enteric Nervous System Using AAV: A Comparison Across Serotypes and Capsid Mutants. *Mol. Ther.* 23, 488–500.

(205) Coulombe, J., Gamage, P., Gray, M. T., Zhang, M., Tang, M. Y., Woulfe, J., Saffrey, M. J., and Gray, D. A. (2014) Loss of UCHL1 promotes age-related degenerative changes in the enteric nervous system. *Front. Aging Neurosci.* 6, 129.

(206) Gray, M. T. (2014) On α -synuclein in the human enteric nervous system. University of Ottawa.

(207) Green, F., Samaranch, L., Zhang, H. S., Manning-Bog, A., Meyer, K., Forsayeth,

- J., and Bankiewicz, K. S. (2016) Axonal transport of AAV9 in nonhuman primate brain. *Gene Ther.* 23, 520–526.
- (208) Jukam, D., Shariati, S. A. M., and Skotheim, J. M. (2017) Zygotic genome activation in vertebrates. *Dev. Cell* 42, 316–332.
- (209) Eissenberg, J. C., James, T. C., Foster-Hartnett, D. M., Hartnett, T., Ngan, V., and Elgin, S. C. R. (1990) Mutation in a heterochromatin-specific chromosomal protein is associated with suppression of position-effect variegation in *Drosophila melanogaster*. *Proc. Natl. Acad. Sci. USA* 87, 9923–9927.
- (210) Wallrath, L. L., and Elgin, S. C. R. (1995) Position effect variegation in *Drosophila* is associated with an altered chromatin structure. *Genes Dev.* 9, 1263–1277.
- (211) Eissenberg, J. C. (1989) Position effect variegation in *Drosophila*: Towards a genetics of chromatin assembly. *BioEssays* 11, 14–17.
- (212) Lu, B. Y., Ma, J., and Eissenberg, J. C. (1998) Developmental regulation of heterochromatin-mediated gene silencing in *Drosophila*. *Development* 125, 2223–2234.
- (213) Irizarry, M. C., Growdon, W., Gomez-Isla, T., Newell, K., George Julia M, Clayton, D. F., and Hyman, B. T. (1998) Nigral and cortical Lewy bodies and dystrophic nigral neurites in Parkinson's disease and cortical Lewy body disease contain alpha-synuclein immunoreactivity. *J. Neuropathol. Exp. Neurol.* 57, 334–337.
- (214) Salegio, E., Samaranch, L., Kells, A., Mittermeyer, G., San Sebastian, W., Zhou, S., Beyer, J., Forsayeth, J., and Bankiewicz, K. (2013) Axonal transport of adeno-associated viral vectors is serotype-dependent. *Gene Ther.* 20, 348–352.
- (215) Oleshko, N. N., Maiskii, V. A., Cherkes, V. A., and Kolomiets, B. P. (1983) Divergence of axon collaterals of substantia nigra neurons in the rat forebrain: Double labeling with fluorochromes and horseradish peroxidase. *Neurophysiology* 15, 375–383.
- (216) Matsuda, W., Furuta, T., Nakamura, K. C., Hioki, H., Fujiyama, F., Arai, R., and Kaneko, T. (2009) Single nigrostriatal dopaminergic neurons form widely spread and highly dense axonal arborizations in the neostriatum. *J. Neurosci.* 29, 444–453.
- (217) Hoggan, M. D., Blacklow, N. R., and Rowe, W. P. (1966) Studies of small DNA viruses found in various adenovirus preparations: Physical, biological and immunological characteristics. *Proc. Natl. Acad. Sci.* 55, 1467–1474.
- (218) Wang, D., Tai, P. W. L., and Gao, G. (2019) Adeno-associated virus vector as a platform for gene therapy delivery. *Nat. Rev. Drug Discov.* 18, 358–378.
- (219) Altman, J. (1962) Are new neurons formed in the brains of adult mammals? *Science (80-)*. 135, 1127–1128.
- (220) Rae, A. S. (1993) Nodules of cellular proliferation in sheep olfactory ventricle. *Clin. Neuropathol.* 13, 17–18.
- (221) Curtis, M. A., Kam, M., Nannmark, U., Anderson, M. F., Axell, M. Z., Wikkelso, C., Holtås, S., van Roon-Mom, W. M. C., Björk-Eriksson, T., Nordborg, C., Frisén, J., Dragunow, M., Faull, R. L. M., and Eriksson, P. S. (2007) Human neuroblasts migrate to the olfactory bulb via a lateral ventricular extension. *Science (80-)*. 315, 1243–1249.
- (222) Gheusi, G., Cremer, H., Mclean, H., Chazal, G., Vincent, J.-D., and Lledo, P.-M. (2000) Importance of newly generated neurons in the adult olfactory bulb for odor discrimination. *Proc. Natl. Acad. Sci.* 97, 1823–1828.
- (223) Panzanelli, P., Fritschy, J. M., Yanagawa, Y., Obata, K., and Sassoè-Pognetto, M. (2007) GABAergic phenotype of periglomerular cells in the rodent olfactory bulb. *J. Comp. Neurol.* 502, 990–1002.
- (224) Gengatharan, A., Bammann, R. R., and Saghatelyan, A. (2016) The role of astrocytes in the generation, migration, and integration of new neurons in the adult olfactory bulb. *Front. Neurosci.* 10, 149.
- (225) Faiz, M., Acarin, L., Castellano, B., and Gonzalez, B. (2005) Proliferation dynamics of germinative zone cells in the intact and excitotoxically lesioned postnatal rat brain. *BMC*

Neurosci. 6, 26.

(226) Aguilar Martínez, N., Aguado Carrillo, G., Saucedo Alvarado, P. E., Mendoza García, C. A., Velasco Monroy, A. L., and Velasco Campos, F. (2018) Clinical importance of olfactory function in neurodegenerative diseases. *Rev. Médica del Hosp. Gen. México* 81, 268–275.

(227) Doty, R. L., Deems, D. A., and Stellar, S. (1988) Olfactory dysfunction in parkinsonism: A general deficit unrelated to neurologic signs, disease stage, or disease duration. *Neurology* 38, 1237–1244.

(228) Höglinger, G. U., Rizk, P., Muriel, M. P., Duyckaerts, C., Oertel, W. H., Caille, I., and Hirsch, E. C. (2004) Dopamine depletion impairs precursor cell proliferation in Parkinson disease. *Nat. Neurosci.* 7, 726–735.

(229) Freundlieb, N., François, C., Tandé, D., Oertel, W. H., Hirsch, E. C., and Höglinger, G. U. (2006) Dopaminergic substantia nigra neurons project topographically organized to the subventricular zone and stimulate precursor cell proliferation in aged primates. *J. Neurosci.* 26, 2321–2325.

(230) Zapiec, B., Dieriks, B. V., Tan, S., Faull, R. L. M., Mombaerts, P., and Curtis, M. A. (2017) A ventral glomerular deficit in Parkinson's disease revealed by whole olfactory bulb reconstruction. *Brain* 140, 2722–2736.

(231) Marxreiter, F., Regensburger, M., and Winkler, J. (2013) Adult neurogenesis in Parkinson's disease. *Cell. Mol. Life Sci.* 70, 459–473.

(232) Desplats, P., Spencer, B., Crews, L., Pathel, P., Morvinski-Friedmann, D., Kosberg, K., Roberts, S., Patrick, C., Winkler, J., and Masliah, E. (2012) Alpha-synuclein induces alterations in adult neurogenesis in Parkinson disease models via p53-mediated repression of Notch1. *J. Biol. Chem.* 287, 31691–31702.

(233) Yu, S.-J., Tseng, K.-Y., Shen, H., Harvey, B. K., and Airavaara, M. (2013) Local administration of AAV-BDNF to subventricular zone induces functional recovery in stroke rats. *PLoS One* 8, e81750.

(234) Henry, R. A., Hughes, S. M., and Connor, B. (2007) AAV-mediated delivery of BDNF augments neurogenesis in the normal and quinolinic acid-lesioned adult rat brain. *Eur. J. Neurosci.* 25, 3513–3525.

(235) Millson, G. C., Kimberlin, R. H., Jane Manning, E., and Collis, S. C. (1979) Early distribution of radioactive liposomes and scrapie infectivity in mouse tissues following administration by different routes. *Vet. Microbiol.* 4, 89–99.

(236) Head, M. W., Yull, H. M., Ritchie, D. L., Bishop, M. T., and Ironside, J. W. (2009) Pathological investigation of the first blood donor and recipient pair linked by transfusion-associated variant creutzfeldt-jakob disease transmission. *Neuropathol. Appl. Neurobiol.* 35, 433–436.

(237) McNulty, E. E., Nalls, A. V., Xun, R., Denkers, N. D., Hoover, E. A., and Mathiason, C. K. (2020) In vitro detection of haematogenous prions in white-tailed deer orally dosed with low concentrations of chronic wasting disease. *J. Gen. Virol.* 101, 347–361.

(238) Sisó, S., González, L., and Jeffrey, M. (2010) Neuroinvasion in prion diseases: The roles of ascending neural infection and blood dissemination. *Interdiscip. Perspect. Infect. Dis.* 2010, 747892.

(239) Scranton, R. A., Fletcher, L., Sprague, S., Jimenez, D. F., and Digicaylioglu, M. (2011) The rostral migratory stream plays a key role in intranasal delivery of drugs into the CNS. *PLoS One* 6, e18711.

(240) Duvernoy, H. M., and Risold, P.-Y. (2007) The circumventricular organs: An atlas of comparative anatomy and vascularization. *Brain Res. Rev.* 56, 119–147.

(241) Jang, A., Lee, H.-J., Suk, J.-E., Jung, J.-W., Kim, K.-P., and Lee, S.-J. (2010) Non-classical exocytosis of α -synuclein is sensitive to folding states and promoted under stress conditions. *J. Neurochem.* 113, 1263–1274.

- (242) Lee, H. J., Suk, J. E., Patrick, C., Bae, E. J., Cho, J. H., Rho, S., Hwang, D., Masliah, E., and Lee, S. J. (2010) Direct transfer of α -synuclein from neuron to astroglia causes inflammatory responses in synucleinopathies. *J. Biol. Chem.* 285, 9262–9272.
- (243) Peretto, P., Merighi, A., Fasolo, A., and Bonfanti, L. (1997) Glial tubes in the rostral migratory stream of the adult rat. *Brain Res. Bull.* 42, 9–21.
- (244) Liu, G., Martins, I. H., Chiorini, J. A., and Davidson, B. L. (2005) Adeno-associated virus type 4 (AAV4) targets ependyma and astrocytes in the subventricular zone and RMS. *Gene Ther.* 12, 1503–1508.
- (245) Rey, N. L., Wesson, D. W., and Brundin, P. (2018) The olfactory bulb as the entry site for prion-like propagation in neurodegenerative diseases. *Neurobiol. Dis.* 109, 226–248.
- (246) Lalancette-Hébert, M., Phaneuf, D., Soucy, G., Weng, Y. C., and Kriz, J. (2009) Live imaging of Toll-like receptor 2 response in cerebral ischaemia reveals a role of olfactory bulb microglia as modulators of inflammation. *Brain* 132, 940–954.
- (247) Ding, X., and Xie, F. (2015) Olfactory mucosa: Composition, enzymatic localization, and metabolism, in *Handbook of Olfaction and Gustation* (Doty, R. L., Ed.), pp 63–92. John Wiley & Sons, Inc, Hoboken, NJ, USA.
- (248) Chen, M., Reed, R. R., and Lane, A. P. (2019) Chronic inflammation directs an olfactory stem cell functional switch from neuroregeneration to immune defense. *Cell Stem Cell* 25, 513.
- (249) Chen, H., Zhang, S. M., Hernán, M. A., Schwarzchild, M. A., Willett, W. C., Colditz, G. A., Speizer, F. E., and Ascherio, A. (2003) Nonsteroidal anti-inflammatory drugs and the risk of Parkinson disease. *JAMA Neurol.* 60, 1059–1064.
- (250) Gagne, J. J., and Power, M. C. (2010) Anti-inflammatory drugs and risk of Parkinson disease: A meta-analysis. *Neurology* 74, 995–1002.
- (251) Wahner, A. D., Bronstein, J. M., Bordelon, Y. M., and Ritz, B. (2007) Nonsteroidal anti-inflammatory drugs may protect against Parkinson disease. *Neurology* 69, 1836–1842.
- (252) Kim, S., Kwon, S.-H., Kam, T.-I., Panicker, N., Karuppagounder, S. S., Lee, S., Lee, J. H., Kim, W. R., Kook, M., Foss, C. A., Shen, C., Lee, H., Kulkarni, S., Pasricha, P. J., Lee, G., Pomper, M. G., Dawson, V. L., Dawson, T. M., and Ko, H. S. (2019) Transneuronal Propagation of Pathologic α -Synuclein from the Gut to the Brain Models Parkinson's Disease. *Neuron* 1–15.
- (253) Mao, X., Ou, M. T., Karuppagounder, S. S., Kam, T. I., Yin, X., Xiong, Y., Ge, P., Umanah, G. E., Brahmachari, S., Shin, J. H., Kang, H. C., Zhang, J., Xu, J., Chen, R., Park, H., Andrabi, S. A., Kang, S. U., Gonçalves, R. A., Liang, Y., Zhang, S., Qi, C., Lam, S., Keiler, J. A., Tyson, J., Kim, D., Panicker, N., Yun, S. P., Workman, C. J., Vignali, D. A. A., Dawson, V. L., Ko, H. S., and Dawson, T. M. (2016) Pathological α -synuclein transmission initiated by binding lymphocyte-activation gene 3. *Science* (80-). 353, aah3374.
- (254) Hauser, R. A., Lyons, K. E., McClain, T., Carter, S., and Perlmutter, D. (2009) Randomized, double-blind, pilot evaluation of intravenous glutathione in Parkinson's disease. *Mov. Disord.* 24, 979–983.
- (255) Mischley, L. K., Conley, K. E., Shankland, E. G., Kavanagh, T. J., Rosenfeld, M. E., Duda, J. E., White, C. C., Wilbur, T. K., De La Torre, P. U., and Padowski, J. M. (2016) Central nervous system uptake of intranasal glutathione in Parkinson's disease. *npj Park. Dis.* 2, 16002.
- (256) Mischley, L. K., Lau, R. C., Shankland, E. G., Wilbur, T. K., and Padowski, J. M. (2017) Phase IIb study of intranasal glutathione in Parkinson's disease. *J. Parkinsons. Dis.* 7, 289–299.
- (257) Treuting, P. M., and Dintzis, S. M. (2012) Lower Gastrointestinal Tract. *Comp. Anat. Histol.* 177–192.
- (258) Berndt, A., Wilhelm, A., Jugert, C., Pieper, J., Sachse, K., and Methner, U. (2007) Chicken cecum immune response to *Salmonella enterica* serovars of different levels of

invasiveness. *Infect. Immun.* 75, 5993–6007.

(259) Swaggerty, C. L., Kogut, M. H., He, H., Genovese, K. J., Johnson, C., and Arsenault, R. J. (2017) Differential levels of cecal colonization by *Salmonella enteritidis* in chickens triggers distinct immune kinome profiles. *Front. Vet. Sci.* 4, 214.

Contributions of Collaborators

Madison T. Gray produced the BiSyn cassette and added it into the original CAG-floxed β -geo construct in place of the XhoI to NotI sites. Madison also built the map of the BiSyn vector in SnapGene.

Dr. Josée Coulombe produced the original BiSyn chimeras and performed the intercrosses necessary to achieve the three BiSyn mouse lines. She undertook the majority of the animal care work and the initial genotyping. Josée harvested zygotes following positive copulation plugs and removed ovaries for expression experiments.

Dr. Douglas A. Gray generated Figure #, which was initially appended to the grant proposal for the Michael J. Fox Foundation grant, which was used to generate the BiSyn mice. He performed all mentioned transfections and assisted with z-stack microscopy images.

Dr. John Woulfe captured all confocal microscopy images at the University of Ottawa Faculty of Medicine core facility.

Appendices

Appendix A: Copyright permission for reproduction of Figure 1

ELSEVIER LICENSE
TERMS AND CONDITIONS
May 11, 2020

This Agreement between Ottawa Hospital Research Institute -- Kianna Mau ("You") and Elsevier ("Elsevier") consists of your license details and the terms and conditions provided by Elsevier and Copyright Clearance Center.

License Number	4826000783108
License date	May 11, 2020
Licensed Content Publisher	Elsevier
Licensed Content Publication	Biological Psychiatry
Licensed Content Title	Therapeutic strategies for neurodegenerative disorders: Emerging clues from parkinson's disease
Licensed Content Author	Carsten R Bjarkam, Jens C Sørensen
Licensed Content Date	Aug 15, 2004
Licensed Content Volume	56
Licensed Content Issue	4
Licensed Content Pages	4
Start Page	213
End Page	216
Type of Use	reuse in a thesis/dissertation
Portion	figures/tables/illustrations
Number of figures/tables/illustrations	1
Format	electronic
Are you the author of this Elsevier article?	No
Will you be translating?	No
Title	Bifluorescent complementation of alpha-synuclein aggregation in vivo
Institution name	Ottawa Hospital Research Institute, University of Ottawa
Expected presentation date	Aug 2020
Portions	Figure 1 on page 2 Ottawa Hospital Research Institute 501 Smyth Rd
Requestor Location	Ottawa, ON K1H 8M2 Canada Attn: Ottawa Hospital Research Institute
Publisher Tax ID	GB 494 6272 12
Total	0.00 CAD

Appendix B: Copyright permission for reproduction of Figure 2

SPRINGER NATURE LICENSE TERMS AND CONDITIONS

May 24, 2020

This Agreement between Ottawa Hospital Research Institute -- Kianna Mau ("You") and Springer Nature ("Springer Nature") consists of your license details and the terms and conditions provided by Springer Nature and Copyright Clearance Center.

License Number	4835420930779
License date	May 24, 2020
Licensed Content Publisher	Springer Nature
Licensed Content Publication	Journal of Neural Transmission
Licensed Content Title	Idiopathic Parkinson's disease: possible routes by which vulnerable neuronal types may be subject to neuroinvasion by an unknown pathogen
Licensed Content Author	H. Braak et al
Licensed Content Date	Jan 1, 2003
Type of Use	Thesis/Dissertation
Requestor type	academic/university or research institute
Format	electronic
Portion	figures/tables/illustrations
Number of figures/tables/illustrations	1
Will you be translating?	no
Circulation/distribution	1 - 29
Author of this Springer Nature content	no
Title	Bifluorescent complementation of alpha-synuclein aggregation in vivo
Institution name	Ottawa Hospital Research Institute, University of Ottawa
Expected presentation date	Aug 2020
Portions	Figure 5 a -b Ottawa Hospital Research Institute 501 Smyth Rd
Requestor Location	Ottawa, ON K1H 8M2 Canada Attn: Ottawa Hospital Research Institute
Total	0.00 CAD

Appendix C: Copyright permission for reproduction of Figure 3

JOHN WILEY AND SONS LICENSE TERMS AND CONDITIONS

May 27, 2020

This Agreement between Ottawa Hospital Research Institute -- Kianna Mau ("You") and John Wiley and Sons ("John Wiley and Sons") consists of your license details and the terms and conditions provided by John Wiley and Sons and Copyright Clearance Center.

License Number	4837150326303
License date	May 27, 2020
Licensed Content Publisher	John Wiley and Sons
Licensed Content Publication	Neuropathology and Applied Neurobiology
Licensed Content Title	Parkinson's disease: a dual-hit hypothesis
Licensed Content Author	H. Braak, K. Del Tredici, C. H. Hawkes
Licensed Content Date	Oct 24, 2007
Licensed Content Volume	33
Licensed Content Issue	6
Licensed Content Pages	16
Type of use	Dissertation/Thesis
Requestor type	University/Academic
Format	Electronic
Portion	Figure/table
Number of figures/tables	1
Will you be translating?	No
Title	Bifluorescent complementation of alpha-synuclein aggregation in vivo
Institution name	Ottawa Hospital Research Institute, University of Ottawa
Expected presentation date	Aug 2020
Portions	Figure 3 Ottawa Hospital Research Institute 501 Smyth Rd
Requestor Location	Ottawa, ON K1H 8M2 Canada Attn: Ottawa Hospital Research Institute
Publisher Tax ID	EU826007151
Total	0.00 CAD

Appendix D: Copyright permission for reproduction of Figure 4

JOHN WILEY AND SONS LICENSE TERMS AND CONDITIONS

May 25, 2020

This Agreement between Ottawa Hospital Research Institute -- Kianna Mau ("You") and John Wiley and Sons ("John Wiley and Sons") consists of your license details and the terms and conditions provided by John Wiley and Sons and Copyright Clearance Center.

License Number	4836091258605
License date	May 25, 2020
Licensed Content Publisher	John Wiley and Sons
Licensed Content Publication	Wiley Books
Licensed Content Date	Dec 31, 1969
Licensed Content Pages	10
Type of use	Dissertation/Thesis
Requestor type	University/Academic
Format	Electronic
Portion	Figure/table
Number of figures/tables	1
Will you be translating?	No
Title	Bifluorescent complementation of alpha-synuclein aggregation in vivo
Institution name	Ottawa Hospital Research Institute, University of Ottawa
Expected presentation date	Aug 2020
Portions	Figure 1.1 Ottawa Hospital Research Institute 501 Smyth Rd
Requestor Location	Ottawa, ON K1H 8M2 Canada Attn: Ottawa Hospital Research Institute
Publisher Tax ID	EU826007151
Total	0.00 CAD

Appendix E: Copyright permission for reproduction of Figure 5

SPRINGER NATURE LICENSE TERMS AND CONDITIONS

May 25, 2020

This Agreement between Ottawa Hospital Research Institute -- Kianna Mau ("You") and Springer Nature ("Springer Nature") consists of your license details and the terms and conditions provided by Springer Nature and Copyright Clearance Center.

License Number	4835971460347
License date	May 25, 2020
Licensed Content Publisher	Springer Nature
Licensed Content Publication	Springer eBook
Licensed Content Title	The Enteric Nervous System and Gastrointestinal Innervation: Integrated Local and Central Control
Licensed Content Author	John B. Furness, Brid P. Callaghan, Leni R. Rivera et al
Licensed Content Date	Jan 1, 2014
Type of Use	Thesis/Dissertation
Requestor type	academic/university or research institute
Format	electronic
Portion	figures/tables/illustrations
Number of figures/tables/illustrations	1
Will you be translating?	no
Circulation/distribution	1 - 29
Author of this Springer Nature content	no
Title	Bifluorescent complementation of alpha-synuclein aggregation in vivo
Institution name	Ottawa Hospital Research Institute, University of Ottawa
Expected presentation date	Aug 2020
Portions	Figure 3.1 Ottawa Hospital Research Institute 501 Smyth Rd
Requestor Location	Ottawa, ON K1H 8M2 Canada Attn: Ottawa Hospital Research Institute
Total	0.00 CAD

Appendix F: Copyright permission for reproduction of Figure 6

SPRINGER NATURE LICENSE TERMS AND CONDITIONS

May 21, 2020

This Agreement between Ottawa Hospital Research Institute -- Kianna Mau ("You") and Springer Nature ("Springer Nature") consists of your license details and the terms and conditions provided by Springer Nature and Copyright Clearance Center.

License Number	4833931073154
License date	May 21, 2020
Licensed Content Publisher	Springer Nature
Licensed Content Publication	Acta Neuropathologica
Licensed Content Title	Parkinson's disease: an immunohistochemical study of Lewy body-containing neurons in the enteric nervous system
Licensed Content Author	K. Wakabayashi et al
Licensed Content Date	Jan 1, 1990
Type of Use	Thesis/Dissertation
Requestor type	academic/university or research institute
Format	electronic
Portion	figures/tables/illustrations
Number of figures/tables/illustrations	1
Will you be translating?	no
Circulation/distribution	1 - 29
Author of this Springer Nature content	no
Title	Bifluorescent complementation of alpha-synuclein aggregation in vivo
Institution name	Ottawa Hospital Research Institute, University of Ottawa
Expected presentation date	Aug 2020
Portions	Figure 2a-d on page 2 Ottawa Hospital Research Institute 501 Smyth Rd
Requestor Location	Ottawa, ON K1H 8M2 Canada Attn: Ottawa Hospital Research Institute
Total	0.00 CAD

Appendix G: Copyright permission for reproduction of Figure 8

ELSEVIER LICENSE TERMS AND CONDITIONS

May 26, 2020

This Agreement between Ottawa Hospital Research Institute -- Kianna Mau ("You") and Elsevier ("Elsevier") consists of your license details and the terms and conditions provided by Elsevier and Copyright Clearance Center.

License Number	4836671425171
License date	May 26, 2020
Licensed Content Publisher	Elsevier
Licensed Content Publication	Current Opinion in Biotechnology
Licensed Content Title	Regulation of protein function through expression of chimaeric proteins
Licensed Content Author	Didier Picard
Licensed Content Date	Oct 1, 1994
Licensed Content Volume	5
Licensed Content Issue	5
Licensed Content Pages	5
Start Page	511
End Page	515
Type of Use	reuse in a thesis/dissertation
Portion	figures/tables/illustrations
Number of figures/tables/illustrations	1
Format	electronic
Are you the author of this Elsevier article?	No
Will you be translating?	No
Title	Bifluorescent complementation of alpha-synuclein aggregation in vivo
Institution name	Ottawa Hospital Research Institute, University of Ottawa
Expected presentation date	Aug 2020
Portions	Figure 1b Ottawa Hospital Research Institute 501 Smyth Rd
Requestor Location	Ottawa, ON K1H 8M2 Canada Attn: Ottawa Hospital Research Institute
Publisher Tax ID	GB 494 6272 12
Total	0.00 CAD

Appendix H: Copyright permission for reproduction of Figure 19

JOHN WILEY AND SONS LICENSE TERMS AND CONDITIONS

Jun 01, 2020

This Agreement between Ottawa Hospital Research Institute -- Kianna Mau ("You") and John Wiley and Sons ("John Wiley and Sons") consists of your license details and the terms and conditions provided by John Wiley and Sons and Copyright Clearance Center.

License Number	4840300820223
License date	Jun 01, 2020
Licensed Content Publisher	John Wiley and Sons
Licensed Content Publication	BioEssays
Licensed Content Title	Position effect variegation in Drosophila: Towards a genetics of chromatin assembly
Licensed Content Author	Joel C. Eissenberg
Licensed Content Date	Feb 5, 2005
Licensed Content Volume	11
Licensed Content Issue	1
Licensed Content Pages	4
Type of use	Dissertation/Thesis
Requestor type	University/Academic
Format	Electronic
Portion	Figure/table
Number of figures/tables	2
Will you be translating?	No
Title	Bifluorescent complementation of alpha-synuclein aggregation in vivo
Institution name	Ottawa Hospital Research Institute, University of Ottawa
Expected presentation date	Aug 2020
Portions	Figures 1 and 2 Ottawa Hospital Research Institute 501 Smyth Rd
Requestor Location	Ottawa, ON K1H 8M2 Canada Attn: Ottawa Hospital Research Institute
Publisher Tax ID	EU826007151
Total	0.00 CAD

Appendix I: Copyright permission for reproduction of Figure 20

SPRINGER NATURE LICENSE TERMS AND CONDITIONS

Jun 07, 2020

This Agreement between Ottawa Hospital Research Institute -- Kianna Mau ("You") and Springer Nature ("Springer Nature") consists of your license details and the terms and conditions provided by Springer Nature and Copyright Clearance Center.

License Number	4843811073800
License date	Jun 07, 2020
Licensed Content Publisher	Springer Nature
Licensed Content Publication	Nature Reviews Drug Discovery
Licensed Content Title	Adeno-associated virus vector as a platform for gene therapy delivery
Licensed Content Author	Dan Wang et al
Licensed Content Date	Feb 1, 2019
Type of Use	Thesis/Dissertation
Requestor type	academic/university or research institute
Format	electronic
Portion	figures/tables/illustrations
Number of figures/tables/illustrations	1
High-res required	no
Will you be translating?	no
Circulation/distribution	1 - 29
Author of this Springer Nature content	no
Title	Bifluorescent complementation of alpha-synuclein aggregation in vivo
Institution name	Ottawa Hospital Research Institute, University of Ottawa
Expected presentation date	Aug 2020
Portions	Figure 2 Ottawa Hospital Research Institute 501 Smyth Rd
Requestor Location	Ottawa, ON K1H 8M2 Canada Attn: Ottawa Hospital Research Institute
Total	0.00 CAD

Appendix J: Copyright permission for reproduction of Figure 22

THE AMERICAN ASSOCIATION FOR THE ADVANCEMENT OF SCIENCE LICENSE TERMS AND CONDITIONS

Jun 08, 2020

This Agreement between Ottawa Hospital Research Institute -- Kianna Mau ("You") and The American Association for the Advancement of Science ("The American Association for the Advancement of Science") consists of your license details and the terms and conditions provided by The American Association for the Advancement of Science and Copyright Clearance Center.

License Number	4844300875907
License date	Jun 08, 2020
Licensed Content Publisher	The American Association for the Advancement of Science
Licensed Content Publication	Science
Licensed Content Title	Pathological α -synuclein transmission initiated by binding lymphocyte-activation gene 3
Licensed Content Author	Xiaobo Mao, Michael Tianhao Ou, Senthilkumar S. Karuppagounder, Tae-In Kam, Xiling Yin, Yulan Xiong, Preston Ge, George Essien Umanah, Saurav Brahmachari, Joo-Ho Shin, Ho Chul Kang, Jianmin Zhang, Jinchong Xu, Rong Chen, Hyejin Park, Shaída A. Andrabi, Sung Ung Kang, Rafaella Araújo Gonçalves, Yu Liang, Shu Zhang, Chen Qi, Sharon Lam, James A. Keiler, Joel Tyson, Donghoon Kim, Nikhil Panicker, Seung Pil Yun, Creg J. Workman, Dario A. A. Vignali, Valina L. Dawson, Han Seok Ko, Ted M. Dawson
Licensed Content Date	Sep 30, 2016
Licensed Content Volume	353
Licensed Content Issue	6307
Volume number	353
Issue number	6307
Type of Use	Thesis / Dissertation
Requestor type	Scientist/individual at a research institution
Format	Print and electronic
Portion	Figure
Number of figures/tables	1
Title	Bifluorescent complementation of alpha-synuclein aggregation in vivo
Institution name	Ottawa Hospital Research Institute, University of Ottawa
Expected presentation date	Aug 2020
Portions	Graphical abstract with caption title "LAG3 deletion or antibodies to LAG3 delay α -synuclein PFF transmission" Ottawa Hospital Research Institute 501 Smyth Rd
Requestor Location	Ottawa, ON K1H 8M2 Canada Attn: Ottawa Hospital Research Institute
Total	0.00 CAD

Curriculum Vitae

KIANNA J. MAU

EDUCATION

Master of Science in Biochemistry 2017 – 2020
Specialization in Pathology and Experimental Medicine
Ottawa Hospital Research Institute, University of Ottawa
Thesis: Bifluorescent analysis of alpha-synuclein aggregation *in vivo*
Supervisors: Drs. Douglas A. Gray and John Woulfe

Bachelor of Science Honours in Neuroscience and Mental Health 2013 – 2017
Minors in Biology and Psychology
Carleton University
Thesis: A new perspective on Parkinson's disease: pathology begins in the gastrointestinal tract
Supervisor: Dr. Nafisa M. Jadavji

ACADEMIC AWARDS AND ACHIEVEMENTS

University of Ottawa Admission Scholarship
2017 – 2019 (\$15,000)

University of Ottawa Dean's List
2018, 2019

Carleton University Entrance Scholarship
2013 – 2016 (\$9,000)

Carleton University Dean's List
2014, 2015, 2017

Ontario Parks Partners' Bursary Recipient
2015 (\$500)

Carleton University Department of Neuroscience Scholarship
2013 (\$1,000)

RESEARCH ACTIVITY

PEER REVIEWED PUBLICATIONS

Mau KJ, Jadavji NM. (2017). A new perspective on Parkinson's disease: pathology begins in the gastrointestinal tract. *Journal of Young Investigators*. 33(4):1-8.

ABSTRACTS FOR SEMINAR PRESENTATIONS

Mau KJ. Pollution and children's health [Landrigan *et al.*, *Science of the Total Environment* (2019)]. Journal Club, Cancer Therapeutics Program, The Ottawa Hospital Research Institute Cancer Centre, 2019.

Mau KJ, Coulombe J, Woulfe J, Gray DA. Bifluorescent analysis of alpha-synuclein aggregation *in vivo*. University of Ottawa Biochemistry, Microbiology and Immunology Research Day, 2019.

Mau KJ. The magical activation of left amygdala when reading Harry Potter: an fMRI study on how descriptions of supernatural events entertain and enchant [Hsu *et al.*, *PLoS ONE* (2015)]. Journal Club, Cancer Therapeutics Program, The Ottawa Hospital Research Institute Cancer Centre, 2019.

Mau KJ. Bifluorescent analysis of alpha-synuclein aggregation *in vivo*. Work in Progress, Cancer Therapeutics Program, The Ottawa Hospital Research Institute Cancer Centre, 2019.

Mau KJ. Does Parkinson's disease start in the gut? [Lionnet *et al.*, *Acta Neuropathol* (2018)]. Journal Club, Cancer Therapeutics Program, The Ottawa Hospital Research Institute Cancer Centre, 2018.

Mau KJ. Bifluorescent complementation of alpha-synuclein aggregation. Work in Progress, Cancer Therapeutics Program, The Ottawa Hospital Research Institute Cancer Centre, 2018.

ABSTRACTS FOR POSTER PRESENTATIONS

Mau KJ, Coulombe J, Woulfe J, Gray DA. Characterization of novel bifluorescent transgenic mice for Parkinson's disease research. Ottawa Hospital Research Institute Research Day, 2019.

Mau KJ, Coulombe J, Woulfe J, Gray DA. Novel system for Parkinson's research: bifluorescent visualization of alpha-synuclein aggregates. University of Ottawa Faculty of Medicine Annual Research Day, 2019.

Mau KJ, Coulombe J, Woulfe J, Gray DA. Bifluorescent analysis of alpha-synuclein aggregation *in vivo*. University of Ottawa Department of Pathology and Laboratory Medicine Annual Research Day, 2019.

Mau KJ, Coulombe J, Woulfe J, Gray DA. Bifluorescent analysis of alpha-synuclein aggregation *in vivo*. Brain and Mind Research Institute. Brain Health Research Day, 2019.

Mau KJ, Coulombe J, Woulfe J, Gray DA. Bifluorescent analysis of alpha-synuclein aggregation *in vivo*. Ottawa Hospital Research Institute Research Day, 2018.

Mau KJ, Coulombe J, Woulfe, J, Gray DA. Visualization of alpha-synuclein via bifluorescent complementation. Brain and Mind Research Institute. Brain Health Research Day, 2018.

Mau KJ, Coulombe J, Woulfe, J, Gray DA. Visualization of alpha-synuclein via bifluorescent complementation. University of Ottawa Biochemistry, Microbiology, and Immunology Research Day, 2018.

Mau KJ, Coulombe J, Woulfe, J, Gray DA. Visualization of alpha-synuclein via bifluorescent complementation. University of Ottawa Department of Pathology and Laboratory Medicine Annual Research Day, 2018.

Mau KJ, Coulombe J, Woulfe J, Gray DA. Bifluorescent analysis of alpha-synuclein aggregation *in vivo*. Ottawa Hospital Research Institute Research Day, 2017.

Mau KJ, Jadavji NM. A new perspective on Parkinson's disease: pathology begins in the gastrointestinal tract. Carleton University Life Sciences Research Day, 2017.

Mau KJ, Jadavji NM. A new perspective on Parkinson's disease: pathology begins in the gastrointestinal tract. Brain and Mind Research Institute. Brain Health Research Day, 2017.

ACADEMIC EXPERIENCE

Tutor, Paul Menton Centre for Students with Disabilities 2016 – 2020
Carleton University, Ottawa ON

Courses: Developmental Psychology (PSYC 2500), Introduction to Research Methods in Psychology (PSYC 2001), Introduction to Statistics in Psychology (PSYC 2002), Introduction to Mental Health and Disease (NEUR 1201), and University Physics II (PHYS 1008)

Test Proctor, Centre for Accessible Learning 2019
Algonquin College, Ottawa ON

Visual Interpreter, Centre for Accessible Learning 2019
Algonquin College, Ottawa ON

Let's Talk Science 2017 – 2019
University of Ottawa, Ottawa ON
Roles: Classroom Facilitator, Let's Talk Cancer, Ottawa Science Innovation Challenge Poster Judge and Essay Corrector